Turbulent Poiseuille Flow with Uniform Wall Blowing and Suction.

Vom Fachbereich Maschinenbau
an der Technischen Universität Darmstadt
zur Erlangung des akademischen Grades
eines Doktor-Ingenieurs (Dr.-Ing.)
genehmigte

D i s s e r t a t i o n

von

Victor Avsarkisov, M.Sc.
aus Tbilissi, Georgien

Berichterstatter:	Prof. Dr.-Ing. M. Oberlack
Mitberichterstatter:	Apl. Prof. Dr.-Ing. S. Jakirlic
Tag der Einreichung:	21.08.2013
Tag der mündlichen Prüfung:	05.11.2013

Darmstadt, 2014

D17

Erklärung

Hiermit erkläre ich, dass ich die vorliegende Arbeit, abgesehen von den in ihr ausdrücklich genannten Hilfen, selbstständig verfasst habe.

Victor Avsarkisov

Order arise from chaos.

Ilya Prigogine

Contents

Acknowledgement

I would like to express my sincere appreciation to many people who have made significant input in the development of this thesis.

First of all to my advisor, Professor M. Oberlack, who introduced me to the world of scientific research and to the subjects of wall-bounded turbulence and Lie group theory. His perpetual energy and enthusiasm in research extremely motivated me in my study. While his support and guidance were fundamental for the completion of the present thesis. I am grateful to Dr.-Ing. G. Khujadze for his constant interest in my work throughout these years. Special thank to Apl. Prof. S. Hoyas for his help with the DNS code and fruitful discussions during my stays in Valencia and his visit in Darmstadt. I would like to thank Prof. G. Chagelishvili for all lessons that he taught me. It is his merit that I became a scientist. Last but certainly not least, I would like to thank my parents, who are my first physics teachers. They showed me the beauty and conciseness of the laws of nature.

I will never forget all the friends that I have made in FDY: Olga, George, Jan, Andreas N., Roozbeh, Andreas Z. and many others. I will always remember with a smile all the funny moments that we had.

A big thank you to my family members for their support, in particular, to my wife Ana and daughter Lisa.

Special thanks are devoted to the people who did the proofreading of my thesis, in particular Vladimir Skrinnikov, Jan Hau and Valerios Serasidis.

This work was funded by the German Research Foundation (Deutsche Forschungsgemeinschaft, DFG) under the grant number KH 257/2-1 (2010). The computations for the numerical experiments of this thesis were performed in several machines, including HHLR IBM Regatta supercomputer at TU Darmstadt, FUCHS cluster at the University of Frankfurt-am-Main and SuperMUC Petascale System at Leibniz-Rechenzentrum, Garching. Special thanks are due to M. Rampp for providing me an account on the HP Visualization Cluster at the Rechenzentrum Garching (RZG) of the Max Planck Institute for Plasmaphysics (IPP) where I performed visualizations of the data.

Nomenclature

$(\cdot)'$ Root mean square, or quadratic average, of $(\cdot)$.

$(\cdot)^+$ Variable in wall units, normalized using u_τ and ν.

$(\cdot)_b$ Variable at the blowing side.

$(\cdot)_s$ Variable at the suction side.

$(\cdot)_w$ Variable at the wall.

$\bar{(\cdot)}$ Ensemble mean.

$\boldsymbol{f}(t)$ Arbitrary function of time.

$\boldsymbol{H}$ Convective terms.

$\boldsymbol{k}$ Constant rotation matrix.

$\boldsymbol{r} = (r_1, r_2, r_3)$ Space correlation length.

$\boldsymbol{x} = (x_1, x_2, x_3)$ Space coordinate vector.

δ Boundary layer thickness.

η Wall-normal coordinate normalized on the h.

γ New log law slope constant.

κ von Kármán constant.

ϵ Turbulent energy dissipation.

$\mathcal{P}$ Turbulence production.

ν Kinematic viscosity.

ω Vorticity field.

$\overline{(\cdot)}$ Ensemble average.

$\frac{\bar{\mathrm{D}}}{\mathrm{D}t} = \left(\frac{\partial}{\partial t} + \bar{U}_k \frac{\partial}{\partial x_k}\right)$ Mean substantial derivative.

ρ Density.

τ Time correlation length.

τ_w Shear stress at the wall.

$\tilde{(\cdot)}$ Variables normalized on bulk velocity U_b.

$\bar{U}_i$ Mean velocity.

$\overline{u_i p}$ Pressure-velocity two-point correlations.

$\overline{u_i u_k}$ Reynolds stress tensor.

A Displacement height.

a Point of the zero shear stress.

C Additive constant in the log law over smooth walls.

C_1 Transpiration induced additive constant in the log law.

D Turbulence diffusion.

$D^{(\nu)}$ Viscous turbulence diffusion.

$D^{(p)}$ Turbulence diffusion by fluctuating pressure.

$D^{(u)}$ Turbulence diffusion by fluctuating velocity.

e_{ik} Rate of strain tensor.

Gr Grashof number.

h Channel half-height.

$H_{i_{\{n+1\}}}$ Multi-point velocity correlation tensor in instantaneous representation.

$I_{i_{\{n\}}[l]}$ Multi-point pressure correlation tensor in instantaneous representation.

k Turbulent kinetic energy.

l Characteristic length scale.

P Pressure.

$P_{i_{\{n\}}[l]}$ Multi-point pressure correlation tensor in fluctuation representation.

$R_{(ik)j}$ Triple correlation tensor.

$R_{i_{\{n+1\}}}$ Multi-point velocity correlation tensor in fluctuation representation.

R_{ij} Two-point correlation function.

Ra Rayleigh number.

Re Reynolds number.

Ro Rossby number.

t Time coordinate.

U_b Bulk velocity.

U_i Instantaneous velocity.

u_i Velocity fluctuations.

U_∞ Free stream velocity.

u_τ Friction velocity.

U_{max} Maximum velocity.

v_0 Transpiration velocity.

x_i Space coordinate.

DNS Direct Numerical Simulation.

LES Large Eddy Simulation.

MPC Multi-point correlations.

RANS Reynolds-averaged Navier-Stokes.

TPC Two-point correlations.

Abstract

The objective of this thesis is the analysis of a fully developed, turbulent Poiseuille flow with wall transpiration, i.e. uniform blowing and suction on the lower and upper walls correspondingly. In the present study Lie group analysis of two-point correlation (TPC) equations and a set of Direct Numerical Simulations (DNS) of the three-dimensional, incompressible Navier-Stokes equations are used. The former is applied to find symmetry transformations and in turn to derive invariant solutions of the set of two- and multi-point correlation equations, while the latter is used to simulate turbulent channel flow with wall-transpiration at different Reynolds numbers and transpiration velocities. Both tools are used to find new mean velocity scaling laws. Consequently, it is shown that the transpiration velocity is a symmetry breaking, which implies a logarithmic scaling law in the core region of the channel. DNS validates the result of Lie symmetry analysis and, hence, aids establishing a new logarithmic law of deficit-type.

The region of validity of the new logarithmic law is very different from the usual near-wall log-law and the slope constant in the core region differs from the von Kármán constant and is equal to 0.3. Apart from the new log-law, extended forms of the linear viscous sublayer law and the near-wall log-law are derived. It is shown that these extended laws, as a particular case, include classical scaling laws obtained for the non-transpirating case. For the near-wall log-law it is found that transpiration only changes the additive constant (C) leaving the von Kármán constant unaltered.

The results present in the presented thesis indicate that high-Reynolds number and high-transpiration effects counterbalance in the near-wall region and amplify each other in the core region of the flow. It is found that at very high transpiration rates the flow tends to become laminar.

Finally, structural analysis of the near-wall regions reveal that wall-blowing boosts generation of hairpin-type vortical structures and amplifies large scale motions (LSMs).

Third and forth chapters of the present thesis are heavily based on the paper Avsarkisov, Oberlack & Hoyas (2014).

Kurzfassung

Das Ziel dieser Arbeit ist die Untersuchung einer komplett entwickelten, turbulenten Poiseuilleströmung mit Wandtranspiration, d.h. mit einem uniformen Einstrom bzw. Absaugung an der unteren bzw. oberen Wand. Zu diesem Zweck werden eine Lie-Gruppen-Analyse der Gleichungen der Zwei-Punkt-Korrelation (TPC) sowie ein Satz direkter numerischer Simulationen (DNS) der dreidimensionalen, inkompressiblen Navier-Stokes-Gleichungen verwendet. Erstere wird angewandt um Symmetrietransformationen der Gleichungen der Zwei- und Multi-Punkt-Korrelationen zu finden und aus diesen invariante Lösungen zu berechnen, letztere werden verwendet um die turbulente Strömung in einem Kanal mit Wandtranspiration bei verschiedenen Reynoldsnummern und Transpirationsgeschwindigkeiten zu simulieren. Diese beiden Werkzeuge werden zur Bestimmung eines neuen Skalengesetzes für das mittlere Geschwindigkeitsfeld benutzt. Als Folge wird gezeigt, dass die Transpirationsgeschwindigkeit symmetriebrechend wirkt, was ein logarithmisches Skalengesetz in der Kernregion des Kanals impliziert. Die DNS bestätigen das Ergebnis der Lie-Symmetrieanalysis und unterstützen somit die Einführung eines neuen logarithmischen Gesetzes vom Defizittyp.

Der Gültigkeitsbereich des neuen logarithmischen Gesetzes weicht stark von dem des normalen wandnahen Log-Gesetzes ab. Die Steigungskonstante unterscheidet sich von der von Kármán-Konstanten und nimmt einen Wert von 0.3 an. Neben dem neuen Log-Gesetz werden erweiterte Formen des Gesetzes in der linearen viskosen Unterschicht und des wandnahe Log-Gesetzes berechnet. Es wird gezeigt, dass diese erweiterten Gesetze die klassischen Skalengesetze als Spezialfall verschwindender Transpiration beinhalten. Für das wandnahe Log-Gesetz zeigt sich, dass nichtverschwindende Transpiration nur die additive Konstante (C) beeinflusst und die von Kármán-Konstante unverändert bleibt.

Die Ergebnisse in dieser Arbeit zeigen, dass sich Effekte aufgrund großer Reynoldszahlen und hoher Transpiration im wandnahen Bereich aufwiegen und sich im Kernbereich der Strömung gegenseitig verstärken. Für sehr hohe Transpirationsraten wird eine Neigung der Strömung, laminar zu werden, festgestellt .

Schlussendlich zeigt eine Strukturanalysis des wandnahen Bereiches, dass die Einströmung die Generierung von haarnadelförmiger Wirbelstrukturen fördert und großskalige Bewegungen (LSMs) verstärkt.

Das dritte und vierte Kapitel dieser Arbeit basieren stark auf dem Artikel Avsarkisov et al. (2014).

1 Introduction

The problem studied in the present thesis refers to the phenomenon of turbulence that occurs in an incompressible fluid. Although there is no clear and unique definition of this phenomenon, it is usually stated that turbulence is a state of the moving fluid with nonlinear, chaotic, unpredictable and continuously fluctuating properties such as velocity, pressure, etc. Turbulence can appear in every fluid flow where it arises from instabilities when inertial, centrifugal, buoyancy or some other forces exceed viscous forces. Criteria for this instabilities is usually expressed in terms of critical non-dimensional numbers, i.e. Reynolds number (Re), Rossby number (Ro), Rayleigh number (Ra) and Grashof number (Gr).

Turbulent flows play a fundamental role both in nature and in industry. They may be found in atmospheric and ocean currents, in oil pipelines, in combustion engines, pumps and turbines and in the flows over aircraft wings as well as in boat wakes. In spite of the considerable progress in a study of turbulence, there still remain unsolved problems related to a multiscale, nonlinearity and irregularity properties of the turbulence.

The present thesis is devoted to a study of an incompressible turbulent flows in the presence of the rigid walls, namely wall-bounded turbulence. In the near-wall region, turbulent flows are usually accompanied by high mean velocity gradients, therefore they are often associated with a shear flows. There are some very important physical processes that take place in the near-wall region and that govern the overall production and distribution of turbulence in the flow. These processes as well as other types of turbulent flows are studied in several monographs, like Tennekes & Lumley (1972), Frisch (1995), Pope (2000) and Bernard & Wallace (2002).

1.1 Historical overview

A reader who would be interested in a history of development of the turbulence theory will easily find out that this theory is only 150 years old, which is not too long in comparison to the other theories of classical mechanics. The term *turbulenza* is a Latin word and it firstly appeared in XIII century. Later, in XVI century Leonardo Da Vinci used it to define a chaotic motion of water. But only in XVIII century Leonhard Euler (Euler 1757) derived an equation that describes the conservation of momentum for an inviscid fluid. Soon after that in the 1822 Claude Navier (Navier 1822) using molecular theory derived an equation that governs motion of a viscous fluid, he did not recognize significance of viscosity and proposed that viscosity coefficient is an arbitrary function of molecular spacing (Johnson 1998). In the 1845 George Stokes

(Stokes 1845) obtained the momentum equation for a viscous fluid in the currently accepted form (Batchelor 1967)

$$\frac{\partial U_i}{\partial t} + U_k \frac{\partial U_i}{\partial x_k} = -\frac{1}{\rho}\frac{\partial p}{\partial x_i} + \frac{\partial}{\partial x_k}\left[2\nu\left(e_{ik} - \frac{1}{3}\Delta\delta_{ik}\right)\right] \ , \ i,k = 1,2,3, \tag{1.1}$$

where

$$e_{ik} = \frac{1}{2}\left(\frac{\partial U_i}{\partial x_k} + \frac{\partial U_k}{\partial x_i}\right) \quad \text{and} \quad \Delta = e_{ii}$$

is the rate of strain tensor.

In the equation (1.1) t and x_i are time and space coordinates. U_i, P, ρ and ν are respectively the instantaneous velocity, pressure, density and kinematic viscosity. Due to the enormous amount of theoretical, numerical and experimental evidence, it is widely accepted, though not known with certainty, that the Navier-Stokes equation together with the continuity equation

$$\frac{\partial \rho}{\partial t} + \rho\frac{\partial U_i}{\partial x_i} = 0 \, , \ i = 1,2,3, \tag{1.2}$$

accurately predicts and describes the transition to turbulence and the turbulent state itself. Therefore the moment in history when Navier-Stokes equation was obtained is usually associated with the birth of the theory of turbulence. Later in the 1850s G. Hagen (Hagen 1854) and H. Darcy (Darcy 1857) independently measured pressure drop in large pipes and observed that it increases as the mass flow rate increase. Thus in the limit of negligible viscosity the dissipation remains constant. That concludes that turbulence is a dissipative state of the system. Soon after that J. Boussinesq (Boussinesq 1887) distinguished the difference between laminar and turbulent regimes and introduced local averaging of the stationary flow. The laminar/turbulent regime transition was clarified by O. Reynolds, who investigated this process experimentally and postulated that transition criterion could be dependent only on a non-dimensional parameter $Re = U_b\, l/\nu$ that incorporates bulk velocity (U_b) of the flow, characteristic length scale (l) and kinematic viscosity (ν) (Reynolds 1883). Presently this parameter is called Reynolds number. He also decomposed the flow into mean ($\bar{U}_i$) and fluctuating (u_i) parts (Reynolds decomposition) (Reynolds 1895)

$$U_i = \bar{U}_i + u_i, \tag{1.3}$$

and introduced concepts of stresses (Reynolds stresses) and closure problem. As a result much of the modern statistical theory of turbulence is derived from his papers. It is interesting to note that neither Boussinesq nor Reynolds used the term *turbulence* in their papers. It was introduced by William Thomson (later Lord Kelvin) in 1887 (Thomson 1887) and adopted in fluid dynamics by Prandtl in the beginning of the XX century.

It is important to mention a work of L. Keller and A. Friedmann (Keller & Friedmann 1924) who first introduced correlation functions between different points in space and time. This general method was applied to the Reynolds stress equations. Authors constructed equation for two-point correlation (TPC) functions and neglected third moment of velocity fluctuations that appeared in TPC equations. Importance of

the neglected term was recognized only 15 years later by Kolmogorov (Kolmogorov 1941a, Kolmogorov 1941b).

In 1922 Richardson proposed an idea on the physical mechanism of turbulent mixing for large Reynolds numbers (Richardson 1922). According to his assumptions, turbulence generates large scale structures (eddies), which due to certain instability in their turn break down into smaller eddies until they become very small and will be dissipated by viscosity. Thus energy introduced in the turbulent flow creates a hierarchy of eddies of various order. The cascade process described above was obtained by Richardson by purely empirical means, his ideas were further developed by Kolmogorov in 40th of XXth century. In his seminal work Kolmogorov proposed the hypothesis that homogeneous and isotropic turbulence with sufficiently large Reynolds number is universally determined by two parameters: mean rate of dissipation ($\bar{\epsilon}$) and viscosity (ν) (Kolmogorov 1941a). In his second hypothesis Kolmogorov noted that for largest eddies, the viscous effects are unimportant for eddy evolution process and as a result, do not dissipate their energy (Kolmogorov 1941a). Thus, there is no intrinsic length scale in the system and all eddies of the hierarchy are statistically similar to each other. This statistical regime is determined by a single parameter $\bar{\epsilon}$.

In the 70s of XX century a link between spatiotemporal chaos and turbulence was proposed by Ruelle & Takens (1971). Authors assumed that Navier-Stokes equations have a strange attractor, that appears after number of Hopf bifurcations and leads to turbulence (according to Ruelle & Takens (1971) it leads to a weak turbulence). Nowadays, the question of a nonlinear dynamic concerning the presence of relationship between chaos and turbulence still stays open.

In present days turbulence still keeps many of its secrets while the Navier-Stokes existence and smoothness problem, that concerns the mathematical properties of solutions of the Navier-Stokes equations are among the greatest unsolved problems in physics and one of the six Millennium Prize Problems that were stated by the Clay Mathematics Institute in 2000 (the seventh, Poincaré conjecture problem was solved by G. Perelman, but he declined the award in 2010).

1.2 Wall-bounded turbulence

Due to drag energy loss that causes turbulence in the immediate vicinity of walls, the wall-bounded turbulent flows are of great technological importance. Wall-bounded turbulence can be conditionally subdivided into three major types of the flows: pipes, channels and boundary layers. First theoretical and experimental study of the turbulence in wall-bounded flows was performed by Darcy (1857) and Hagen (1854). However, due to complexity of the flows, caused by the presence of the rigid or nearly immovable walls, turbulence in wall-bounded flows remains less understood than in homogeneous flows. This complexity and hence importance of the study, first of all, lies in interconnection between different scales at different distances from the wall.

Being inhomogeneous in wall-normal direction it is important to emphasize that while channel and pipe flows are homogeneous in streamwise and spanwise directions, boundary layers are homogeneous only in spanwise direction. However in the present

thesis I will restrict to the wall-bounded flows with only one (wall-normal) inhomogeneous direction.

In many different textbooks, reviews and articles you will easily find one clear statement that turbulence is a multiscale phenomenon. It becomes especially important when we are talking about wall-bounded turbulence. A specific structural feature that distinguishes wall-bounded flows is the presence of an equilibrium layer near the boundary, which was obtained by Prandtl (1904) who extended his boundary layer theory to the fully developed turbulent flow over smooth walls. He showed that viscous effects in the vicinity of the wall keep their importance even at very high Reynolds numbers, thus, he solved the famous *d'Alembert's paradox*. Prandtl defined two sets of scaling parameters that describe different regions of the turbulent wall-bounded flow (Prandtl 1904). Namely, in the near wall region all variables should be scaled with ν and friction velocity $u_\tau = \sqrt{\tau_w/\rho}$ defined by wall shear stress τ_w, since viscosity is playing key role there. This scaling Prandtl called the *inner* one. In the core region the variables should be scaled with channel half-height h, this scaling is called the *outer* one.

Presently we can easily conclude that the whole classical theory of the wall-bounded turbulence stems from works by Prandtl (1904) and von Kármán (1921), the latter was the first one to compare friction coefficients in laminar and turbulent boundary layers. The classical theory can be found in many books on turbulence like Tennekes & Lumley (1972), Townsend (1976), Pope (2000), Davidson (2004), etc.

We consider a turbulent flow of an incompressible fluid in a channel. The channel height will be denoted as $2h$. In a channel flow with smooth boundaries incorporating the Reynolds decomposition (1.3) into the equations (1.1) the equations of motion for the mean velocity will have following form:

$$0 = -\frac{1}{\rho}\frac{d\bar{P}}{dx_1} - \frac{d\overline{u_1 u_2}}{dx_2} + \nu\frac{d^2\bar{U}_1}{dx_2^2}, \tag{1.4}$$

$$0 = -\frac{1}{\rho}\frac{d\bar{P}}{dx_2} - \frac{d\bar{u}_2^2}{dx_2}, \tag{1.5}$$

$$0 = -\frac{1}{\rho}\frac{d\bar{P}}{dx_3}, \tag{1.6}$$

here statistically averaged quantities are denoted by an overbar, e.g. $\bar{U}_1$ and $\bar{P}$ are mean streamwise velocity and pressure. Whereas fluctuating quantities are denoted by a lower case letters, e.g. $\bar{u}_2$ and $\overline{u_1 u_2}$ are wall-normal velocity fluctuations and Reynolds stress. Integration of (1.5) and (1.6) yields

$$\frac{\bar{P}}{\rho} + \bar{u}_2^2 = \frac{\bar{P}_0}{\rho} \tag{1.7}$$

where $\bar{P}_0$ is a function of x_1 only. Assuming that $\bar{u}_2$ is not a function of x_1 we will obtain that $\partial\bar{P}/\partial x_1 = \partial\bar{P}_0/\partial x_1$. Since the present flow is in steady state, forcing, i.e. the mean pressure gradient, should be constant (this will protect the flow from

streamwise acceleration). Equation (1.4) can be integrated from $x_2 = 0$ upward, to yield

$$0 = -\frac{x_2}{\rho}\frac{d\bar{P}_0}{dx_1} - \overline{u_1 u_2} + \nu\frac{d\bar{U}_1}{dx_2} - u_\tau^2. \tag{1.8}$$

Due to symmetry of the channel flow with respect to the centerline, at the point $x_2 = h$, the shear stress ($\tau = -\rho\overline{u_1 u_2} + \mu\bar{U}_1/dx_2$) is zero and $u_\tau^2 = -(h/\rho)(d\bar{P}_0/dx_1)$. Thus, the momentum equation reduces to

$$-\overline{u_1 u_2} + \nu\frac{d\bar{U}_1}{dx_2} = u_\tau^2\left(1 - \frac{x_2}{h}\right). \tag{1.9}$$

Equation (1.8) can be rewritten in the following non-dimensional form

$$-\frac{\overline{u_1 u_2}}{u_\tau^2} + \frac{\nu}{u_\tau h}\frac{d(\bar{U}_1/u_\tau)}{d(x_2/h)} = 1 - \frac{x_2}{h}. \tag{1.10}$$

At high Reynolds numbers $Re_\tau = u_\tau h/\nu$ viscous term in this non-dimensional form is negligibly small. Since near the wall the shear stress is purely viscous, this equation cannot be used in this region. According to Prandtl (1904) in the near wall region another non-dimensional form of equation (1.9) should be used. In particular, it should be normalized on friction velocity u_τ and viscous length scale ν/u_τ

$$-\frac{\overline{u_1 u_2}}{u_\tau^2} + \frac{d(\bar{U}_1/u_\tau)}{d(x_2 u_\tau/\nu)} = 1 - \frac{\nu}{h u_\tau}\frac{x_2 u_\tau}{\nu}. \tag{1.11}$$

At $Re_\tau \to \infty$ but when $x_2 u_\tau/\nu$ remaining of order one, momentum equation (1.11) reduces to

$$-\frac{\overline{u_1 u_2}}{u_\tau^2} + \frac{d(\bar{U}_1/u_\tau)}{d(x_2 u_\tau/\nu)} = 1. \tag{1.12}$$

Region governed by equation (1.12), according to Tennekes & Lumley (1972), is called the *surface layer*. If the surface is smooth, the solution of the equation (1.12) may be integrated to following form

$$\bar{U}_1^+ = f(x_2^+). \tag{1.13}$$

This equation is called *law of the wall* (Prandtl 1925). Function $f(x_2^+)$ is expected to be independent of the external flow and since streamwise velocity $\bar{U}_1$ should be independent of density ρ, the function $f(x_2^+)$ must be constant. Finally, it was found that in the vicinity of the wall the mean velocity varies linearly with a distance from the wall (Reichardt 1951)

$$\bar{U}_1^+ = x_2^+. \tag{1.14}$$

This region is called a *viscous sublayer* ($x_2^+ < 5$) since viscous effects dominate over turbulent ones. Outside the viscous sublayer the viscosity and inertial effects are of great importance, this region is called a *buffer layer* and it is a most active part of the turbulent flow, since here both mean velocity gradients and the Reynolds stresses are much larger than in any other region. Away from the wall the viscous effects decrease and that affects the flow length scale. In the near wall region the length scale is $x_2^+ = x_2 u_\tau/\nu$ (Kolmogorov scale analogy in homogeneous turbulence) and in the core region it is x_2/h (integral scale analogy in homogeneous turbulence), where

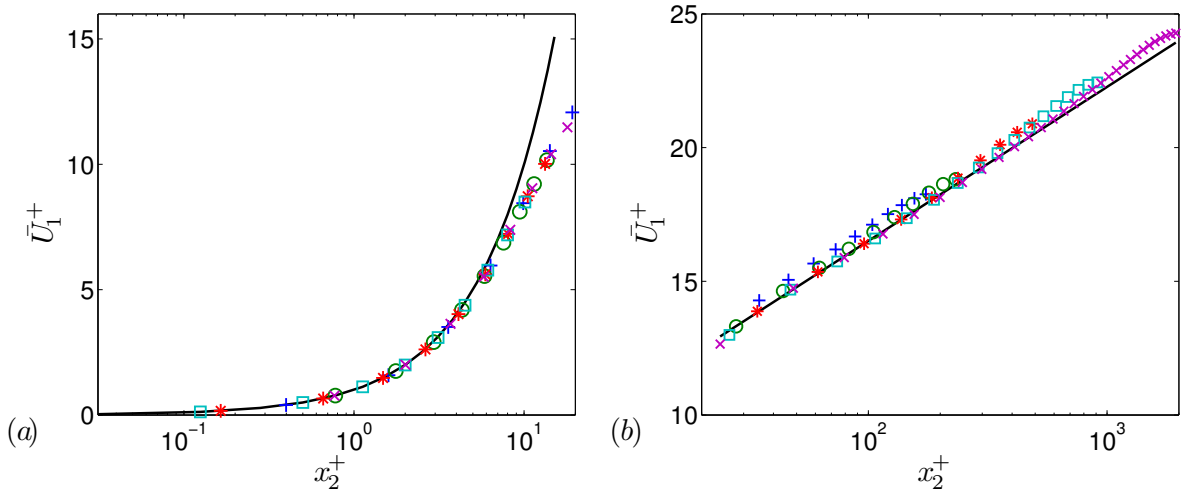

Figure 1.1: Turbulent mean velocity scaling laws. Solid lines correspond to (a) viscous sublayer linear scaling law (1.14). (b) near-wall logarithmic law (1.18). Symbols correspond to DNS data for $(+)$ $Re_\tau = 180$ (del Álamo & Jiménez 2003); $(\bigcirc)$ $Re_\tau = 250$ (Avsarkisov et al. 2011); $(*)$ $Re_\tau = 550$ (del Álamo & Jiménez 2003); $(\square)$ $Re_\tau = 950$ (del Álamo et al. 2004); $(\times)$ $Re_\tau = 2000$ (Hoyas & Jiménez 2006).

h is the height of the half-channel. A part of the flow where both length scales are similarly important is often called intermediate or overlap region. Velocity profile in this region is independent of viscosity and, since $\bar{U}_1 = u_\tau(x_2^+)$,

$$\frac{d\bar{U}_1}{dx_2} = u_\tau \frac{df}{dx_2^+}\frac{dx_2^+}{dx_2} = \frac{u_\tau^2}{\nu}\frac{df}{dx_2^+}. \tag{1.15}$$

Using dimensional analysis and certain physical assumption one may conclude that

$$\frac{df}{dx_2^+} = \left(\kappa \frac{x_2 u_\tau}{\nu}\right)^{-1}, \tag{1.16}$$

here κ is a proportionality constant first found by von Kármán (1930). Finally, mean velocity gradient is found in the following form

$$\frac{d\bar{U}_1}{dx_2} = \frac{u_\tau^2}{\nu}\frac{1}{\kappa x_2^+}, \tag{1.17}$$

that leads to the following result

$$\bar{U}_1^+ = \frac{1}{\kappa}\log\left(x_2^+\right) + C. \tag{1.18}$$

This is the famous logarithmic type mean velocity scaling law universal for all canonical wall-bounded turbulent flows. Since the mean velocity varies as the logarithm of the distance from the wall, the overlap region is also called the *logarithmic region*. Equation (1.18) was first obtained by Theodore von Kármán using similarity arguments (von Kármán 1931). The Kármán constant κ, in principle, should be universal,

though the values for it vary from 0.35 to 0.42, independently from canonical turbulent flow type. The same may be said about additional constant C, its values vary from 4.7 to 5.5, depending on the canonical turbulent flow type.

The logarithmic velocity law may also be derived using Townsend's concept of equilibrium layer (Townsend 1961). According to this concept near-wall region may be represented as a set of the thin, in comparison to h, regions with local energy equilibrium, i.e. when energy production and dissipation are in balance. He showed that this concept leads to a logarithmic mean velocity profile. Another important property of the layers is that the Reynolds stress scaled with friction velocity in such layers should be approximately equal to one $-\overline{u_1 u_2}/u_\tau^2 \approx 1$. This concept together with observation that the characteristic length scale of the equilibrium layers increase within the region of the constant Reynolds stress let Townsend to formulate *the attached eddy hypothesis*, which postulates that main energy containing eddies of the flow that appear in the logarithmic region have widths proportional to distance of their centers to the wall. Therefore, the motion of this eddies is directly influenced by the wall, i.e. they are attached to that wall. With the increase of the Reynolds number the attached (logarithmic) eddies grow in size, which, in turn extends the logarithmic region.

Alternatively to the classical theory of the logarithmic near-wall scaling law J. Nikuradze proposed the $1/7$-exponential law for the mean velocity based on his experimental results of the turbulent flow in the pipe (Nikuradze 1932)

$$\bar{U}_1^+ = 8.74 x_2^{+1/7}. \tag{1.19}$$

Later Barenblatt (1993) assuming a power-type asymptotic behaviour for the non-dimensional function which in classical log-law is known as a von Kármán constant κ, derived power law

$$\bar{U}_1^+ = C x_2^{+\alpha}, \tag{1.20}$$

where both C and α are non-dimensional constants that depend on the log of the Reynolds number. A different type of the power law was obtained by George & Castillo (1997) see also Wosnik, Castillo & George (2000) for the zero pressure gradient turbulent boundary layer. They presumed the existence of a mesolayer between the buffer layer and the outer part of the overlap layer. The viscous stresses in the mesolayer are negligible, but the viscosity produces the Reynolds stress. Using an asymptotic invariance principle to suggest that solutions of the momentum equations for the inner and the outer regions are Reynolds number independent only at infinite Re, they found a power law

$$\bar{U}_1^+ = C(x_2^+ + a^+)^\gamma, \tag{1.21}$$

where the parameters C and γ are functions of boundary layer thickness δ^+ and the parameter a^+ represents a shift of an origin and it is related to the presence of the mesolayer.

Finally, Oberlack (2000) see also Oberlack (2001), Oberlack & Rosteck (2010), Rosteck & Oberlack (2011), applied a Lie group analysis to an infinite set of dimensional multipoint correlation (MPC) equations and showed that log-law is an exact solution of the MPC system of equations. Furthermore, he found that near-wall log-law fundamentally relies on a new statistical translation group. Application of the admitted set of

the symmetries together with boundary conditions and observation that friction velocity u_τ is a symmetry breaking in the near-wall region led to the following classical functional non-dimensional form of the mean velocity

$$\bar{U}_1^+ = \frac{1}{\kappa}\log(x_2^+ + A^+) + C^+. \tag{1.22}$$

Equation (4.27) is a slightly generalized functional form of the logarithmic law of the wall, as it implies the offset A^+ as a displacement height which gives an extended fit of (4.27) to the experimental data (Lindgren, Österlund & Johansson 2004) and that appears, for example, in the log-law for rough-wall-bounded flows (Jackson 1981).

Far from the wall, where length scale is x_2/h the effects of the viscous stress are negligibly small. At high Reynolds numbers ($Re_\tau \to \infty$), but with the length scale remaining of order one ($x_2/h = \mathcal{O}(1)$) momentum equation (1.10) reduces to the following form

$$-\frac{\overline{u_1 u_2}}{u_\tau^2} = 1 - \frac{x_2}{h}. \tag{1.23}$$

This equation does not give explicit information about mean velocity $\bar{U}_1$ itself, but it suggests that velocity scale far from the wall should be friction velocity u_τ. The part of the flow where this equation is valid is called *core region*. Thus the only dimensional parameters in the core region of the turbulent flow are length x_2/h and velocity u_τ scales and channel half-height h. Taking into account Prandtl's mixing length theory (Prandtl 1925), which states that there is a distance through which a fluid element can move from one layer to another without change of its velocity, von Kármán derived the following relation (von Kármán 1930)

$$\frac{d\bar{U}_1}{dx_2} = \frac{u_\tau}{h}\frac{dF(x_2/h)}{d(x_2/h)}. \tag{1.24}$$

Here $F(x_2/h)$ is unknown function, with $dF(x_2/h)/d(x_2/h) = \mathcal{O}(1)$. Integrating (1.24) from channel center towards the walls and taking into account that $\bar{U}_1 = \bar{U}_{1max}|_{x_2/h=1}$, one may obtain the mean velocity scaling law for the core region

$$\frac{\bar{U}_1 - \bar{U}_{1max}}{u_\tau} = F\left(\frac{x_2}{h}\right). \tag{1.25}$$

This is a *velocity defect law* which first was obtained by von Kármán (1930).

In the beginning of the twentieth century it was widely accepted that randomness of the turbulent flow is a local phenomenon and statistical analysis is the only tool that can shed some light on the turbulence problem. With the development of experimental techniques and facilities it became evident that structures (eddies) are present in the turbulent flow and they are flow patterns. Furthermore, in wall-bounded turbulent flows the structures, similarly to the scaling laws derived in this section, characterize different regions of the flow. One of the earliest observations of these structures was reported by Kline, Reynolds, Schraub & Runstadler (1967). They have found low-speed streaks in the near-wall region of the turbulent flow. These coherent structures are located very close to the wall (at $x_2^+ = 5$ above the wall) and elongated in streamwise direction ($\Delta x_1^+ \approx 1000$). Further they observed that low-speed streaks can eject

from the wall, reach the buffer layer and breakup. This violent events are called *bursting*. The dynamics of the low-speed streaks was described by Kim, Kline & Reynolds (1971). According to the continuity equation, if at some point of the near-wall region the fluid is moving outwards from the wall (ejection), then there is an another point of the same region, where the fluid is moving towards the wall (sweep). The sweep motions was observed by Corino & Brodkey (1969) and Grass (1971). Analyzing Reynolds shear stress, responsible for creation of the coherent structures, Wallace, Eckelmann & Brodkey (1972) and Willmarth & Lu (1972) developed *quadrant analysis*, in which the u_1u_2 plane is separated into four quadrants: Q1 ($u_1 > 0, u_2 > 0$), Q2 ($u_1 < 0, u_2 > 0$), Q3 ($u_1 < 0, u_2 < 0$), Q4 ($u_1 > 0, u_2 < 0$). While quadrant Q2 is associated with ejection, quadrant Q4 is associated with sweeps. It was found that in the buffer layer Q2 and Q4 contribute equally, while sweeps dominate closer to the wall and ejections dominate farther from the wall.

Further, away from the wall, in the logarithmic region, the flow is dominated by the quasi-streamwise vortices. They may replicate themselves and organize into the groups of coherent structures. These coherent structures are well interpreted with the concept of hairpin vortices. As it was proposed by Görtler (1942) and Adrian (2007) the structures are packets of self-propelled and self-similar hairpin vortices, where each hairpin represents a single streak ejection motion. In a channel flow the length of a single hairpin vortex may exceed the channel half-height h, while the width is scaled in wall units. An alternative explanation for the quasi-streamwise clusters of vortices was formulated by del Álamo & Jiménez (2006). It was proposed that structures should be separated into two families: attached to the wall and detached from it. Attached ones are self-similar objects from the Q2 quadrant, while detached clusters are small-scale dissipative objects. Attached clusters consist of an elongated low-speed streaks surrounded by two counter-rotating vortices (sweep-ejection pair).

While both proposed models give plausible explanation for the quasi-streamwise coherent vortical structures that are found in the near-wall region, the recent finding, that the structures, that are present in the logarithmic region even when the buffer region is completely destroyed (Flores, Jiménez & del Álamo 2007), suggest the attached cluster model.

1.3 Near-wall scaling laws of the turbulent flows with wall transpiration

Turbulent flow with wall transpiration is first of all technologically important and at the same time difficult object of scientific investigation. Its importance lays in skin friction drag reduction in turbulent wall-bounded flows, that met to reduce environmental impact, and in particular, fuel consumption in ships, aircrafts and vehicles. It is difficult object of investigation because transpiration implies specific boundary conditions that may completely change near-wall region of the flow, i.e. viscous sublayer, buffer layer and near-wall log-region.

First theoretical and experimental studies on this topic are dated from the second half of the 20th century. They were devoted to the turbulent boundary layers in equilibrium conditions (Clauser 1956) with injection and suction. An example of such flow

is a zero pressure gradient boundary layer, an outer layer of this flow has a constant thickness since the growth due to skin friction is compensated by the suction. Most of this studies were based on the mixing-length theory proposed by Prandtl (1925). In particular, it was assumed that fluid eddies originate in a near-wall region and then move towards the turbulent core region where they transfer their momentum to the surroundings. It was also assumed that mixing length is proportional to the distance from the wall $l = \kappa x_2$, where κ is von Kármán constant. This approach facilitated Black & Sarnecki (1958) and Mickley & Davis (1957) to derive a new mean velocity scaling law for the near-wall region of the zero pressure gradient turbulent boundary layer. They called it the bi-logarithmic law

$$u_\tau^2 + v_0 \bar{U}_1 = \left(\frac{v_0}{2\kappa} \log\left(\frac{x_2}{C} \right) \right)^2, \tag{1.26}$$

here κ is von Kármán constant, C is constant of integration and v_0 transpiration velocity. Later Stevenson using the similar assumptions compared his experimental results to the experimental data of Black & Sarnecki (1958) and Mickley & Davis (1957) in two companion papers Stevenson (1963a) and Stevenson (1963b). He found generalized forms of the law of the wall

$$2\frac{u_\tau}{v_0} \left[\left(1 + \frac{v_0 \bar{U}_1}{u_\tau^2} \right)^{\frac{1}{2}} - 1 \right] = \frac{1}{\kappa} \log(x_2^+) + C, \tag{1.27}$$

and shortly afterwards a velocity defect law for the turbulent boundary layer with suction and blowing at zero pressure gradient

$$2\frac{u_\tau}{v_0} \left[\left(1 + \frac{v_0 \bar{U}_\infty}{u_\tau^2} \right)^{\frac{1}{2}} - \left(1 + \frac{v_0 \bar{U}_1}{u_\tau^2} \right)^{\frac{1}{2}} \right] = F(x_2/h), \tag{1.28}$$

where $\bar{U}_\infty$ is a free-stream velocity and $F(x_2/h)$ is a universal function. He stated that in the logarithmic law the slope constant, i.e. the von Kármán constant κ, and the additive constant C are both independent of the transpiration velocity v_0.

Assuming the existence of a joint velocity scale u_τ^2/v_0 for the inner and the outer regions at moderate transpiration rates ($0.04 \leq v_0/u_\tau \leq 0.04$) (Tennekes 1965) obtained a new form of the "limit" law of the wall for the boundary layer flow with transpiration, which he called semi-logarithmic law

$$-\frac{v_0 \bar{U}_1}{u_\tau^2} = 0.06 \log\left(-\frac{v_0 x_2}{\nu} \right) - 11 \left(\frac{v_0}{u_\tau} \right) + A \left(\frac{\kappa v_0}{\nu} \right), \tag{1.29}$$

and a "limit" velocity defect law

$$v_0 \frac{\bar{U}_1 - \bar{U}_\infty}{u_\tau^2} = G\left(\frac{x_2}{h}; \frac{dp}{dx}; \frac{v_0 \bar{U}_\infty}{u_\tau^2} \right), \tag{1.30}$$

here G is a universal function. This assumption followed from the result of Clauser (1956) that the primary variable in an overlap region of the turbulent boundary layer is the wall shear stress τ_w or equivalently the friction velocity u_τ. Tennekes called these

laws "limit" assuming that at very small transpiration rates ($v_0/u_\tau < 0.04$) the skin friction coefficient $c_f = 2(u_\tau/\bar{U}_\infty)^2$ is not compensated by the suction rate and there is no joint velocity scale for inner and outer layers, however he is not certain. Quoting Tennekes: "This conclusion is clearly tentative, awaiting further experimental and/or theoretical confirmation" (Tennekes 1965, p. 698).

Structural analysis of the boundary layer flow with uniform suction revealed (Antonia, Krishnamoorthy, Fulachier, Anselmet & Benabid 1986) that transpiration increases the stability and the streamwise coherence of the near-wall low-speed streaks. Further it was found that suction increases an average length and decrease spanwise oscillations of the streaks. Finally, they concluded that the suction stabilizes near-wall region reducing turbulent energy production, i.e. Reynolds stresses, temperature variances and heat fluxes.

In order to correctly predict a wall stress for large eddy simulations (LES) of the wall-bounded flows with transpiration Piomelli, Ferziger & Moin (1989) developed a new approximate boundary conditions in which the wall stress is specified by the velocity in the core of the flow. Authors used Schumann-type boundary conditions Schumann (1975) extended by Grötzbach (1987). It was assumed that the wall stress τ_w correlates with the mean velocity $\bar{U}_1$ in the logarithmic region. They have derived a modified linear mean velocity scaling law for the viscous sublayer

$$\bar{U}_1^+ = \frac{1}{v_0^+}\left(\exp^{v_0^+ x_2^+} - 1\right) \quad (x_2 \leq x_2^+), \tag{1.31}$$

and modified logarithmic law of the wall

$$\bar{U}_1^+ = \bar{U}_0^+ + \frac{\sqrt{1+\bar{U}_0^+ v_0^+}}{\kappa}\log\left(\frac{x_2^+}{x_{2\,0}^+}\right) + \frac{v_0^+}{4}\left[\frac{1}{\kappa}\log\left(\frac{x_2^+}{x_{2\,0}^+}\right)\right]^2 \quad (x_2 \geq x_2^+), \tag{1.32}$$

here $x_{2\,0}^+$ is the edge point of the inner layer and $\bar{U}_0^+$ is the velocity at that point. v_0^+ is a transpiration rate and κ is a von Kármán constant. The values for $x_{2\,0}^+ = \bar{U}_0^+ = 11$ are obtained applying the condition $v_0 = 0$, i.e. requiring convergence of (1.31) and (1.32) to the classical laws for the flow without transpiration.

1.4 Motivation

Summarizing all the studies mentioned in §1.3 we may conclude that there is no comprehensive experimental, numerical or analytical investigation of the Poiseuille flow with uniform wall blowing and suction and, in particular, of the mean velocity scaling laws of this flow based on first principles. This difficulty first of all may be traced back to the complexity of the admitted flow type, although it is possible to find an analytical solution of the laminar channel flow with wall transpiration (see Appendix A). Another problem that arises in the study of mean velocity scaling laws is the determination of an appropriate velocity scale as there are multiple of them including v_0, u_τ on both walls and U_b being the bulk velocity, as well as the proper choice of equations on which the analysis should be based on. Due to all the above mentioned issues the near-wall regions of the wall-bounded flows with blowing or suction are

poorly studied, it is not clear how blowing and suction affect shear stress distribution, or how turbulent kinetic energy is being produced and distributed in the flow.

The aim of the present thesis is to investigate near-wall and core regions of the turbulent channel flow with wall transpiration and to shed some light on the listed above problems. In particular, to perform numerical study, collect and analyze low and high order statistical data and to find near-wall and core region mean velocity scaling laws. The latter task is of particular importance since the motivation for this study was a forecast of the new mean velocity scaling law that was made with a Lie group analysis. It was found that transpiration velocity v_0 is a symmetry breaking in the core region of the channel flow with blowing and suction and that a new mean velocity logarithmic type scaling law is to be expected.

Special attention will be paid to Reynolds number effects that are present in wall-bounded turbulence. DNSes of a turbulent channel flow with blowing and suction with a different moderate Reynolds numbers and wide range of the transpiration rates were performed. The results from these simulations will contribute to the understanding of the role of blowing and suction in the dynamics of the near-wall and core regions.

Another objective that is attempted in the present thesis is to study how blowing and suction affect near-wall streaks and coherent vortical structures. Recent results suggest that suction stabilizes low-speed streaks (Antonia et al. 1986) and creates large spanwise roller structures (Jiménez, Uhlmann, Pinelli & Kawahara 2001).

1.5 Contents

The present thesis is structured in five chapters. In the first chapter, basic equations of the fluid dynamics theory will be introduced. It will be shown how application of the new boundary conditions with wall transpiration will affects momentum and two-point correlation equations.

In the second chapter, the eight DNSes of the turbulent channel with wall blowing and suction that have been run during last two years of the PhD will be presented. This chapter also includes some general analytical results that were obtained from comparison of the performed DNS data to the results without transpiration.

In the third chapter, a Lie group symmetry analysis will be introduced. It will be shown that a new mean velocity scaling law was predicted with Lie group theory and it is based on two of the new statistical groups which have no direct counterparts in the Euler and Navier-Stokes equations for the instantaneous velocities.

In the fourth chapter, a new mean velocity scaling law obtained with the Lie group analysis will be validated. It will be also shown that classical linear and near-wall mean velocity scaling laws are found in a modified form in the channel flow with wall blowing and suction.

Finally, in the fifth chapter, a coherent structures that usually occur in the near-wall region of the turbulent flow will be analyzed. Further, effects of the wall blowing and suction on the small scale near-wall coherent structures as well as on the large scale

structures will be discussed. It will be shown that blowing boosts hairpin structures production, while suction harms near-wall regeneration cycle.

2 Basic equations

2.1 Basic equations for the turbulent channel flow

As the present thesis is devoted to the study of the physical phenomena that occurs in the moving incompressible Newtonian fluid, that has constant physical properties, it seems logical to start analysis with the Navier-Stokes and continuity equations written for incompressible Newtonian fluid. In its most general form the Navier-Stokes equation was presented in the Introduction chapter of this thesis (see equation (1.1)), while for the incompressible flow this equation will take the form

$$\frac{\partial U_i}{\partial t} + U_k \frac{\partial U_i}{\partial x_k} = -\frac{\partial P^*}{\partial x_i} + \nu \frac{\partial^2 U_i}{\partial x_k \partial x_k}\,,\ i,k = 1,2,3, \tag{2.1}$$

where ν is the kinematic viscosity with dimensions L^2T^{-1} and $P^* = P/\rho$ is the kinematic pressure, i.e. the physical pressure divided by the constant density. The asterisk will be omitted throughout the thesis.

The continuity equation (1.2), for an incompressible fluid, will reduce to the following form

$$\frac{\partial U_i}{\partial x_i} = 0\,,\ i = 1,2,3. \tag{2.2}$$

Taking the divergence of the equation (2.1) and using equation (2.2) we will obtain Poisson equation for the pressure

$$\nabla^2 P = -\frac{\partial^2}{\partial x_i \partial x_j}(U_i U_j)\,,\ i = 1,2,3. \tag{2.3}$$

Thus, in the incompressible flows, equation (2.3) allows to simplify the turbulence problem by expressing the pressure field with velocity.

2.2 One-point statistics: Reynolds equations

In order to simplify the mathematical description of turbulence, following the procedure proposed by Reynolds (1895), we will write the instantaneous velocity $U_i(\boldsymbol{x},t)$ and pressure $P(\boldsymbol{x},t)$ as a sum of the mean $\bar{U}_i(\boldsymbol{x},t)$, $\bar{P}(\boldsymbol{x},t)$ and the fluctuation $u_i(\boldsymbol{x},t)$, $p(\boldsymbol{x},t)$ from the mean

$$U_i(\boldsymbol{x},t) = \bar{U}_i(\boldsymbol{x},t) + u_i(\boldsymbol{x},t)\,,\ i = 1,2,3, \tag{2.4}$$

$$P(\boldsymbol{x},t) = \bar{P}(\boldsymbol{x},t) + p(\boldsymbol{x},t)\,. \tag{2.5}$$

These notations for the statistically averaged (mean) and fluctuating quantities will be used throughout the present thesis. In honor of O. Reynolds, this decomposition

technique is called *Reynolds decomposition*. There are various ways to obtain the mean quantity that depends on the type of the flow. If the flow is statistically stationary we may average any quantity over time to obtain *time mean*. If the flow is periodic it is possible to average over a number of periods to obtain *phase averaged mean*. Finally, if the flow is non-stationary and non-periodic we may obtain an *ensemble mean* by averaging over a number of samples. Irrespective to the type of the averaging Reynolds decomposition of the two arbitrary instantaneous variables

$$A = \bar{A} + a\,, \tag{2.6}$$
$$B = \bar{B} + b\,, \tag{2.7}$$

should satisfy the following relations:

- addition or subtraction

$$\overline{A \pm B} = \overline{A} \pm \overline{B} = \bar{A} \pm \bar{B} \tag{2.8}$$

- multiplication with a constant α

$$\overline{\alpha A} = \alpha \overline{A} = \alpha \bar{A} \tag{2.9}$$

- multiplication

$$\overline{ab} \neq 0 \tag{2.10}$$

- differentiation and integration (x_i is the time and space coordinate)

$$\overline{\frac{\partial A}{\partial x_i}} = \frac{\partial \overline{A}}{\partial x_i} = \frac{\partial \bar{A}}{\partial x_i} \qquad \overline{\int A dx_i} = \int \overline{A} dx_i = \int \bar{A} dx_i \tag{2.11}$$

According to the definition the mean value of the fluctuations is equal to zero

$$\overline{u_i}(\boldsymbol{x}, t) = 0\,, \tag{2.12}$$
$$\overline{p}(\boldsymbol{x}, t) = 0\,, \tag{2.13}$$

but the average of the square of a fluctuation is not zero. Thus, we may introduce the root mean square (r.m.s.) value of the velocity fluctuation as follows

$$u'_{(i)}(\boldsymbol{x}, t) = \overline{u^2_{(i)}(\boldsymbol{x}, t)}^{1/2}\,, \tag{2.14}$$

while the index in brackets implies no summation. It is also called a fluctuation intensity. This quantity is widely used in the turbulence theory as an indicator of the various effects and phenomenas. Application of the Reynolds decomposition to the continuity equation (2.2) and averaging over time results in the following equations

$$\frac{\partial \bar{U}_i(\boldsymbol{x}, t)}{\partial x_i} = 0\,, \tag{2.15}$$
$$\frac{\partial \overline{u_i}(\boldsymbol{x}, t)}{\partial x_i} = 0\,, \tag{2.16}$$

which show that mean and fluctuating velocities, due to the linearity of the decomposition (2.4), separately satisfy the continuity equation.

Application of the equations (2.4) and (2.5) to the Navier-Stokes equations (2.1) and averaging over time term by term leads to the Reynolds averaged Navier-Stokes (RANS) equations for the incompressible Newtonian fluid

$$\frac{\partial \bar{U}_i}{\partial t} + \bar{U}_k \frac{\partial \bar{U}_i}{\partial x_k} = -\frac{\partial \bar{P}}{\partial x_i} + \nu \frac{\partial^2 \bar{U}_i}{\partial x_k \partial x_k} - \frac{\partial \overline{u_i u_k}}{\partial x_k}, \ i = 1, 2, 3, \tag{2.17}$$

here $\overline{u_i u_k}$ is the Reynolds stress tensor. Simple term by term comparison of the equations (2.1) with (2.17) shows that the mean velocity equation is the Navier-Stokes equation written in terms of the mean variables, which has an additional term that involves Reynolds stress. In other words, mean motion equations (2.15) and (2.17) along with the mean velocity and pressure have the third independent variable $\overline{u_i u_k}$. This is the famous *closure problem* discovered by Reynolds (1895). It states that a new nonlinear term that arise from the convective acceleration of the flow cannot be closed using RANS and continuity equations only.

In the present study we are investigating statistically stationary turbulent channel flow of an incompressible fluid with a uniform wall-normal blowing and suction. For the present flow we have the following boundary condition (BC) at the wall

$$U_i(x_1; x_2 = 0,\, 2h; x_3) = (0;\, v_0;\, 0)^T, \tag{2.18}$$

where v_0 is a transpiration velocity. Because of the periodic BC in streamwise direction and general homogeneity in this direction, continuity leads to a constant wall-normal velocity across the channel height, i.e.

$$\bar{U}_2(x_2) = v_0. \tag{2.19}$$

As we employ the BC $U_i(x_1; x_2 = 0,\, 2h; x_3) = (0;\, v_0;\, 0)^T$ for the DNS together with (2.18) it implies that all fluctuations vanish at the wall , i.e. $u_i = 0$. Therefore all Reynolds stresses also vanish at the wall.

With this, we obtain the streamwise component of mean momentum equation for the steady state

$$v_0 \frac{d\bar{U}_1}{dx_2} = -\frac{d\bar{P}}{dx_1} - \frac{d\overline{u_1 u_2}}{dx_2} + \nu \frac{d^2 \bar{U}_1}{dx_2^2}. \tag{2.20}$$

The analysis of equation (2.20) presented below in a chapter 5 employs a mean friction velocity as a non-dimensionalization parameter. Which is by definition a measure of the pressure gradient

$$u_\tau \equiv \sqrt{\frac{u_{\tau b}^2 + u_{\tau s}^2}{2}} = \sqrt{\frac{1}{\rho} \frac{|\tau_{wb}| + |\tau_{ws}|}{2}} = \sqrt{h \left| \frac{\partial \bar{P}}{\partial x_1} \right|}. \tag{2.21}$$

The local friction velocities are defined as

$$u_{\tau b} = \sqrt{\nu \left| \frac{\partial \bar{U}_1}{\partial x_2} \right|_b}, \quad u_{\tau s} = \sqrt{\nu \left| \frac{\partial \bar{U}_1}{\partial x_2} \right|_s}. \tag{2.22}$$

Here and subsequently subscripts $(\cdot)_b$ and $(\cdot)_s$ correspond to variables taken on the blowing and the suction side respectively. For variables at the wall we use the subscript $(\cdot)_w$. Dimensionless variables in the near-wall scaling will have the superscript plus

$$x_i^+ = \frac{x_i u_\tau}{\nu}, \quad \bar{U}_i^+ = \frac{\bar{U}_i}{u_\tau}, \quad \overline{u_i u_k}^+ = \frac{\overline{u_i u_k}}{u_\tau^2}, \quad v_0^+ = \frac{v_0}{u_\tau}, \quad \tau^+ = \frac{\tau}{(|\tau_{wb}| + |\tau_{ws}|)/2}. \tag{2.23}$$

Note, that here u_τ is the mean friction velocity, which is a global parameter. Specific differences on each wall and the corresponding differences in scaling will be discussed in the subsections 5.2 and 5.3. We employ the channel half-width h as a core-region length scaling parameter. The bulk mean velocity is defined as

$$U_b = \frac{1}{2h} \int_0^{2h} \bar{U}_1(x_2) dx_2. \tag{2.24}$$

As the pressure gradient is specified as a constant, equation (2.20) may be integrated once and rearranged to obtain

$$\tau(x_2) - v_0 \bar{U}_1 = -\overline{u_1 u_2} + \nu \frac{d\bar{U}_1}{dx_2} - v_0 \bar{U}_1 = x_2 \frac{d\bar{P}}{dx_1} + c_1. \tag{2.25}$$

Here c_1 is a constant that in the canonical channel flow is defined as ρu_τ^2 (Tennekes & Lumley 1972). Due to different wall conditions of the channel flow with transpiration the wall shear stresses on the blowing and suction walls are different, which brought the necessity to use a local friction velocity in (2.25) rather than a global one.

2.3 Reynolds stress and turbulent kinetic energy transport equations

In the previous section it was shown that Reynolds decomposition leads to the closure problem, i.e. it reveals a new variables (the Reynolds stresses) in the Navier-Stokes equations that are products of two fluctuating velocities. Assuming that construction of new equations that involves the Reynolds stresses will solve the closure problem lets write a transport equation for the Reynolds stresses. By subtracting the Reynolds equations (2.17) from the Navier-Stokes equations (2.1) and using equations (2.4) and (2.5) we obtain a transport equation for the velocity fluctuations u_i

$$\frac{\partial u_i}{\partial t} + (\bar{U}_k + u_k) \frac{\partial u_i}{\partial x_k} = -u_k \frac{\partial \bar{U}_i}{\partial x_k} - \frac{\partial p}{\partial x_i} + \nu \frac{\partial^2 u_i}{\partial x_k \partial x_k} + \frac{\partial \overline{u_i u_k}}{\partial x_k}, \ i = 1, 2, 3, \tag{2.26}$$

Assuming now that the order of application of differentiation and averaging operations may be interchanged

$$\overline{\frac{\partial}{\partial t}u_i u_j} = \overline{u_j \frac{\partial u_i}{\partial t}} + \overline{u_i \frac{\partial u_j}{\partial t}}, \tag{2.27}$$

after certain mathematical operations we obtain the following equation for the Reynolds stress

$$\begin{aligned} \frac{\bar{\mathrm{D}}\overline{u_i u_j}}{\bar{\mathrm{D}}t} &= -\overline{u_i u_k}\frac{\partial \bar{U}_j}{\partial x_k} - \overline{u_j u_k}\frac{\partial \bar{U}_i}{\partial x_k} + \overline{p\left(\frac{\partial u_i}{\partial x_j} + \frac{\partial u_j}{\partial x_i}\right)} - 2\nu\overline{\frac{\partial u_i}{\partial x_k}\frac{\partial u_j}{\partial x_k}} \\ &+ \frac{\partial}{\partial x_k}\left[\nu\frac{\partial \overline{u_i u_j}}{\partial x_k} - \overline{p(u_i\delta_{jk} + u_j\delta_{ik})} - \overline{u_i u_j u_k}\right]. \end{aligned} \tag{2.28}$$

here

$$\frac{\bar{\mathrm{D}}}{\bar{\mathrm{D}}t} = \left(\frac{\partial}{\partial t} + \bar{U}_k\frac{\partial}{\partial x_k}\right) \tag{2.29}$$

is the mean substantial derivative.

Apart from already known mean velocity and Reynolds stress terms equation (2.28) contains some new ones, which show that the system is not closed. These terms are, first of all, triple products of velocity fluctuations (the last term on the r.h.s. of (2.28)) and pressure strain term (the third term on the r.h.s. of (2.28)). Appearance of these terms shows that the system of equations cannot be closed by adding a new equations for higher velocity moments. In equations for the triple correlations we will find fourth-order correlations and the products of pressure and Reynolds stress, which still will be unclosed. This finding gave rise to a number of semi-empirical theories of turbulence, which pursued only one aim: to close the system of equations by expressing higher order correlations with $\overline{u_i}$ and $\overline{u_i u_j}$, using some additional hypotheses and assumptions.

By setting $i = j$ and summing each term in equation (2.28) over i we obtain turbulent kinetic energy equation

$$\frac{\bar{\mathrm{D}}k}{\bar{\mathrm{D}}t} = \mathcal{P} - \epsilon + \mathcal{D}. \tag{2.30}$$

where the following notations are used

- Turbulent kinetic energy

$$k = \frac{1}{2}\overline{u_i u_i} \tag{2.31}$$

- Turbulence production due to mean-flow deformation

$$\mathcal{P} \equiv \frac{1}{2}\mathcal{P}_{ii} = -\overline{u_i u_k}\frac{\partial \bar{U}_i}{\partial x_k} \tag{2.32}$$

- Turbulence dissipation by the viscous forces

$$\epsilon \equiv \frac{1}{2}\epsilon_{ii} = \nu\overline{\frac{\partial u_i}{\partial x_k}\frac{\partial u_i}{\partial x_k}} \tag{2.33}$$

- Diffusive transport of turbulence ($\mathcal{D}^{(\nu)}$ is viscous, $\mathcal{D}^{(p)}$ by fluctuating pressure and $\mathcal{D}^{(u)}$ by fluctuating velocity, correspondingly)

$$\mathcal{D} = \mathcal{D}^{(\nu)} + \mathcal{D}^{(p)} + \mathcal{D}^{(u)} = \frac{\partial}{\partial x_k}\left[\nu\frac{\partial k}{\partial x_k} - \overline{pu_i}\delta_{ik} - \overline{ku_k}\right]. \tag{2.34}$$

Turbulence kinetic energy equation (2.30) is the one of the most important equations in the turbulence theory. In many cases it helps to study the major physical mechanism that take place in the turbulent flows.

2.4 The two-point correlation equations

In a previous sections we obtained equations that describe the flow in one particular point in space and time. In other words, statistical data that may be obtained by integration of these equations represents only one point of the flow, but it is unable to provide information about turbulence structure. In order to overcome this limitations and to study turbulent eddies, that exist in a variety of different scales in the turbulent flow, a two-point correlation (TPC) functions can be used. TPC function (R_{ij}) is a product of two fluctuating quantities (a_i, a_j) taken at two different points in space or/and time

$$\begin{aligned} \boldsymbol{x}, \boldsymbol{x}' &= \boldsymbol{x} + \boldsymbol{r} \\ t, t' &= t + \tau. \end{aligned}$$

Here $\boldsymbol{r}$ and τ are the distances between two points in space and time, correspondingly. Thus, the TPC tensor function is defined as follows

$$R_{ij}(\boldsymbol{x}, t, \boldsymbol{r}, t') = \overline{a_i(\boldsymbol{x}, t), a_j(\boldsymbol{x}', t')}. \tag{2.35}$$

Presently we are dealing with a statistically stationary wall-bounded turbulent flow, which means that all the statistics, including two- and multi-point correlations are invariant under a shift in time. Thus, we consider only space correlations and in order to obtain TPC equation for the velocity fluctuations we may employ equations (2.26) written for two different fluctuating velocities (u_i and u_j) in two different systems of coordinate ($\boldsymbol{x}^{(1)}$ and $\boldsymbol{x}^{(2)}$), correspondingly. Connection between these two systems is established through the following transformation for coordinates

$$\begin{cases} \boldsymbol{x}^{(1)} = & \boldsymbol{x} \\ \boldsymbol{x}^{(2)} = & \boldsymbol{x} + \boldsymbol{r} \end{cases} \tag{2.36}$$

and for their derivatives

$$\begin{cases} \dfrac{\partial}{\partial \boldsymbol{x}^{(1)}} = \dfrac{\partial}{\partial \boldsymbol{x}}\dfrac{\partial \boldsymbol{x}}{\partial \boldsymbol{x}^{(1)}} + \dfrac{\partial}{\partial \boldsymbol{r}}\dfrac{\partial \boldsymbol{r}}{\partial \boldsymbol{x}^{(1)}} = \dfrac{\partial}{\partial \boldsymbol{x}} - \dfrac{\partial}{\partial \boldsymbol{r}} \\ \dfrac{\partial}{\partial \boldsymbol{x}^{(2)}} = \dfrac{\partial}{\partial \boldsymbol{x}}\dfrac{\partial \boldsymbol{x}}{\partial \boldsymbol{x}^{(2)}} + \dfrac{\partial}{\partial \boldsymbol{r}}\dfrac{\partial \boldsymbol{r}}{\partial \boldsymbol{x}^{(2)}} = \dfrac{\partial}{\partial \boldsymbol{r}} \end{cases} \tag{2.37}$$

Using transformations (2.36) and (2.37) for the equations (2.26) written for velocity fluctuations u_i and u_j and multiplying equation for u_i velocity fluctuation taken in the point $\boldsymbol{x}$ on u_j and equation for u_j in the point $\boldsymbol{x}+\boldsymbol{r}$ on u_i, correspondingly, it is possible to sum them up to obtain an evolution equation for the TPC function R_{ij} (Hinze 1959)

$$\begin{aligned} \frac{\bar{\mathrm{D}}R_{ij}}{\bar{\mathrm{D}}t} \;+\; & R_{kj}\frac{\partial \bar{U}_i(\boldsymbol{x},t)}{\partial x_k} + R_{ik}\left.\frac{\partial \bar{U}_j(\boldsymbol{x},t)}{\partial x_k}\right|_{\boldsymbol{x}+\boldsymbol{r}} + \left[\bar{U}_k(\boldsymbol{x}+\boldsymbol{r},t) - \bar{U}_k(\boldsymbol{x},t)\right]\frac{\partial R_{ij}}{\partial r_k} \\ & + \frac{\partial \overline{pu}_j}{\partial x_i} - \frac{\partial \overline{pu}_j}{\partial r_i} + \frac{\partial \overline{u_i p}}{\partial r_j} - \nu\left[\frac{\partial^2 R_{ij}}{\partial x_k \partial x_k} - 2\frac{\partial^2 R_{ij}}{\partial x_k \partial r_k} + 2\frac{\partial^2 R_{ij}}{\partial r_k \partial r_k}\right] \\ & + \frac{\partial R_{(ik)j}}{\partial x_k} - \frac{\partial}{\partial r_k}\left[R_{(ik)j} - R_{i(jk)}\right] = 0, \end{aligned} \tag{2.38}$$

where the second and third order correlation tensors are defined as

$$\begin{aligned} R_{ij}(\boldsymbol{x},\boldsymbol{r};t) = \overline{u_i(\boldsymbol{x},t)u_j(\boldsymbol{x}+\boldsymbol{r},t)},\ \overline{pu}_j = \overline{p(\boldsymbol{x},t)u_j(\boldsymbol{x}+\boldsymbol{r},t)}, \\ R_{(ik)j}(\boldsymbol{x},\boldsymbol{r};t) = \overline{u_i(\boldsymbol{x},t)u_k(\boldsymbol{x},t)u_j(\boldsymbol{x}+\boldsymbol{r},t)},\ \overline{u_i p} = \overline{u_i(\boldsymbol{x},t)p(\boldsymbol{x}+\boldsymbol{r},t)}, \\ R_{i(jk)}(\boldsymbol{x},\boldsymbol{r};t) = \overline{u_i(\boldsymbol{x},t)u_j(\boldsymbol{x}+\boldsymbol{r},t)u_k(\boldsymbol{x}+\boldsymbol{r},t)}. \end{aligned}$$

and the mean substantial derivative has the form shown above (see eq. (2.29)). Continuity equations for the TPC have the following form

$$\frac{\partial R_{ij}}{\partial x_i} - \frac{\partial R_{ij}}{\partial r_i} = 0, \quad \frac{\partial R_{ij}}{\partial r_j} = 0 \tag{2.39}$$

$$\frac{\partial R_{(ik)j}}{\partial x_i} - \frac{\partial R_{(ik)j}}{\partial r_i} = 0, \quad \frac{\partial R_{(ik)j}}{\partial r_j} = 0 \tag{2.40}$$

$$\frac{\partial R_{i(jk)}}{\partial x_i} - \frac{\partial R_{i(jk)}}{\partial r_i} = 0, \quad \frac{\partial R_{i(jk)}}{\partial r_j} = 0 \tag{2.41}$$

$$\tag{2.42}$$

and

$$\frac{\partial \overline{pu}_i}{\partial r_i} = 0, \quad \frac{\partial \overline{u_j p}}{\partial x_j} - \frac{\partial \overline{u_j p}}{\partial r_j} = 0. \tag{2.43}$$

In the present study Lie group analysis is used to find symmetry transformations and in turn self-similar solutions of the TPC equations. For the present flow the TPC equations (2.38) reduce to the following form

$$\begin{aligned}\bar{U}_2\frac{\partial R_{ij}}{\partial x_2} \quad + \quad & R_{2j}\delta_{i1}\,\frac{\partial \bar{U}_1(x_2)}{\partial x_2} + R_{i2}\delta_{1j}\,\frac{\partial \bar{U}_1(x_2)}{\partial x_2}\bigg|_{x_2+r_2} + \frac{\partial \overline{pu}_j}{\partial x_i} - \frac{\partial \overline{pu}_j}{\partial r_i} \\ & + \frac{\partial \overline{u_i p}}{\partial r_j} + \left[\bar{U}_1(x_2+r_2) - \bar{U}_1(x_2)\right]\frac{\partial R_{ij}}{\partial r_1} - \nu\left[\frac{\partial^2 R_{ij}}{\partial x_2 \partial x_2} - 2\,\frac{\partial^2 R_{ij}}{\partial x_2 \partial r_2} + 2\frac{\partial^2 R_{ij}}{\partial r_k \partial r_k}\right] \\ & + \frac{\partial R_{(i2)j}}{\partial x_2} - \frac{\partial}{\partial r_k}\left[R_{(ik)j} - R_{i(jk)}\right] = 0, \end{aligned} \tag{2.44}$$

since

$$\bar{U}_i = (\bar{U}_1(x_2), \bar{U}_2, 0) \tag{2.45}$$

and, we recall, $\bar{U}_2 = v_0$, as well as the TPC have a reduced form

$$\begin{gathered} R_{ij} = R_{ij}(x_2, \boldsymbol{r}),\ \overline{pu}_j = \overline{pu}_j(x_2, \boldsymbol{r}),\ \overline{u_i p} = \overline{u_i p}(x_2, \boldsymbol{r}), \\ R_{(ik)j} = R_{(ik)j}(x_2, \boldsymbol{r}),\ R_{i(jk)} = R_{i(jk)}(x_2, \boldsymbol{r}). \end{gathered}$$

For this special case with wall transpiration continuity equations will also have a reduced form

$$\frac{\partial R_{2j}}{\partial x_2} - \frac{\partial R_{2j}}{\partial r_2} = 0, \quad \frac{\partial R_{ij}}{\partial r_j} = 0 \tag{2.46}$$

$$\frac{\partial R_{(ik)j}}{\partial x_2} - \frac{\partial R_{(ik)j}}{\partial r_2} = 0, \quad \frac{\partial R_{(ik)j}}{\partial r_j} = 0 \tag{2.47}$$

$$\frac{\partial R_{i(jk)}}{\partial x_2} - \frac{\partial R_{i(jk)}}{\partial r_2} = 0, \quad \frac{\partial R_{i(jk)}}{\partial r_j} = 0 \tag{2.48}$$

$$\tag{2.49}$$

and

$$\frac{\partial \overline{pu}_i}{\partial r_2} = 0, \quad \frac{\partial \overline{u_j p}}{\partial x_j} - \frac{\partial \overline{u_j p}}{\partial r_j} = 0. \tag{2.50}$$

2.5 The multi-point correlation equations

It is possible to expand the correlation approach from two- to a multi-point correlations (MPC). There are two different forms of the MPC equations (Oberlack & Rosteck 2010). The first one is based on the fluctuating quantities, similarly to the equation (2.38), and has the following form in absolute coordinates

$$\begin{aligned}\frac{\partial R_{i_{\{n+1\}}}}{\partial t} + \sum_{l=0}^{n}\Bigg[& \bar{U}_{k_{(l)}}(\boldsymbol{x}_{(l)})\frac{\partial R_{i_{\{n+1\}}}}{\partial x_{k_{(l)}}} + R_{i_{\{n+1\}}[i_{(l)}\mapsto k_{(l)}]}\frac{\partial \bar{U}_{i_{(l)}}(\boldsymbol{x}_{(l)})}{\partial x_{k_{(l)}}} \\ & + \frac{\partial P_{i_{\{n\}}[l]}}{\partial x_{i_{(l)}}} - \frac{1}{Re}\frac{\partial^2 R_{i_{\{n+1\}}}}{\partial x_{k_{(l)}}\partial x_{k_{(l)}}} - R_{i_{\{n\}}[i_{(l)}\mapsto\emptyset]}\frac{\partial \overline{u_{i_{(l)}} u_{k_{(l)}}}(\boldsymbol{x}_{(l)})}{\partial x_{k_{(l)}}} \end{aligned} \tag{2.51}$$

$$+ \frac{\partial R_{i_{\{n+2\}}[i_{(n+1)}\mapsto k_{(l)}]}[\boldsymbol{x}_{(n+1)} \mapsto \boldsymbol{x}_{(l)}]}{\partial x_{k_{(l)}}}\Bigg] = 0$$

for $n = 0, \ldots, \infty$, where multi-point velocity and pressure correlation tensors are based on fluctuation quantities

$$R_{i_{\{n+1\}}} = R_{i_{(0)}i_{(1)}\ldots i_{(n)}} = \overline{u_{i_{(0)}}(\boldsymbol{x}_{(0)}) \cdot \ldots \cdot u_{i_{(n)}}(\boldsymbol{x}_{(n)})} \tag{2.52}$$

$$P_{i_{\{n\}}[l]} = \overline{u_{i_{(0)}}(\boldsymbol{x}_{(0)}) \cdot \ldots \cdot u_{i_{(l-1)}}(\boldsymbol{x}_{(l-1)}) p(\boldsymbol{x}_{(l)}) u_{i_{(l+1)}}(\boldsymbol{x}_{(l+1)}) \cdot \ldots \cdot u_{i_{(n)}}(\boldsymbol{x}_{(n)})}. \tag{2.53}$$

Continuity equations for the MPC and the pressure-velocity correlations have the following form

$$\frac{\partial R_{i_{\{n+1\}}[l][i_{(l)}\mapsto k_{(l)}]}}{\partial x_{k_{(l)}}} = 0 \quad \text{for} \quad l = 1, ..., n, \tag{2.54}$$

$$\frac{\partial P_{i_{\{n\}}[l][i_{(l)}\mapsto k_{(l)}]}}{\partial x_{k_{(l)}}} = 0 \quad \text{for} \quad k, l = 1, ..., n \quad \text{and} \quad k \neq l. \tag{2.55}$$

However, there is also an instantaneous representation of the MPC equations which involves an instantaneous quantities and has the following form

$$\frac{\partial H_{i_{\{n+1\}}}}{\partial t} + \sum_{l=0}^{n} \left[\frac{\partial H_{i_{\{n+2\}}[i_{(n+1)}\mapsto k_{(l)}]}[\boldsymbol{x}_{(n+1)} \mapsto \boldsymbol{x}_{(l)}]}{\partial x_{k_{(l)}}} + \frac{\partial I_{i_{\{n\}}[l]}}{\partial x_{i_{(l)}}} - \frac{1}{Re} \frac{\partial^2 H_{i_{\{n+1\}}}}{\partial x_{k_{(l)}} \partial x_{k_{(l)}}} \right] = 0, \tag{2.56}$$

for $n = 0, \ldots, \infty$, where

$$H_{i_{\{n+1\}}} = \overline{U_{i_{(0)}}(\boldsymbol{x}_{(0)}) \cdot \ldots \cdot U_{i_{(n)}}(\boldsymbol{x}_{(n)})}, \tag{2.57}$$

$$I_{i_{\{n\}}[l]} = \overline{U_{i_{(0)}}(\boldsymbol{x}_{(0)}) \cdot \ldots \cdot U_{i_{(l-1)}}(\boldsymbol{x}_{(l-1)}) P(\boldsymbol{x}_{(l)}) U_{i_{(l+1)}}(\boldsymbol{x}_{(l+1)}) \cdot \ldots \cdot U_{i_{(n)}}(\boldsymbol{x}_{(n)})}. \tag{2.58}$$

and

$$\frac{\partial H_{i_{\{n+1\}}[i_{(l)}\mapsto k_{(l)}]}}{\partial x_{k_{(l)}}} = 0 \quad \text{for} \quad l = 1, ..., n+1 \tag{2.59}$$

$$\frac{\partial I_{i_{\{n\}}[l][i_{(l)}\mapsto k_{(l)}]}}{\partial x_{k_{(l)}}} = 0 \quad \text{for} \quad k, l = 1, ..., n \quad \text{and} \quad k \neq l. \tag{2.60}$$

The advantage of the instantaneous representation (2.56) over the fluctuation one (2.51) is in linearity of the equations of the former, while equations (2.51) are non-linear.

In the paper (Oberlack & Rosteck 2010) a direct link between the instantaneous (see eq. (2.56)) and fluctuating (see eq. (2.51)) approaches was shown

$$H_{i_{(0)}} = \bar{U}_{i_{(0)}} \tag{2.61}$$

$$H_{i_{(0)}i_{(1)}} = \bar{U}_{i_{(0)}}\bar{U}_{i_{(1)}} + R_{i_{(0)}i_{(1)}} \tag{2.62}$$

$$\begin{aligned} H_{i_{(0)}i_{(1)}i_{(2)}} &= \bar{U}_{i_{(0)}}\bar{U}_{i_{(1)}}\bar{U}_{i_{(2)}} + R_{i_{(0)}i_{(1)}i_{(2)}} \\ &\quad + R_{i_{(0)}i_{(1)}}\bar{U}_{i_{(2)}} + R_{i_{(0)}i_{(2)}}\bar{U}_{i_{(1)}} + R_{i_{(1)}i_{(2)}}\bar{U}_{i_{(0)}} \end{aligned} \tag{2.63}$$

$$\vdots \qquad \vdots$$

where the indices represent different correlation points in space.

For the present case with the uniform wall-blowing and suction the MPC equations in the fluctuation approach will reduce to the following form

$$\begin{aligned} &\bar{U}_2\frac{\partial R_{i\{n+1\}}}{\partial x_2} + R_{i_{\{n+1\}}[i_{(0)}\mapsto 2]}\delta_{i_{(0)}1}\frac{\partial \bar{U}_1(x_2)}{\partial x_2} + \sum_{l=1}^{n-1} R_{i_{\{n+1\}}[i_{(l)}\mapsto 2]}\delta_{i_{(l)}1}\frac{\partial \bar{U}_1(x_2+r_{2_{(l)}})}{\partial x_2} \\ &+\frac{\partial P_{i_{\{n\}}[0]}}{\partial x_2}\delta_{i_{(0)}2} + \sum_{l=1}^{n-1}\left(\frac{\partial P_{i_{\{n-1\}}[l]_p}}{\partial r_{i_{(l)}(l)}} - \frac{\partial P_{i_{\{n-1\}}[0]_p}}{\partial r_{i_{(0)}(l)}}\right) + \sum_{l=1}^{n}\left[\bar{U}_1(\boldsymbol{x}+\boldsymbol{r}_{(l)}) - \bar{U}_1(\boldsymbol{x})\right]\frac{\partial R_{i_{\{n+1\}}}}{\partial r_{k_{(l)}}} \\ &-\nu\left[\frac{\partial^2 R_{i_{\{n+1\}}}}{\partial x_2\partial x_2} + \sum_{l=1}^{n-1}\left(-2\frac{\partial^2 R_{i_{\{n+1\}}}}{\partial x_2\partial r_{2(l)}} + \sum_{m=1}^{n-1}\frac{\partial^2 R_{i_{\{n+1\}}}}{\partial r_{k(m)}\partial r_{k(l)}} + \frac{\partial^2 R_{i_{\{n+1\}}}}{\partial r_{k(l)}\partial r_{k(l)}}\right)\right] \\ &-R_{i_{\{n\}}[0]_\emptyset}\frac{\partial \overline{u_{i_{(0)}}u_2}(\boldsymbol{x})}{\partial x_2} - \sum_{l=1}^{n-1} R_{i_{\{n\}}[0]_\emptyset}\frac{\partial \overline{u_{i_{(l)}}u_2}(x_2+r_{2(l)})}{\partial r_{k(l)}} \\ &+\frac{\partial R_{i_{\{n+2\}}[i_{(n)}\mapsto 2]}[\boldsymbol{r}_{(n)}\mapsto 0]}{\partial x_2} - \sum_{l=1}^{n+1}\frac{\partial R_{i_{\{n+2\}}[i_{(n)}\mapsto k]}[\boldsymbol{r}_{(n)}\mapsto 0]}{\partial r_{k(l)}} \\ &+\sum_{l=1}^{n+1}\frac{\partial R_{i_{\{n+2\}}[i_{(n)}\mapsto k]}[\boldsymbol{r}_{(n)}\mapsto \boldsymbol{r}_{(l)}]}{\partial r_{k(l)}} = 0 \end{aligned} \tag{2.64}$$

In instantaneous approach the MPC equations (2.56) for the channel flow with uniform wall blowing and suction will have the form

$$\begin{aligned} &\frac{\partial H_{i_{\{n+1\}}[i_{(l)}\mapsto 2]}[\boldsymbol{r}_{(n)}\mapsto 0]}{\partial x_2} + \frac{\partial I_{i_{\{n-1\}}[0]_p}}{\partial x_{i_{(0)}}} + \sum_{l=0}^{n}\left[\frac{\partial H_{i_{\{n+2\}}[i_{(n+1)}\mapsto k]}[\boldsymbol{r}_{(n+1)}\mapsto \boldsymbol{r}_{(l)}]}{\partial r_{k_{(l)}}}\right. \\ &+\frac{\partial I_{i_{\{n\}}[l]_p}}{\partial x_{i_{(l)}(l)}} - \frac{\partial H_{i_{\{n+2\}}[i_{(n+1)}\mapsto k]}[\boldsymbol{r}_{(n+1)}\mapsto 0]}{\partial r_{k_{(l)}}} - \frac{\partial I_{i_{\{n\}}[0]_p}}{\partial r_{i_{(l)}(l)}} - \frac{1}{Re}\sum_{m=0}^{n}\frac{\partial^2 H_{i_{\{n+1\}}}}{\partial r_{k_{(l)}}\partial r_{k_{(m)}}} \\ &\left.-\frac{1}{Re}\frac{\partial^2 H_{i_{\{n+1\}}}}{\partial r_{k_{(l)}}\partial r_{k_{(l)}}} + \frac{2}{Re}\frac{\partial^2 H_{i_{\{n+1\}}}}{\partial x_2\partial r_{2(l)}}\right] - \frac{1}{Re}\frac{\partial^2 H_{i_{\{n+1\}}}}{\partial x_2\partial x_2} = 0, \\ &\text{for} \quad n = 1, ..., \infty, \end{aligned} \tag{2.65}$$

3 DNS of turbulent Poiseuille flow with wall transpiration

3.1 Introduction

Turbulence is a fundamental property of any flow relevant in industry, nature or meteorology. It is also one of the most important unsolved problems in physics. The complex behavior of turbulence is described by the Navier-Stokes equations (2.1) and the continuity equation (2.2). A complete description of a turbulent flow, where the flow variables are space and time dependent, can only be obtained by Direct Numerical Simulation (DNS) techniques, where all the significant scales are resolved. Since the size of the smallest turbulent eddies is proportional to $Re^{-3/4}$, the computational cost in 3D simulations scales as $Re^{11/4}$, which apparently is a serious computational challenge with increasing Reynolds numbers. Although there exists another techniques to model turbulence (RANS and LES being the most famous), DNS is the only feasible technique to study the physics of turbulence in every detail, despite its high cost.

Some of the most advanced DNS simulations of turbulent channel flows have been conducted by Prof. J. Jiménez group at the School of Aeronautics of the Universidad Politécnica de Madrid (Technical University of Madrid), see for instance (Jiménez (2004), Jiménez, del Álamo & Flores (2004), del Álamo et al. (2004), del Álamo & Jiménez (2006), Hoyas & Jiménez (2006), Flores & Jiménez (2006)). The simulation of Hoyas & Jiménez (2006) is, up to now, still the "record" simulation in terms of the achieved Reynolds number. In the present thesis the code of Hoyas & Jiménez (2006) is used to perform numerical experiments of the turbulent Poiseuille flow with uniform wall blowing and suction, as it is shown in figure 3.1.

In the classical non-transpirating plane turbulent channel flow all statistical quantities are symmetric or antisymmetric with respect to the channel centerline. This includes symmetric distribution of the mean velocity, the normal Reynolds stresses, and point symmetric distributions of viscous and turbulent shear stresses including values of shear stresses at the walls. These results are consistent with zero total shear stress and zero mean velocity gradient in the center of the channel. In the presence of wall transpiration, all these symmetries are broken. Furthermore, the occurrence of an additional term in the streamwise component of the mean momentum equation modifies the classical universal scaling laws (linear viscous sublayer and law of the wall) for non-transpirating wall-bounded flows. In comparison to the other wall-bounded flows with specific, non-standard boundary conditions, turbulent channel, i.e. Poiseuille flow with wall transpiration is a relatively new subject of investigation. The only experimental study of this flow of an incompressible fluid known to the authors was conducted by Zhapbasbayev & Isakhanova (1998) (see also Zhapbasbayev & Yershin (2003)). They collected statistics for the mean velocity and turbulent stresses

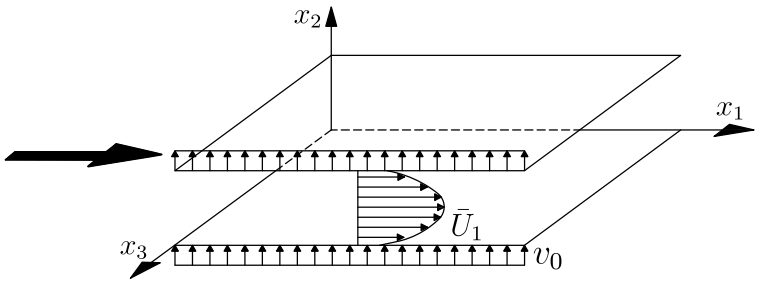

Figure 3.1: Schematic view of the channel flow with wall transpiration. Fluid is blown through the lower wall and removed from the upper wall with a constant rate.

for different Reynolds numbers and a variety of small transpiration velocity numbers in the range $0 < v_0/u_\tau < 0.05$. Thereafter, they employed the experimental data to evaluate a Reynolds stress transport model developed by Launder and co-authors (see e.g. Hanjalić & Launder (1972b), Launder, Reece & Rodi (1975)).

In the literature only a few DNS studies of the turbulent channel flow with blowing and suction were reported. Sumitani & Kasagi (1995) studied turbulent channel flow with uniform wall transpiration and heat transfer. The walls were kept isothermal, while their temperatures vary. The Reynolds number and the transpiration rate were held constant at Re_τ=150 and v_0/u_τ=0.05. Various statistical quantities including mean velocity and mean temperature, Reynolds stresses, and turbulent heat fluxes were obtained. Energy budgets and temperature correlations were also calculated. One key overall result they have found was that blowing stimulates the near-wall turbulence and creates an excessive amount of small scale coherent streamwise vortical structures while suction suppresses turbulence and at the same time creates large scale near-wall coherent structures. Nikitin & Pavel'ev (1998) performed DNS computations at Re_τ=356, 681.2 for v_0/u_τ=0.112, 0.118, respectively. They showed that blowing and suction increase the friction coefficient. Apart from this, they investigated the near-wall logarithmic region of the mean velocity profile and found that the slope constant of the log-law at the blowing wall is not constant and increases with the increase of transpiration rate. Here it is important to mention that they used the local friction velocity at each wall as the velocity scale. This is rather natural to do so, however, presently we employ an averaged friction velocity from both walls, which is a measure of the pressure gradient, collapsing our DNS data to a considerably extended range. Chung & Sung (2001) investigated the initial relaxation of a turbulent channel flow after a sudden application of blowing and suction. Later, Chung, Sung & Krogstad (2002), extended this by modulating the near-wall turbulence with uniform wall blowing and suction. They confirmed that suction increases the turbulence anisotropy, while blowing acts on the transverse components of the velocity fluctuations (u_2 and u_3) and hence decreases the anisotropy in the near-wall region. The most recent study on a turbulent wall-bounded flow with transpiration is a numerical one conducted by Schlatter & Örlü (2011). They showed that in turbulent boundary layers the uniform suction considerably changes the mean velocity profile and they found the modified coefficients for the log-law to be $\kappa = 0.82$ and $C = 9.2$.

The numerical experiments presented in this chapter aim to clarify how transpiration affects near-wall and core regions of the turbulent channel flow with wall transpiration at moderate and large Reynolds numbers. Due to the uniform blowing and suction a properties of the corresponding near-wall regions will be considerably different from each other. It will be also natural to expect that the properties of this regions will be different from the near-wall region of the non-transparent channel flow. These simulations allow to study three different regions: the wall-blowing region, the wall-suction region and the core region with a constant transverse velocity. High resolution of the present simulations, large variety of the governing parameters such as transpiration velocity v_0 and Reynolds number Re_τ and the absence of the previous comprehensive studies of the Poiseuille flow with transpiration constitute the significance of these numerical experiments.

The present chapter is organized as follows. Description of the numerical code, boundary conditions and code validation results are presented in §3.2. The effect of the blowing and suction on the mean flow is discussed in §3.3. Conclusions are summarized in §3.4.

3.2 Numerical experiments

3.2.1 Mathematical model

For the intended DNS a CFD algorithm employing a Fourier-Compact Finite Difference method to solve the Navier-Stokes equations was used. In the dimensionless form the governing equations for an incompressible flow have the following form

$$\frac{\partial U_i^+}{\partial t^+} = -\frac{\partial P^+}{\partial x_i^+} + H_i^+ + \frac{1}{Re_\tau}\nabla^2 U_i^+, \tag{3.1}$$

$$\frac{\partial U_i^+}{\partial x_i^+} = 0, \tag{3.2}$$

where $\boldsymbol{U}$ is velocity field, $\boldsymbol{\omega}$ is vorticity field and $\boldsymbol{H}$, which includes the convective terms and the mean pressure gradient, have the following form

$$\boldsymbol{U} = (U_1, U_2, U_3), \tag{3.3}$$

$$\boldsymbol{\omega} = \boldsymbol{\nabla} \times \boldsymbol{U} = (\omega_1, \omega_2, \omega_3), \tag{3.4}$$

$$\boldsymbol{H} = (\boldsymbol{U} \times \boldsymbol{\omega}) - \frac{1}{2}\nabla(\boldsymbol{U} * \boldsymbol{U}) = (H_1, H_2, H_3). \tag{3.5}$$

Independent variables t, x_i, instantaneous velocity and pressure U_i, P and convective term H_i in dimensionless form are

$$t^+ = \frac{t u_\tau^2}{\nu},\ \ x_i^+ = \frac{x_i u_\tau}{\nu},\ \ U_i^+ = \frac{U_i}{u_\tau},\ \ P = \frac{P}{u_\tau^2},\ \ H_i^+ = \frac{H_i \nu}{u_\tau^3}. \tag{3.6}$$

$(\cdot)^+$ denotes non-dimesionalization of the physical quantity using friction velocity u_τ and channel half-height h and it is omitted from here on. For the present DNS study

instead of impermeability and no-slip BCs we employed the boundary conditions (2.18).

3.2.2 Numerical methods and algorithms

As it was already mentioned in the introduction to this chapter, for the DNS we were using the code developed in the School of Aeronautical Engineering, Technical University of Madrid. The code integrates the Navier-Stokes equations for an incompressible fluid in the velocity-vorticity formulation (Dennis, Ingham & Cook 1979)

$$\frac{\partial \nabla^2 U_2}{\partial t} = h_{U_2} + \frac{1}{Re_\tau}\nabla^4 U_2, \tag{3.7}$$

$$\frac{\partial \omega_2}{\partial t} = h_{\omega_2} + \frac{1}{Re_\tau}\nabla^2 \omega_2, \tag{3.8}$$

$$f + \frac{\partial U_2}{\partial x_2} = 0, \tag{3.9}$$

where

$$h_{U_2} = -\frac{\partial}{\partial x_2}\left(\frac{\partial H_1}{\partial x_1} + \frac{\partial H_3}{\partial x_3}\right) + \left(\frac{\partial^2}{\partial x_1^2} + \frac{\partial^2}{\partial x_3^2}\right) H_2, \tag{3.10}$$

$$\omega_2 = \frac{\partial U_1}{\partial x_3} - \frac{\partial U_3}{\partial x_1},\ h_{\omega_2} = \frac{\partial H_1}{\partial x_3} - \frac{\partial H_3}{\partial x_1}, \tag{3.11}$$

$$f = \frac{\partial U_1}{\partial x_1} + \frac{\partial U_3}{\partial x_3}, \tag{3.12}$$

i.e. in the form of two evolution equations for the Laplacian of the wall-normal velocity $\nabla^2 U_2$ (see equation (3.7)) and for the wall-normal vorticity ω_2 (see equation (3.8)), so pressure is not computed during the run. The remarkable property of the formulation is that it is independent whether or not the frame of reference is inertial, i.e. non-inertial effects are present only in initial and boundary conditions (Speziale 1987). In this form 70-80 % of simulation time and 99% of inter-domain communication is based on calculation of h_{ω_2} and h_{U_2}.

Numerics and the main ideas are based on the original code made by (Kim, Moin & Moser 1987), but presently none of the original code subroutines remain in it. In the streamwise and spanwise directions (x_1, x_3) it uses a spectral formulation (Fourier series), which has the following form

$$\varphi(x_1, x_2, x_3) = \sum_{\alpha'=0}^{N_{x_1}-1} \sum_{\beta'=0}^{N_{x_3}-1} \widehat{\varphi}_{\alpha',\beta'}(x_2) e^{ic_\alpha \alpha' x_1} e^{ic_\beta \beta' x_3} \tag{3.13}$$

where

$$c_\alpha = 2\pi L_{x_2}/L_{x_1}, \quad c_\beta = 2\pi L_{x_2}/L_{x_3}. \tag{3.14}$$

Equation (3.14) may be rewritten in the following form

$$\varphi(x_1, x_2, x_3) = \sum_{k_{x_1}}^{N_{x_1}-1} \sum_{k_{x_3}}^{N_{x_3}-1} \widehat{\varphi}_{k_{x_1},k_{x_3}}(x_2) e^{i(k_{x_1}x_1 + k_{x_3}x_3)}, \tag{3.15}$$

with

$$k_{x_1} = c_\alpha \alpha', \quad k_{x_3} = c_\beta \beta'. \tag{3.16}$$

Thus, governing equation (3.7-3.9) and boundary conditions (2.18) in phase space have the form

$$-\partial_t(k_{x_1}^2 + k_{x_3}^2 - \partial_{x_2x_2})\widehat{U}_2 = \widehat{h}_{U_2} + \frac{1}{Re}(k_{x_1}^4 + k_{x_3}^4 + \partial_{x_2x_2x_2x_2})\widehat{U}_2, \tag{3.17}$$

$$\partial_t \widehat{\omega}_{x_2} = \widehat{h}_{\omega_2} - \frac{1}{Re_\tau}(k_{x_1}^2 + k_{x_3}^2 - \partial_{x_2x_2})\widehat{\omega}_{x_2}, \tag{3.18}$$

$$\widehat{\omega}_{x_2}(x_2 = 0,\, 2h) = 0, \tag{3.19}$$

$$\partial_{x_2}\widehat{U}_2(x_2 = 0,\, 2) = 0, \;\; \widehat{U}_2(x_2 = 0,\, 2h) = v_0. \tag{3.20}$$

In the wall-normal direction, (x_2), a seven-point compact finite difference scheme with fourth-order consistency and extended spectral-like resolution (Lele 1992) is applied. Using this discretization scheme, first and second derivatives will have the form

$$D_j + \sum_{m=1}^{M} b_m(D_{j+m} + D_{j-m}) = \frac{1}{h}\sum_{n=1}^{N} a_n(U_{j+n} - U_{j-n}), \; N = M = 7. \tag{3.21}$$

$$D_j^{(2)} + \sum_{m=1}^{M} b_m(D_{j+m}^{(2)} + D_{j-m}^{(2)}) = \frac{a_0 U_j + \sum_{n=1}^{N} a_n(U_{j+n} - U_{j-n})}{h^2}, \; N = M = 5. \tag{3.22}$$

Compared to the traditional finite difference approximations the scheme used in this code provides a better representation of the shorter length scales. It has a pure central difference form (except near the boundaries), i.e. it has no built-in artificial dissipation. It is, therefore, necessary that the applications to which this scheme is applied be such that there is a physically well defined cutoff for the smallest scales. In other words the smallest scales should be determined physically and not numerically.

For the time discretization, a third-order semi-implicit Runge-Kutta (R-K) algorithm (Spalart, Moser & Rogers 1991) is implemented. It allows to write the system of equations for the unknown vector function $\boldsymbol{U}$ in the following form

$$\frac{\partial \boldsymbol{U}}{\partial t} = L(\boldsymbol{U}) + N(\boldsymbol{U}), \tag{3.23}$$

here L and N are linear and non-linear operator, correspondingly. They only implicitly dependent on t. In Navier-Stokes equations L contains the viscous and pressure terms, while operator N represents the convective term. Any linear term can be included in either operator. The scheme needs three substeps to advance from $\boldsymbol{U}_n$, at time t, to $\boldsymbol{U}_{n+1}$, at time $t + \delta t$

$$\boldsymbol{U}' = \boldsymbol{U}_n + \delta t[L(\alpha_1 \boldsymbol{U}_n + \beta_1 \boldsymbol{U}') + \gamma_1 N_n], \tag{3.24}$$

$$\boldsymbol{U}'' = \boldsymbol{U}' + \delta t[L(\alpha_2 \boldsymbol{U}' + \beta_2 \boldsymbol{U}'') + \gamma_2 N' + \xi_1 N_n], \tag{3.25}$$

$$\boldsymbol{U}_{n+1} = \boldsymbol{U}'' + \delta t[L(\alpha_3 \boldsymbol{U}'' + \beta_3 \boldsymbol{U}_{n+1}) + \gamma_3 N'' + \xi_2 N'], \tag{3.26}$$

where $N_n \equiv N(\boldsymbol{U}_n), N' \equiv N(\boldsymbol{U}')$ and $N'' \equiv N(\boldsymbol{U}'')$. $\alpha_i, \beta_i, \gamma_i, \xi_i$ are unknown coefficients. It is a low-storage, hybrid implicit/explicit modification of the three-substep R-K scheme designed by A. Wray (Kennedy, Carpenter & Lewis 2000). The advantage of this scheme is that it needs only the minimum of storage, i.e. the same as the Euler explicit scheme.

The code is written in Fortran77, MPI parallelized and does compile and run on different machines and compiler (IBM and Intel). It has planes-lines parallelization scheme. For each sub-step of R-K scheme, the data set is distributed in $x_2 - x_3$ complex planes, therefore, the number of processors must be divisible by the number of the complex planes. Essentially the code does the following steps:

1. Calculation of velocity and vorticity in Fourier-Physical-Fourier (F-P-F) space. Transformation of x_3 from Fourier space into physical space. It is necessary for computation of the nonlinear terms of the Navier-Stokes equations. This transformation takes 10% of R-K substep.

2. Move the data set from x_2 - x_3 planes into x_1-lines using MPI routines (40% of R-K substep).

3. Transformation of the data to physical space in x_1 and computation of nonlinear terms. Then nonlinear terms are transformed back into x_1-Fourier space (all together 10% of R-K substep).

4. Then nonlinear terms are moved back into x_2 - x_3 planes (20% of R-K substep).

5. Transformation of the nonlinear terms in F-P-F space and solution of the viscous problem (20% of R-K substep). Then move to the next substep of the R-K.

The code demonstrates excellent speed-up for a large amount of processors. In order to save time and memory, the code computes only a few statistics and spectra. Many other quantities are computed in the post-process stage, using images of the fields saved each few hundreds time steps. The cost of computing almost any imaginable (and useful) quantity is of the same order of magnitude that computing just one time-step advance, providing that a parallel post-process code is available.

In order to keep a forcing constant during the run a fixed mass-flow rate is employed in the code. The bulk velocity U_b is kept constant in the code through the adaptation of the pressure gradient at every time step. All quantities in the code are normalized by the channel half width h of the channel and a bulk velocity U_b, that defines the scaling in which the code works. A new boundary conditions with uniform blowing and suction instead of the no-slip and impermeability were implement in the code.

For validation of the modified code DNS we have used the results of numerical simulation of the fully turbulent Poiseuille flow with uniform blowing and suction conducted by Sumitani & Kasagi (1995). Reynolds number $Re_\tau = 150$ and uniform transpiration rate $v_o/u_\tau = 0.03$ were adopted from Sumitani & Kasagi (1995). The results

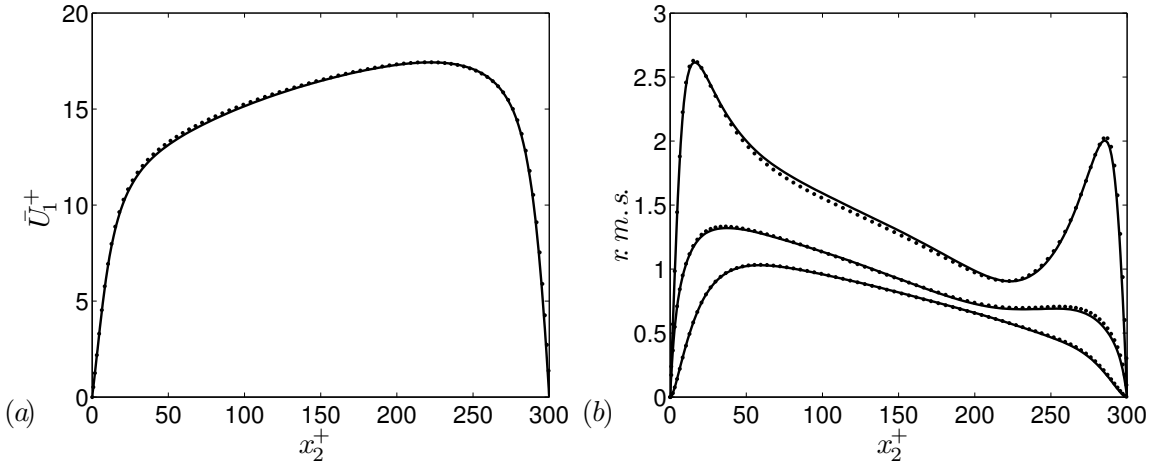

Figure 3.2: Comparison of the low order turbulence statistics of the performed DNS (dotted line) to the results of Sumitani & Kasagi (1995) (solid line). (a) Mean velocity profiles. (b) Turbulence intensities, from top to the bottom: u_1^+, u_3^+, u_2^+.

of validation are presented on the figures 3.2(a, b) and 3.3. We considered the box size $8\pi \times 2 \times 6\pi$, unlike $5\pi \times 2 \times 2\pi$ which was used in the benchmark case. The resolution in the streamwise direction was 2.4 times higher than in the benchmark case, in spanwise direction the resolution was kept the same and in wall-normal direction we took 251 grid points, unlike 145 that were employed by Sumitani & Kasagi (1995). Simulation time was $1000U_b/h$. As may be taken from the figures 3.2 and 3.3 present numerical simulation results are in good agreement with DNS of Sumitani & Kasagi (1995). Validation results shown here were included in Avsarkisov et al. (2011).

Some other validation tests like laminar flow simulation and grid convergence test were performed. It was shown that low (i.e. mean velocity $\bar{U}_1$) and high (i.e. Reynolds stress $\overline{u_1 u_2}$) order statistics of the computed flow fields are not sensitive to the computational meshes that were based on the reasonable estimates of the cell size. Results of these studies are not presented here due to their simplicity.

It was proven that the present code is stable and produces correct results, and that it may be used for numerical simulation of the fully developed turbulent channel flow with wall transpiration.

3.3 Statistical data

Production runs can be divided into three sets depending on the friction Reynolds number Re_τ. The first two simulation sets consists of four cases for different transpiration rates, while the highest Reynolds number simulation set consists of only two cases for small and medium transpiration numbers. A complete summary of the flow and the numerical parameters are given in Table 1. Using the DNS and the experimental results of Sumitani & Kasagi (1995) and Antonia et al. (1986) we concluded that for the smaller Reynolds number simulations ($Re_\tau = 250$) it will be sufficient to use a $4\pi h \times 2h \times 2\pi h$ box. A validation of this assumption may be taken from figure

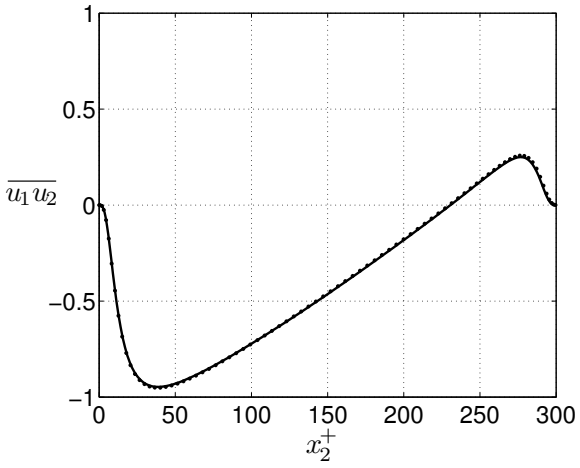

Figure 3.3: Comparison of the turbulent Reynolds stress of the performed DNS (dotted line) to the results of Sumitani & Kasagi (1995) (solid line).

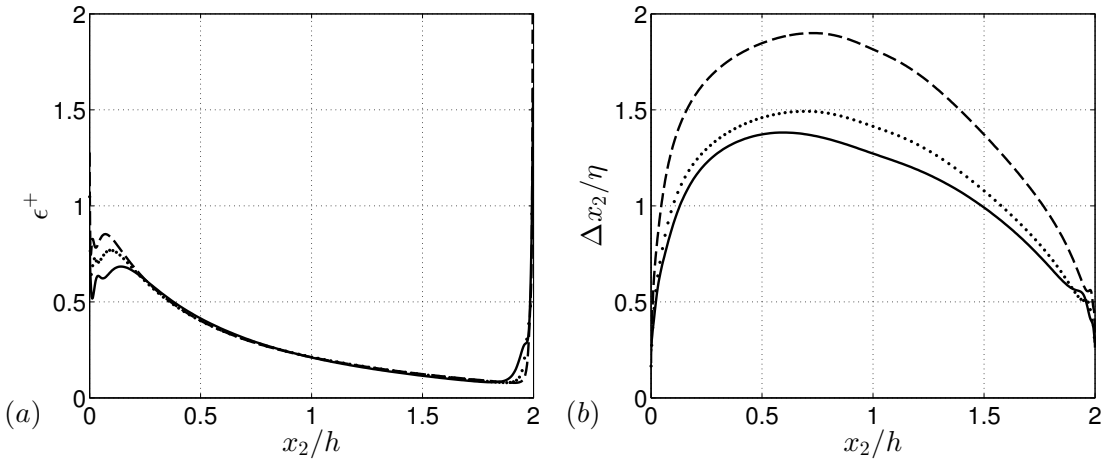

Figure 3.4: (a) Distribution of the dissipation. (b) Resolution in terms of local Kolmogorov scale $\eta = (\nu^3/\epsilon)^{1/4}$. On each plot profiles for different Reynolds numbers are shown: $Re_\tau = 250$ —; $Re = 480$: ····; $Re_\tau = 850$ - - .

6.1, where the results for the two-point cross correlation function $R_{12}/\sqrt{(\overline{u_1 u_2})^2}$ for $Re_\tau = 250, v_0^+ = 0.16$ are shown. For higher Reynolds numbers we selected a box similar to the one that was used in del Álamo & Jiménez (2003), del Álamo et al. (2004) and Hoyas & Jiménez (2006). Due to an increased dissipation at the blowing side, as it may be taken from figure 3.4(a), we had to use more grid points in wall normal direction than it is usually taken in a classical channel flow DNS to keep the resolution of $\Delta x_2 = 1.8\eta$ approximately constant in terms of the local Kolmogorov length scale η, see figure 3.4(b).

As it was mentioned in the introduction to the present chapter, the existence of the uniform transpiration implies an asymmetry not only for the mean velocity profile, but also for the distribution of the stresses. Blowing redistributes Reynolds shear stress into the core region while suction creates a very high wall-normal gradient of the streamwise velocity in the vicinity of the suction wall. With growing transpiration

Re_τ	v_0^+	v_0/U_b	L_{x_1}/h	L_{x_3}/h	Δx_1^+	Δx_3^+	N_{x_1}	N_{x_2}	N_{x_3}	N_F	$u_\tau T/h$
250	0	0	4π	2π	4.1	6.1	768	251	256	48	100
250	0.05	0.003	4π	2π	4.1	6.1	768	251	256	161	150
250	0.1	0.0069	4π	2π	4.2	6.1	768	251	256	197	70
250	0.16	0.0164	4π	2π	4.2	6.2	768	251	256	161	120
250	0.26	0.05	4π	2π	4.2	6.2	768	251	256	136	150
480	0	0	8π	6π	15.3	11.7	768	385	768	95	31
480	0.05	0.003	8π	6π	15.6	11.7	768	385	768	226	41
480	0.1	0.0075	8π	6π	15.6	11.7	768	385	768	310	40
480	0.16	0.0164	8π	6π	15.7	11.8	768	385	768	212	25
480	0.26	0.049	8π	6π	15.8	11.8	768	385	768	214	30
850	0.05	0.0026	8π	6π	6.8	5.1	3072	471	3072	160	26
850	0.16	0.016	8π	6π	7	5.2	3072	471	3072	205	22

Table 3.1: Summary of the simulations. $v_0^+ = v_0/u_\tau$ is the transpiration rate. L_{x_1}, L_{x_3}, Δx_1^+ and Δx_3^+ are respectively the periodic dimensions of the numerical box and the resolutions in streamwise and spanwise directions. $N_{x_1}, N_{x_2}, N_{x_3}$ are numbers of collocation points in streamwise, wall-normal and spanwise directions, correspondingly. N_F is the number of accumulated statistical fields. T is the computational time spanned by those fields.

rate this asymmetry is amplified exhibiting an ever increasing difference in physical properties between the canonical channel flow and the flow with transpiration, as may be taken from the figures 3.5-3.7. In the vicinity of the blowing wall the transpiration velocity produces extra Reynolds shear stress and suppresses the viscous stress, while the reverse is observed on the suction side. At high transpiration rates, i.e. $0.16 < v_0/u_\tau < 0.26$, the Reynolds shear stress vanishes on the suction side, while the viscous stress disappears on the blowing one, as it can be taken from the figures 3.5(d,e), 3.6(d,e) and 3.7(a). The flow in the near-wall region is rather particular and very different from the classical Poiseuille flow as in this region the transpiration velocity is only an order of magnitude smaller than the streamwise velocity. As a result, and in contrast to the classical flow, streamlines in the near-wall region are perpendicular to the wall. Further away from the wall they are strongly bent towards the downstream direction. A first theoretical attempt to study turbulent Poiseuille flow at high transpiration rates was made in a paper by (Vigdorovich & Oberlack 2008), who used the method of matched asymptotic expansions to show that the skin friction vanishes at the blowing wall, while the point of maximum streamwise velocity approaches the suction wall.

A second critical effect, that can be taken from the figures 3.5 - 3.7, is the non-coincidence of the points of zero turbulent shear stress ($x_2 = a$) with the point of zero viscous stress. Usually located in the center of the channel, as it is shown on the figures 3.5(b), 3.6(b) and 3.7(a), i.e. $a = h$, the point of zero shear stress is shifted towards the blowing wall while the point of maximum velocity moves towards the suction side.

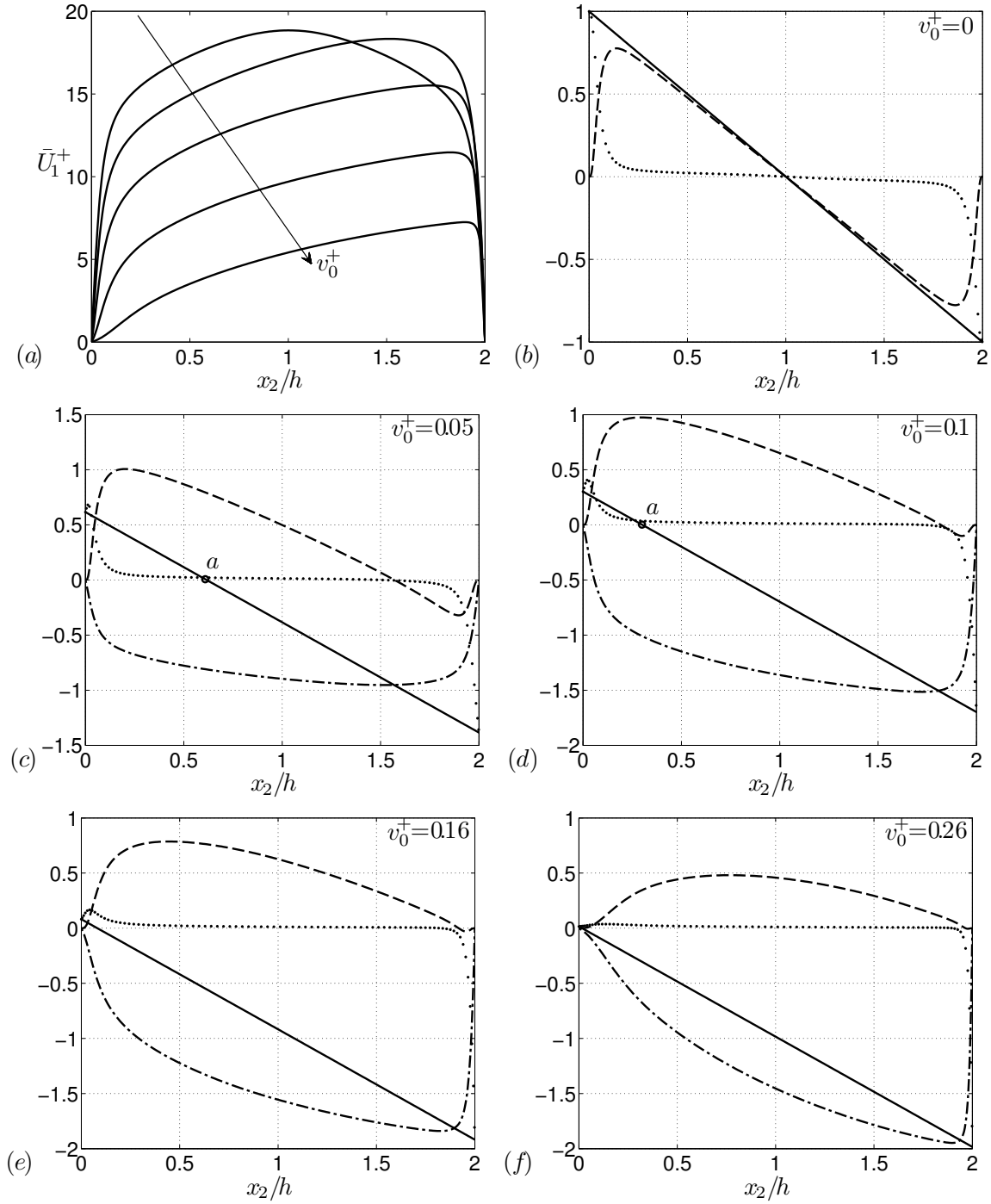

Figure 3.5: Mean velocity and shear stress distribution profiles at $Re_\tau = 250$ and $v_0^+ = 0.0, 0.05, 0.1, 0.16, 0.26$. (a) mean velocity profiles. Figures (b)-(f) depict shear stress distributions with increasing transpiration rate. $\overline{u_1 u_2}^+$: **--** ; $\frac{d\bar{U}_1^+}{dx_2^+}$: ····; $\frac{\tau}{(|\tau_{wb}| + |\tau_{ws}|)/2}$: **—** ; $v_0^+ \bar{U}_1^+$: **-·-**. Blowing wall is at $x_2 = 0$ and suction wall is at $x_2 = 2h$. The point of zero shear stress measured from the blowing wall is denoted by a.

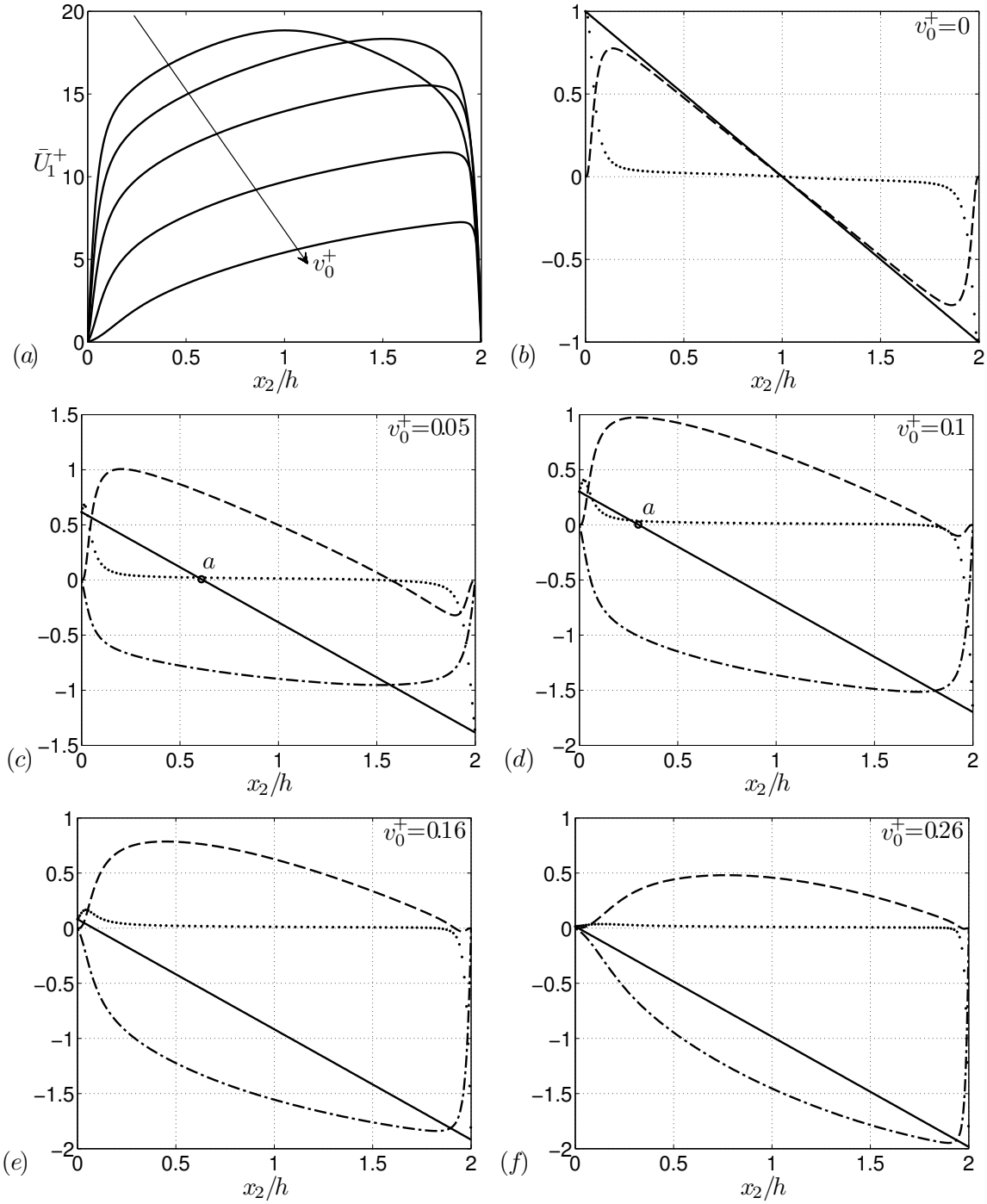

Figure 3.6: The same as on figure 3.5 but for $Re_\tau = 480$.

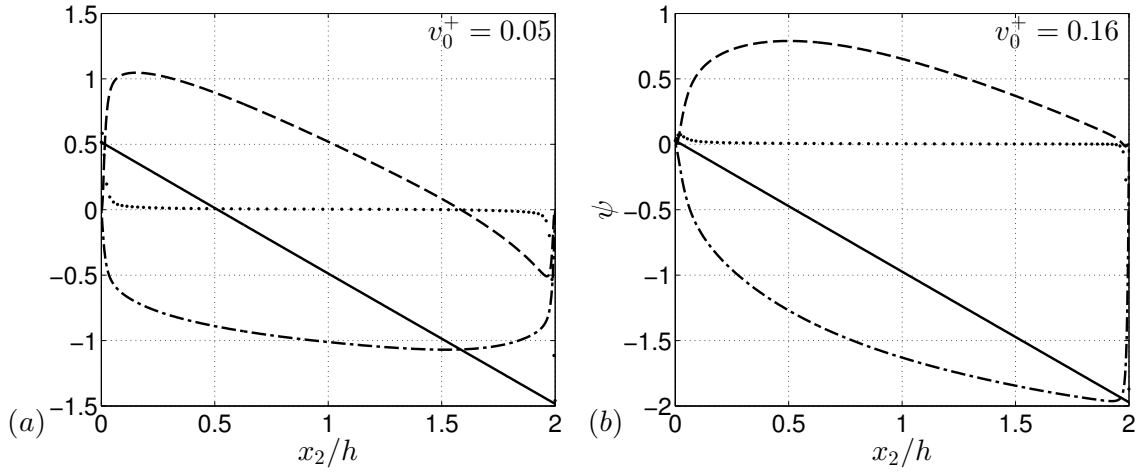

Figure 3.7: The same as on figure 3.5 but for $Re_\tau = 850$.

The convective momentum transport $v_0\bar{U}_1$ drives these two points apart and with increasing transpiration rate, the point of zero shear stress approaches the blowing wall, while the point of zero viscous stress tends towards the suction wall. The non-coincidence of the different location of the two points with $\tau(x_2) = 0$ and $\bar{U}_{1max}(x_2)$ may not only be induced by transpiration. This effect, however, may also be observed in the turbulent channel flows with asymmetric boundary conditions such as, rough wall/smooth wall conditions (see e.g. Hanjalić & Launder (1972a)), or, generally speaking, when the values of the stresses at the wall τ_w are different on the upper and the lower walls. From simple geometrical considerations one may derive the relation

$$\frac{a}{h} = \frac{\tau_{wb}}{(|\tau_{wb}| + |\tau_{ws}|)/2}, \tag{3.27}$$

which indicates that the position of the zero-shear-stress point depends on the values of the both shear stresses at the walls, i.e. τ_{wb} and τ_{ws}.

It is possible to study how blowing and suction amplify or decrease the turbulent kinetic energy by calculation of the production over the dissipation rate $\mathcal{P}/\epsilon$. In canonical channel flow production peak occurs at $x_2^+ \approx 20$ in buffer layer, and a short dissipative region $40 < x_2^+ < 100$ follows it. Low blowing, that is approximately $v_0^+ \approx 0.05$ decrease the turbulent energy production and slightly shifts the maximum peak from the wall, that can be taken from the figures 3.8(a),(c). With increase of the blowing rate the maximum peak is shifted further from the wall and production rate starts to grow. At $v_0^+ \approx 0.15$ the peak reaches the rate $\mathcal{P}/\epsilon = 1.8$ which is the maximum for the channel flow without transpiration, but it is situated in the central part of the buffer layer at $x_2^+ \approx 30 - 40$. At higher transpiration rate the peak of the maximum ratio moves to the upper boundary of the buffer layer $x_2^+ \approx 60 - 100$ and reaches the maximum rate $\mathcal{P}/\epsilon = 2$.

At the suction wall the behavior of the rate $\mathcal{P}/\epsilon$ is completely different, that can be taken from the figures 3.8(b),(d). At low transpiration rates the maximum peak exceeds the one for zero transpiration rate. With increase of transpiration rate the maximum peak dramatically decrease and at high transpiration rate $v_0^+ = 0.26$ the maximum rate is $\mathcal{P}/\epsilon = 0.25$.

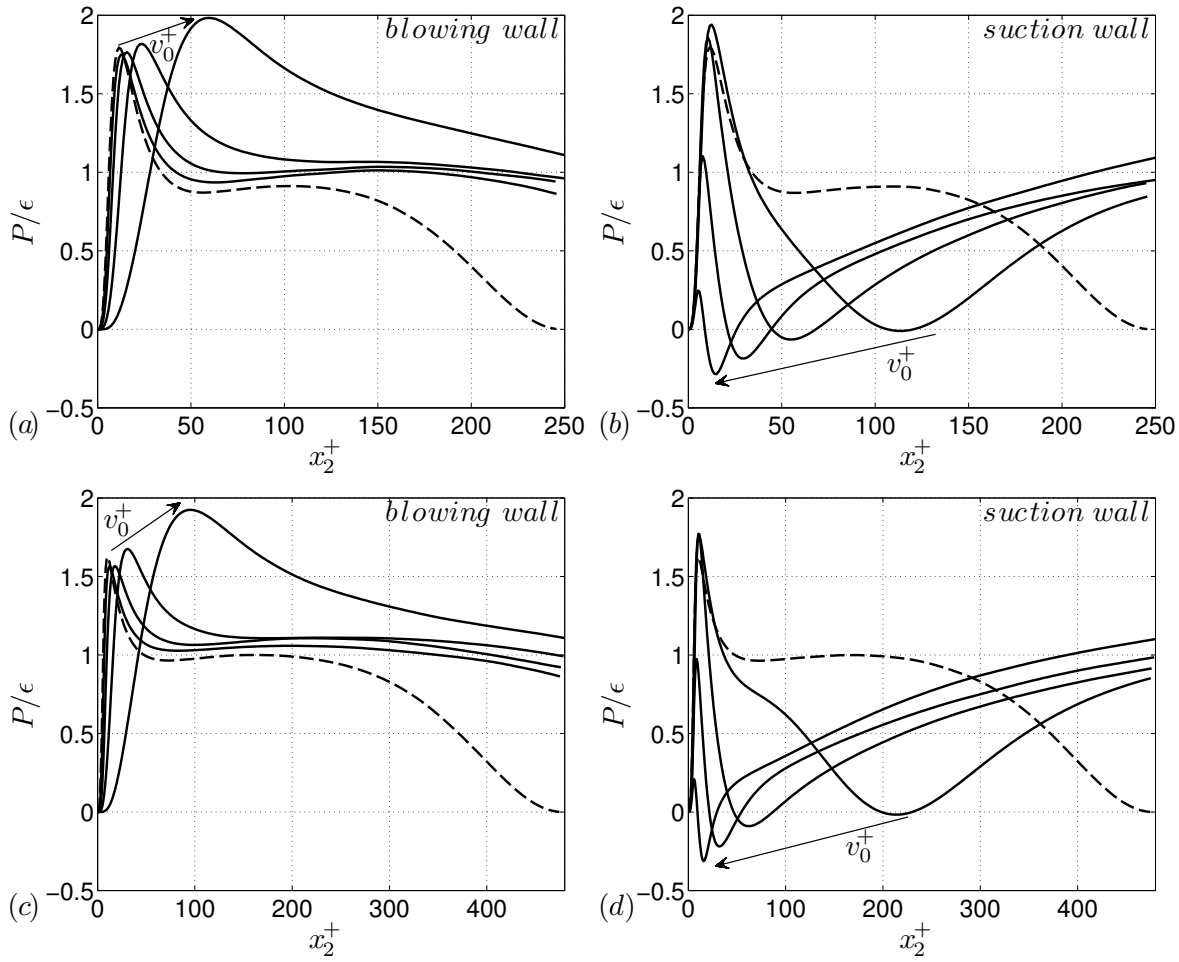

Figure 3.8: Ratio of turbulent energy production to dissipation. (a)-(b) at $Re_\tau = 250$. (c)-(d) at $Re_\tau = 480$. Flow without transpiration: **- -** . In direction of arrow: $v_0/u_\tau = 0.05, 0.1, 0.16, 0.26$.

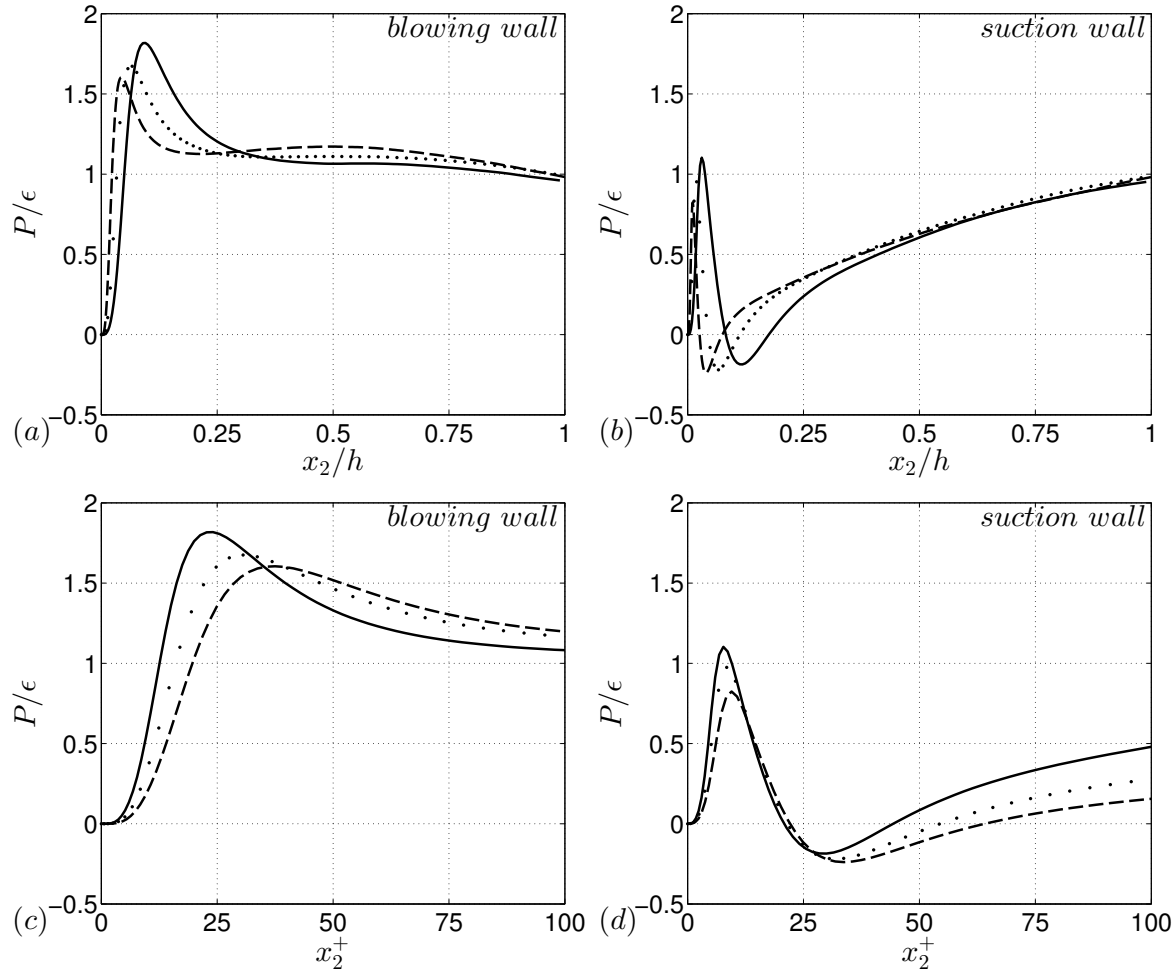

Figure 3.9: Ratio of turbulent energy production to dissipation at $v_0/u_\tau = 0.16$. (a)-(b) are plotted in outer scaling. (c)-(d)- are in the near-wall scaling. On each plot profiles for different Reynolds numbers are shown: $Re_\tau = 250$ —— ; $Re = 480$: ·····; $Re_\tau = 850$ - - .

Position of the peak is also changing, but this shift to the suction wall is negligibly small in comparison to the shift of the maximum peak at the blowing wall. Another important feature of the turbulent flow near the suction wall is a steep decrease to the negative values that follows the maximum peak of ratio of the turbulent energy production to dissipation $\mathcal{P}/\epsilon$. The region with negative $\mathcal{P}/\epsilon$ ratio appears when the point of zero Reynolds stress do not coincide with the point of maximum velocity and it was first reported by Hanjalić & Launder (1972a). To quote Hanjalić: "For a fully developed flow, the non-coincidence of the surfaces of zero shear stress and mean rate of strain means that, over a portion of the flow, the production of turbulent energy (which arises exclusively from the working of the Reynolds shear stresses against the mean velocity gradient) is negative; that is, locally there is a loss of turbulence energy to the mean motion" (Hanjalić & Launder (1972a), pp 302-303). The region with negative $\mathcal{P}/\epsilon$ ratio becomes smaller as the suction increase, while the minimum (negative) peak becomes larger. At very high transpiration rates it is larger then the maximum peak of $\mathcal{P}/\epsilon$ rate. Thus, at these transpiration rates the amount of turbulent kinetic energy produced at the suction wall is smaller than amount of turbulent kinetic energy transferred to the mean flow in the same near-wall region.

Another important conclusion that may be obtained from the figures 3.8 is that the anisotropy induced by the wall-blowing propagates far away from the wall, while the wall-suction induced anisotropy is localized in a very small region close to the wall.

All the effects described above occur only in the viscous sublayer or in the buffer layer. However in all turbulent wall-bounded flows there is a region where $\mathcal{P}/\epsilon \approx 1$, that is a local property of the turbulence. It is situated in the near-wall region and is usually associated with the logarithmic mean velocity scaling law. It is found not only in the canonical flows but also in a channel flows with specific boundary conditions like wall-roughness (Flores & Jiménez 2006) and transpiration. As it may be taken from the figures 3.8 in turbulent channel flow with wall transpiration it occurs only on the blowing wall and only at the small and moderate transpiration rates $0 < v_0^+ < 0.16$. At very high transpiration rates $v_0^+ \geq 0.26$ the equilibrium layer of $\mathcal{P}/\epsilon$ does not exist. That is an indicator that there is no logarithmic region in the flow. Later, in the chapter 5 similar conclusion will be obtained from analysis of the near-wall mean velocity scaling law. It will be also shown that at very high transpiration rates the log-law does not exist. Thus, we may conclude that when transpiration velocity is too high the blowing inflates the buffer region and eliminates the logarithmic region. An interesting conclusion may be obtained from the comparison of the $\mathcal{P}/\epsilon$ ratios at different Reynolds numbers when the transpiration velocities are equal, see figures 3.9. It appears that with increase of the Reynolds number the maximum peak decrease in size on blowing as well as on suction wall. It is also evident that the ratio in logarithmic region is larger then one and it depends on the Reynolds number. Collapse of the $\mathcal{P}/\epsilon$ profiles in the core region agrees with most of the results for the symmetric flows over smooth and rough walls, and it shows, that in the core region of the flow transpiration effects are equally unimportant at different Reynolds numbers. Thus, unlike the near-wall region, there is no correlation between Reynolds number and transpiration velocity in the core region. Later in the chapter 5 it will be shown that a new mean ve-

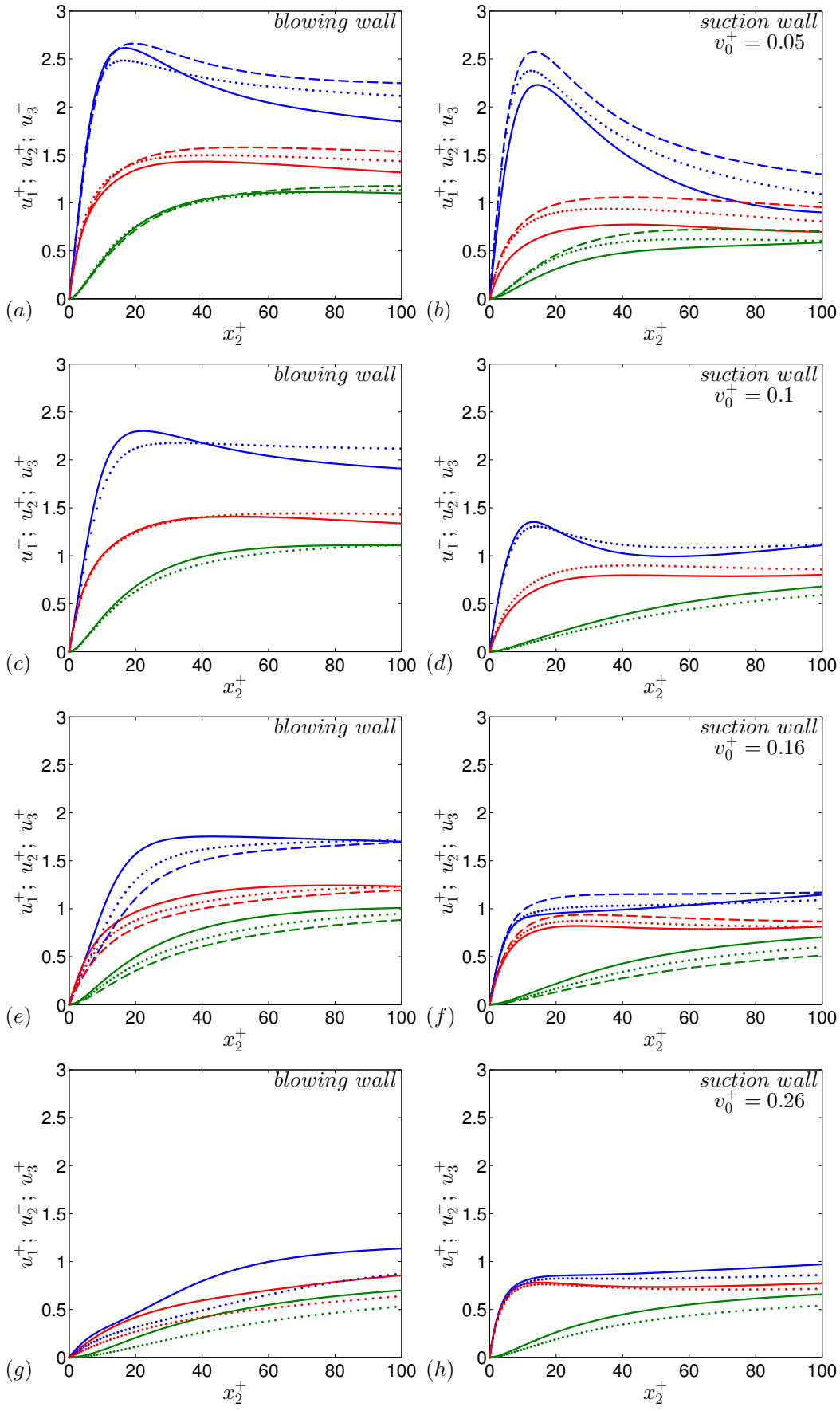

Figure 3.10: Rms velocity profiles in wall coordinates. On each plot profiles for different Reynolds numbers are shown: $Re_\tau = 250$ —; $Re = 480$: ···; $Re_\tau = 850$ - - -. From top to bottom: u_1^+(blue), u_3^+(red), u_2^+(green).

locity scaling law is found in the core region of the turbulent flow with wall blowing and suction.

It is well known that fluctuation intensities in wall-bounded turbulence display some important Reynolds number effects that take place in the vicinity of the wall as well as in the core region. Previously it was shown that the Reynolds stress distributions and the mean velocity distributions of the channel flow with blowing and suction are not symmetric about centerline of the channel presently we may imply that fluctuation intensities are also asymmetric.

In the canonical channel flow the peak value of the u_1 fluctuation component is located in buffer region at $x_2^+ \approx 15$ and it increase with increasing Reynolds number. In the present flow simulation we observe that the peak value at the blowing wall is higher for the smaller Reynolds numbers and at the suction wall it is higher for the higher Reynolds numbers but only for the small suction rates, as may be taken from the figure 3.10(b). The near-wall peak decreases as blowing/suction increase. That indicates that at the blowing wall Reynolds number and blowing effects balance each other while at the suction wall this effects amplify each other. The near-wall peak of u_1 is a characteristic feature of the near-wall streaks (Kline et al. 1967) which are involved in the near-wall regeneration cycle proposed by Jiménez & Pinelli (1999). Damping of this peak which we may take from the figures 3.10($a - h$) suggests that streaks are destroyed and the regeneration cycle is broken. Interesting enough, both blowing and suction are very effective in damping the peak of u_1.

Recently it was found that damping of the spanwise component of the velocity fluctuations is an effective method of reducing of the turbulent friction, i.e. the drag reduction (Frohnapfel, Hasegawa & Kasagi 2010). Analysis of the rms velocity fluctuations of the present simulations revealed that it may be damped by both blowing and suction. However, as may be taken from the figures 3.10($g - h$) only high blowing damps u_3, while suction collapses velocity profiles of u_1^+ and u_3^+ in the small region $x_2^+ < 5$ at the wall. This may be an indicator of the long coherent structures elongated in the streamwise direction that were found by Antonia et al. (1986) in the turbulent boundary layer with uniform suction.

Wall-normal velocity fluctuations are usually associated with the sweeps and ejections that occur in the buffer region. u_2 together with u_1 is used in a quadrant analysis (it was described in the Introduction chapter), which is a useful tool in study of the near-wall coherent structures. Present DNS study reveals that small suction suppress wall-normal velocity fluctuations in the near-wall region, while blowing of the same rate leaves its profile practically unchanged, as it may be taken from the figures 3.10(a, c, e). This might be an indication that low- and high-speed fluid moving events such as ejections and sweeps, respectively, that are typical for the near-wall region, are very sensitive to the wall suction. However, detailed analysis of these structures is required.

3.4 Conclusions

In the present chapter we have studied the effect of the wall transpiration boundary conditions on the inner and core regions of the turbulent channel flow. Four different uniform transpiration rates at three different Reynolds numbers have been explored (see table 3.1), in order to analyze these effects.

Reproduction of the DNS results of Sumitani & Kasagi (1995) proved that changes that were made inside the DNS code are correct and it is possible to run production runs at high Reynolds numbers and transpiration rates.

It was shown that blowing and suction create asymmetry of the streamwise mean velocity profile about centerline of the flow, which makes it much harder to understand and explain. Further it was found that blowing and suction considerably change streamwise velocity gradients and Reynolds stresses in the near-wall regions, this changes affect shear stresses at the walls and in the near wall regions. As a result friction velocities at the walls are very different from each other. This fact rises the question of the proper velocity scale in the near-wall region.

It is well known that in the near-wall region of the canonical channel flow the friction velocity averaged on both walls, which is, in fact, similar to the friction velocity values calculated at the walls, is a velocity scale that collapses low (mean and fluctuating velocity, fluctuating vorticity) and high (Reynolds stresses, triple correlations) order statistical data. Using present DNS results we investigated different velocity scalings such as near-wall friction velocities ($u_{\tau b}, u_{\tau s}$), friction velocity averaged on both walls (u_τ), transpiration velocity (v_0) and bulk velocity (U_b) and came up to conclusion that u_τ is a proper scaling parameter as it is a measure of the streamwise gradient of the pressure.

Apart from that, results obtained in the present chapter helped to understand interaction between near-wall and core regions in the presence of the wall transpiration. In particular, it was shown that high transpiration rate is able to broaden buffer layer and to directly link it with the core region. This is one of the high transpiration effects that was not studied before and requires much deeper analysis, due to its singularity. This result supports in part the recent finding that the logarithmic region is independent from the near-wall region, which was obtained by numerical studying of the wall turbulence created without walls (Mizuno & Jiménez 2013).

Another important result of this chapter is a finding that turbulent kinetic energy may be transfered to the mean flow, which was first obtained by Hanjalić & Launder (1972a). Presently we have found that at very high transpiration rates turbulence production may become smaller then the turbulence energy extraction by the mean flow. This could make a convincing argument for the flow relaminarization that presumably is taking place in the channel flow at very high transpiration rates.

Finally, from analysis of the turbulence velocity fluctuations we have studied some important near-wall high-Reynolds number effects that exhibit transpiration effects. In particular, it was shown that high transpiration is damping near-wall velocity streaks and breaking regeneration cycle.

Further it was found that even small suction rates are able to effectively reduce spanwise velocity fluctuations and, as a consequence of that, to reduce a drag.

4 Lie symmetry based turbulent scaling laws

4.1 History of Lie symmetry analysis

Lie group analysis is a powerful, and in fact unifying mathematical tool to solve differential equations, using Lie symmetries. It arose from the Galois' work (Galois 1830) who discovered that the algebraic solution of an equation is related to the structure of a group of permutations related to the equation. Galois was the first one who introduced term *le groupe* and classified algebraic equations in terms of group theory.

In the beginning of the 1870th Sophus Lie introduced *finite continuous groups* (Lie 1874) to mathematical society and showed how these groups should be applied to the theory of differential equations. Lie's ideas stem from the view of F. Klein, who assumed that geometry of space is determined by the group of its symmetries, Klein named this concept *Erlangen Program* (Klein 1872). Lie combined geometric ideas of Klein with works of Poisson and Jacobi on the explicit solutions of the differential equations of mechanics. Using group concept of Galois Lie explicitly showed that solutions of the differential equations are determined by the group of its symmetries, which is being called now *Lie group* (Lie (1888), Lie (1891), Lie (1896)). Lie's key idea was to analyze the group action employing its infinitesimals (locally). Thus, a Lie group is a mathematical object with an algebraic and at the same time a topological structure and a property that allows us to do differential calculus on it. It allows us to perform algebraic operations and define continuous function because of topology.

Ten years after Lie's discovery, in 1880th W. Killing independently of Lie introduced and classified all finite dimensional real Lie algebras (Killing 1889). He also discovered exceptional simple Lie algebras and found out that the only simple Lie algebras are associated with linear, symmetric and orthogonal groups. A complete classification of the simple Lie algebras was performed by E. Cartan in his thesis (Cartan 1894). Later he developed method of prolongations that helps to find solutions of PDE, this method allows to determine all singular solutions of PDE. It is also used in a *Cartan's exterior calculus*, that helps in finding of solutions and Lie symmetry transformations of a systems of PDEs. Cartan also developed a theory of an infinite groups of transformations (Cartan 1905). He extended Lie's structure theory for finite groups to an infinite ones and generalized Lie's third fundamental theorem to infinite groups. Apart from that, Cartan studied the problem of the possible forms of the equation of gravitation. He was trying to unify gravitational and electro-magnetic fields using Lie group theory (Cartan (1922), Cartan (1923-1924)). His findings later served as a basis of Einstein's unified field theory. From then on, an interaction between the physics and the group theory start to grow rapidly, covering different fields of physics. A rather comprehensive overview on the recent developments of the applications of Lie

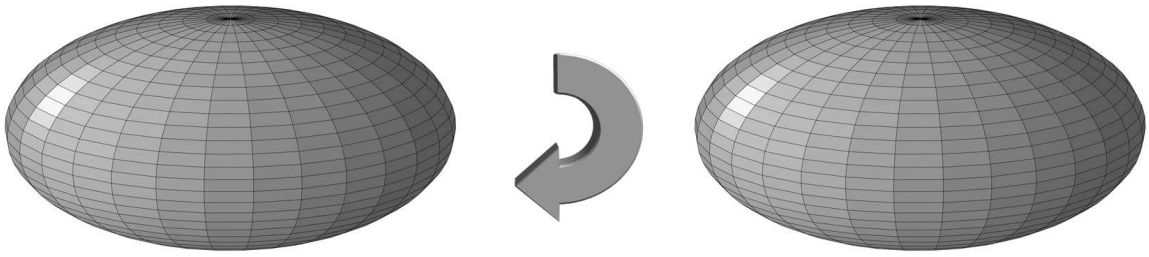

Figure 4.1: Invariant transformation.

group theory may be found in Olver (1986), Ibragimov (1995b), Ibragimov (1995a), Ibragimov (1996), Bluman & Anco (2002), Bluman, Cheviakov & Anco (2010).

At the beginning of 1990s it became possible to find the Lie symmetry groups of large number of differential equations in symbolic representation using numerical methods. Most of the programs use prolonged vector fields method (Olver 1986) like SYMMGRP.MAX (Champagne, Hereman & Winternitz 1991), DIMSYM (Sherring, Head & Prince 1997) and some others. Others, like REDUCE employ Cartan's exterior calculus (Cartan 1946) via the Harrison-Estabrook procedure. There are also programs written for commercial computer algebra systems like *Maple*® and *Mathematica*®.

Lie group symmetry analysis yields broadly applicable technique to find solutions of ordinary differential equations (ODEs) in a closed form. It allows to characterize standard solution methods for the first order or linear ODEs in terms of symmetries. It also allows to reduce the solution of nonlinear ODEs to a series of quadratures. In application to the partial differential equations (PDEs), Lie group analysis leads to the conservation laws. Using the concept of adjoint equations it becomes possible to construct the Lagrangian of the system. With help of Lie group analysis all symmetries of the system, inherited by the adjoint equations, may be found. Once the Lagrangian is constructed and the symmetries are found, Noether's theorem is applied to determine the conservation laws. In fact, each symmetry of the system of PDEs, which was found by Lie group analysis, corresponds to a conservation law.

Apart from that, Lie group analysis is used to find the group invariant solutions, the invariant center manifolds in bifurcation theory (Cicogna & Gaeta 1993) and many more.

4.2 Lie group analysis

As it was mentioned in the introduction to the present chapter, Lie groups have certain duality in their properties. These mathematical objects may be classified according to their algebraic properties (groups may be simple, semisimple, solvable, nilpotent and abelian) and topological (connectedness and compactness). Thus, according to the concept of Lie group we may establish certain analogy between symmetry of a geometric object and a differential equation. Similarly to the geometric object that

stays invariant under certain virtual motion, that may be taken from figure 4.1, a differential equation

$$D(\boldsymbol{x}, \boldsymbol{U}) = 0 \tag{4.1}$$

is form invariant under the global transformation

$$\boldsymbol{x}^* = f(\boldsymbol{x}, \boldsymbol{U}; a), \;\; \boldsymbol{U}^* = g(\boldsymbol{x}, \boldsymbol{U}; a), \tag{4.2}$$

i.e. it does not change its functional form

$$D(\boldsymbol{x}, \boldsymbol{U}) = 0 \iff D(\boldsymbol{x}^*, \boldsymbol{U}^*) = 0, \tag{4.3}$$

where $\boldsymbol{x}$ and $\boldsymbol{U}$ are the independent and dependent variables respectively and a is a constant and it is called the group parameter.

Let us now assume that the transformation (4.2) possess group properties (*associativity*, *identity*, *inverse*, *closure*), thus it is a one-parameter (a) Lie group of transformations. Taylor series expansion of the transformation (4.2) about $a = 0$ with an identity transformation corresponding to $a = 0$ will yield

$$\begin{aligned}
\boldsymbol{x}^* =& \boldsymbol{x} + a\frac{\partial f(\boldsymbol{x}, \boldsymbol{U}; a)}{\partial a}\bigg|_{a=0} + \frac{1}{2}a^2\frac{\partial^2 f(\boldsymbol{x}, \boldsymbol{U}; a)}{\partial a^2}\bigg|_{a=0} + ... \\
=& \boldsymbol{x} + a\frac{\partial f(\boldsymbol{x}, \boldsymbol{U}; a)}{\partial a}\bigg|_{a=0} + \mathcal{O}(a^2); \qquad (4.4) \\
\boldsymbol{U}^* =& \boldsymbol{U} + a\frac{\partial g(\boldsymbol{x}, \boldsymbol{U}; a)}{\partial a}\bigg|_{a=0} + \frac{1}{2}a^2\frac{\partial^2 g(\boldsymbol{x}, \boldsymbol{U}; a)}{\partial a^2}\bigg|_{a=0} + ... \\
=& \mathbf{U} + a\frac{\partial g(\boldsymbol{x}, \boldsymbol{U}; a)}{\partial a}\bigg|_{a=0} + \mathcal{O}(a^2). \qquad (4.5)
\end{aligned}$$

Using the following notations

$$\Psi(\boldsymbol{x}, \boldsymbol{U}) = \frac{\partial f(\boldsymbol{x}, \boldsymbol{U}; a)}{\partial a}\bigg|_{a=0}, \tag{4.6}$$

$$\Phi(\boldsymbol{x}, \boldsymbol{U}) = \frac{\partial g(\boldsymbol{x}, \boldsymbol{U}; a)}{\partial a}\bigg|_{a=0}, \tag{4.7}$$

we will finally obtain the transformation (4.2) in an infinitesimal form which also contains all essential information

$$\boldsymbol{x}^* = \boldsymbol{x} + a\Psi(\boldsymbol{x}, \boldsymbol{U}) + \mathcal{O}(a^2), \tag{4.8}$$

$$\boldsymbol{U}^* = \boldsymbol{U} + a\Phi(\boldsymbol{x}, \boldsymbol{U}) + \mathcal{O}(a^2). \tag{4.9}$$

According to Lie's first theorem (Bluman et al. 2010), the global form of the transformation (4.2) may be obtained from the corresponding infinitesimals (4.8) and (4.9) by integration of the following first order system

$$\frac{d\boldsymbol{x}^*(a)}{da} = \Psi(\boldsymbol{x}^*(a), \boldsymbol{U}^*(a)), \tag{4.10}$$

$$\frac{d\boldsymbol{U}^*(a)}{da} = \Phi(\boldsymbol{x}^*(a), \boldsymbol{U}^*(a)), \tag{4.11}$$

using the initial conditions

$$a = 0 : \boldsymbol{x}^*(a) = \boldsymbol{x} \text{ and } \boldsymbol{U}^*(a) = \boldsymbol{U}. \tag{4.12}$$

This theorem shows, that the concept of infinitesimal transformation, introduced by Sophus Lie, plays an important role in applications to the differential equations. In particular, it allows to replace complicated nonlinear symmetry conditions with the linear ones.

It is possible to construct an invariant solution of a given PDE system from invariants of a local symmetry of the PDE, which in its turn satisfy the invariant surface condition, a constraint that arises from an auxiliary PDE system. Let us call $\boldsymbol{y} = \boldsymbol{\Theta}(\boldsymbol{x})$ a group invariant solution if

- $\boldsymbol{y} - \boldsymbol{\Theta}(\boldsymbol{x})$ is invariant function under the multi-parameter Lie symmetry group X, where
$$X = \xi_i \frac{\partial}{\partial x_i} + \eta_j \frac{\partial}{\partial y_j} \tag{4.13}$$
- $\boldsymbol{y} = \boldsymbol{\Theta}(\boldsymbol{x})$ is a solution of the differential equation.

Taking these two conditions into account we obtain that

$$X[\boldsymbol{y} - \boldsymbol{\Theta}(\boldsymbol{x})] = 0, \quad \text{where} \quad \boldsymbol{y} = \boldsymbol{\Theta}(\boldsymbol{x}). \tag{4.14}$$

Taking into account (4.13) equation (4.14) will transform into the following hyperbolic system

$$\xi_k(\boldsymbol{x}, \boldsymbol{\Theta}) \frac{\partial \theta_l}{\partial x_k} = \eta_l(\boldsymbol{x}, \boldsymbol{\Theta}). \tag{4.15}$$

The system (4.16) can be solved by the method of characteristics and in its final form it represents the characteristic condition

$$\begin{aligned} \frac{dx_1}{\xi_1(\boldsymbol{x}, \boldsymbol{\Theta})} = \frac{dx_2}{\xi_2(\boldsymbol{x}, \boldsymbol{\Theta})} = \cdots = \frac{dx_m}{\xi_m(\boldsymbol{x}, \boldsymbol{\Theta})} \\ = \frac{dy_1}{\eta_1(\boldsymbol{x}, \boldsymbol{\Theta})} = \frac{dy_2}{\eta_2(\boldsymbol{x}, \boldsymbol{\Theta})} = \cdots = \frac{dy_n}{\eta_n(\boldsymbol{x}, \boldsymbol{\Theta})}. \end{aligned} \tag{4.16}$$

and it is usually referred as an invariant surface condition. Solving the system 4.16 we obtain $m - 1$ new independent variables, so there is one dependent variable eliminated. Thus we obtain, that the set of independent variables in the PDE may be reduced by one.

The method of derivation of the invariant solution can be used in the turbulence theory for generation of a scaling laws. In particularly, it was successfully used in Oberlack (2001), Oberlack & Rosteck (2010) to find a classical near-wall mean velocity scaling law. In the present thesis this method was used to find a new mean velocity scaling law for the channel center (Avsarkisov et al. 2014).

4.3 Symmetry analysis in fluid mechanics

The first attempts to use symmetry groups in a fluid mechanics belongs to German mathematician Felix Klein, who, as we already know, was helping S. Lie in the development of his ideas. Klein incorporated fluid dynamics ideas in a book Klein (1882) in which function theory was treated in a geometric way by connecting potential theory and conformal mappings.

The most important result that made possible the usage of Lie groups analysis in fluid dynamics is also related to F. Klein. He, together with D. Hilbert, invited Mrs. E. Noether at the University of Göttingen, where she proved a theorem that presently is known as a *Noether's first theorem*. Soon this theorem became a fundamental tool of the modern theoretical physics and, in particular, of the theory of fluid mechanics. It states that any continuous symmetry of the action of a physical system is a conserved quantity and it corresponds to a certain conservation law. Despite a significance of this discovery for the fluid mechanics the major results were obtained only 50 years later, when the group theory was introduced in the field.

A constitutive role in the development of the symmetry-based analysis in fluid mechanics is due to discovery of J. Fourier that every physical quantity may be written with exponents and after the transformation the quantity will be given in terms of certain *fundamental units* (Fourier 1822). Thus, physical quantity appears to be invariant under the transformation. This finding gave rise to the so called *Inspectional Analysis* (Ruark 1935) which formulated a concept of *dynamic similitude* of fluids. According to this concept (Birkhoff 1950): two fluid motions Φ and Φ' are called dynamically similar if they can be described by coordinate systems which are related by transformations of space-time-mass, of the form

$$\begin{aligned} x_i' =& \alpha x_i, \\ t' =& \beta t, \\ m' =& \gamma m. \end{aligned} \tag{4.17}$$

In 1926 Mrs. T. Ehrenfest-Afanassjewa proposed that Inspectional Analysis is valid not only for the form transformations (4.17), but also to any group of transformations (Ehrenfest-Afanassjewa 1926). With this statement she demonstrated that the concept of group transformations is valuable tool in fluid mechanics. Shortly afterward, it was realized that it is possible to integrate the differential equations of fluid mechanics using group transformations, using property that if a system of PDE is invariant under a certain group of transformations, then solution of the system will also be invariant under this group of transformations. Finally, the method of search for symmetric solutions of PDE was described and successfully used by Bechert (1941a), Bechert (1941b) and Sedov (1945).

The calculation and classification of all one parameter Lie symmetry groups of the Euler equations was performed by Buchnev (1971). The author showed that the Euler equations, i.e. equation (1.1) with $\nu = 0$ admit a ten-parameter symmetry group, and derived the infinitesimal generators (Oberlack 2000)

$$
\begin{aligned}
\mathrm{X}_1 &= \frac{\partial}{\partial t} \ , && \Big\} \text{ time translation} \\
\mathrm{X}_2 &= x_i\frac{\partial}{\partial x_i} + U_j\frac{\partial}{\partial U_j} + 2P\frac{\partial}{\partial P} \ , && \Big\} \text{ space and time scalings} \\
\mathrm{X}_3 &= t\frac{\partial}{\partial t} - U_i\frac{\partial}{\partial U_i} - 2P\frac{\partial}{\partial P} \ , && \\
\mathrm{X}_4 &= f_1(t)\frac{\partial}{\partial x_1} + \frac{\mathrm{d}f_1(t)}{\mathrm{d}t}\frac{\partial}{\partial U_1} - x_1\frac{\mathrm{d}^2 f_1(t)}{\mathrm{d}t^2}\frac{\partial}{\partial P} \ , && \Big\} \text{ moving coordinates} \\
\mathrm{X}_5 &= f_2(t)\frac{\partial}{\partial x_2} + \frac{\mathrm{d}f_2(t)}{\mathrm{d}t}\frac{\partial}{\partial U_2} - x_2\frac{\mathrm{d}^2 f_2(t)}{\mathrm{d}t^2}\frac{\partial}{\partial P} \ , && \\
\mathrm{X}_6 &= f_3(t)\frac{\partial}{\partial x_3} + \frac{\mathrm{d}f_3(t)}{\mathrm{d}t}\frac{\partial}{\partial U_3} - x_3\frac{\mathrm{d}^2 f_3(t)}{\mathrm{d}t^2}\frac{\partial}{\partial P} \ , && \\
\mathrm{X}_7 &= x_2\frac{\partial}{\partial x_1} - x_1\frac{\partial}{\partial x_2} + U_2\frac{\partial}{\partial U_1} - U_1\frac{\partial}{\partial U_2} \ , && \Big\} \text{ rotations} \\
\mathrm{X}_8 &= x_1\frac{\partial}{\partial x_3} - x_3\frac{\partial}{\partial x_1} + U_1\frac{\partial}{\partial U_3} - U_3\frac{\partial}{\partial U_1} \ , && \\
\mathrm{X}_9 &= x_3\frac{\partial}{\partial x_2} - x_2\frac{\partial}{\partial x_3} + U_3\frac{\partial}{\partial U_2} - U_2\frac{\partial}{\partial U_3} \ , && \\
\mathrm{X}_{10} &= f_4(t)\frac{\partial}{\partial P} \ , && \Big\} \text{ pressure changes}
\end{aligned}
\tag{4.18}
$$

with $f_1(t)$-$f_3(t)$ being at least differentiable twice and $f_4(t)$ may have arbitrary time dependence. In global form these symmetry groups are (Oberlack 2000)

$$
\begin{aligned}
T_1 &: \ t^* = t + k_1 \ , \ \boldsymbol{x}^* = \boldsymbol{x} \ , \ \boldsymbol{U}^* = \boldsymbol{U} \ , \ P^* = P \ , \\
T_2 &: \ t^* = t \ , \ \boldsymbol{x}^* = \mathrm{e}^{k_2}\boldsymbol{x} \ , \ \boldsymbol{U}^* = \mathrm{e}^{k_2}\boldsymbol{U} \ , \ P^* = \mathrm{e}^{2k_2}P \ , \\
T_3 &: \ t^* = \mathrm{e}^{k_3}t \ , \ \boldsymbol{x}^* = \boldsymbol{x} \ , \ \boldsymbol{U}^* = \mathrm{e}^{-k_3}\boldsymbol{U} \ , \ P^* = \mathrm{e}^{-2k_3}P \ , \\
T_4 - T_6 &: \ t^* = t \ , \ \boldsymbol{x}^* = \boldsymbol{x} + \boldsymbol{f} \ , \ \boldsymbol{U}^* = \boldsymbol{U} + \frac{\mathrm{d}\boldsymbol{f}}{\mathrm{d}t} \ , \ P^* = P - \boldsymbol{x}\cdot\frac{\mathrm{d}^2\mathbf{f}}{\mathrm{d}t^2} \ , \\
T_7 - T_9 &: \ t^* = t \ , \ \boldsymbol{x}^* = \boldsymbol{k}\cdot\boldsymbol{x} \ , \ \boldsymbol{U}^* = \boldsymbol{k}\cdot\boldsymbol{U} \ , \ P^* = P \ , \\
T_{10} &: \ t^* = t \ , \ \boldsymbol{x}^* = \boldsymbol{x} \ , \ \boldsymbol{U}^* = \boldsymbol{U} \ , \ P^* = P + f_4(t),
\end{aligned}
\tag{4.19}
$$

here $k_1 - k_4$ are constant group parameters, $\boldsymbol{k}$ is a constant rotation matrix with the following properties: $\boldsymbol{k}\cdot\boldsymbol{k}^\intercal = \boldsymbol{k}^\intercal\cdot\boldsymbol{k} = \boldsymbol{I}$ and $|\boldsymbol{k}| = 1$. Function of time is $\boldsymbol{f}(t) = (k_4 f_1(t), k_5 f_2(t), k_6 f_3(t))^\intercal$ and $f_4(t)$ is an arbitrary function of time. Similarly to the equations (4.18) the first symmetry T_1 in (4.19) represents translation in time. T_2 and T_3 correspond to the scaling of space and time. $T_4 - T_6$ describe the invariance of the equations with respect to the translation in space for constant $f_1 - f_3$. If $f_1 - f_3$ are linear functions of time, $T_4 - T_6$ represent the classical Galilei invariance. The symmetries $T_7 - T_9$ describe finite rotation invariance of the equations. Finally, T_{10} shows that the equations are invariant under an addition of the arbitrary time dependent function $f_4(t)$ to the pressure.

For the Navier-Stokes equations in 2D the full transformation group was examined by Puhnachev (1960), while the complete set of infinitesimal generators for three-dimensional case was obtained later by Bytev (1972).

Some exact solutions of the Navier-Stokes equations for the steady state were derived by Boisvert, Ames & Srivastava (1983). Later in the paper Grauel & Steeb (1985) similarity solutions for Euler and Navier-Stokes equations were found. They showed that such solutions lead to reduction of the original system of PDE to ODE or to PDE with lower number of independent variables.

For the Reynolds averaged Navier-Stokes equations (2.17) the symmetry groups (4.19) have the following form (Oberlack & Rosteck 2010)

$$\begin{aligned}
&\bar{T}_1:\ t^*=t+k_1,\ \ \boldsymbol{x}^*=\boldsymbol{x},\ \ \bar{\boldsymbol{U}}^*=\bar{\boldsymbol{U}},\ \ \bar{P}^*=\bar{P},\ \ \overline{u_iu_k}^*=\overline{u_iu_k}.\\
&\bar{T}_2:\ t^*=t,\ \ \boldsymbol{x}^*=\mathrm{e}^{k_2}\boldsymbol{x},\ \ \bar{\boldsymbol{U}}^*=\mathrm{e}^{k_2}\bar{\boldsymbol{U}},\ \ \bar{P}^*=\mathrm{e}^{2k_2}\bar{P},\ \ \overline{u_iu_k}^*=\mathrm{e}^{2k_2}\overline{u_iu_k}.\\
&\bar{T}_3:\ t^*=\mathrm{e}^{k_3}t,\ \ \boldsymbol{x}^*=\boldsymbol{x},\ \ \bar{\boldsymbol{U}}^*=\mathrm{e}^{-k_3}\bar{\boldsymbol{U}},\ \ \bar{P}^*=\mathrm{e}^{-2k_3}\bar{P},\ \ \overline{u_iu_k}^*=\mathrm{e}^{-2k_3}\overline{u_iu_k}.\\
&\bar{T}_4{-}\bar{T}_6:\ t^*=t\ ,\ \ \boldsymbol{x}^*=\boldsymbol{x}+\mathbf{f}(t),\ \ \bar{\boldsymbol{U}}^*=\bar{\boldsymbol{U}}+\frac{\mathrm{d}\boldsymbol{f}}{\mathrm{d}t},\ \ \bar{P}^*=\bar{P}-\boldsymbol{x}\cdot\frac{\mathrm{d}^2\boldsymbol{f}}{\mathrm{d}t^2},\ \ \overline{u_iu_k}^*=\overline{u_iu_k}.\\
&\bar{T}_7{-}\bar{T}_9:\ t^*=t,\ \ \boldsymbol{x}^*=\boldsymbol{k}\cdot\boldsymbol{x},\ \ \bar{\boldsymbol{U}}^*=\boldsymbol{k}\cdot\bar{\boldsymbol{U}},\ \ \bar{P}^*=\bar{P}\ ,\ \ \overline{u_iu_k}^*=A_{ik}\otimes\overline{u_iu_k}.\\
&\bar{T}_{10}:\ t^*=t\ ,\ \ \boldsymbol{x}^*=\boldsymbol{x},\ \ \bar{\boldsymbol{U}}^*=\bar{\boldsymbol{U}},\ \ \bar{P}^*=\bar{P}+f_4(t),\ \ \overline{u_iu_k}^*=\overline{u_iu_k}.
\end{aligned}\tag{4.20}$$

The space and time correlation functions in the theory of turbulence was first introduced by (Keller & Friedmann 1924). Various authors derived the complete system of two-point correlation equations (see e.g. Hinze (1959), McComb (1990)), while (Keller & Friedmann 1924) were also the first who closed it by writing the third moment via the second moment and the mean. Later it was found, that higher order correlations may indeed not be neglected and the infinite number of the multi-point correlation (MPC) equations rather than two-point correlation should be taken into account.

The idea of using multi-point correlations belongs to Kolmogorov who introduced a structure function of an arbitrary order in his inertial-range theory (Kolmogorov (1941a), Kolmogorov (1941b)) for a locally homogeneous random fields. The infinite set of the dimensional MPC equations, derived from Navier-Stokes equations, was introduced by Oberlack (2000) in the study of the symmetry induced scaling laws and, in particular, near-wall log-law, in the turbulent shear flows. Later Oberlack & Rosteck (2010) derived a two different sets of MPC equations. In particular, it was shown that the MPC equations may be written for the instantaneous values $(\mathbf{U}, P)$ or for the fluctuating quantities $(\mathbf{u}, p)$. In addition to the above described symmetries (see eq. (4.18), (4.19)), MPC equations (2.56) and (2.51) admit new statistical symmetries that cannot be found in Euler and Navier-Stokes equations (Oberlack 2001). The new statistical symmetries in instantaneous representation have the following form (Oberlack & Rosteck 2010)

$$\bar{T}'_s:\ t^*=t,\ \ \boldsymbol{x}^*=\boldsymbol{x},\ \ \boldsymbol{r}^*_{(l)}=\boldsymbol{r}_{(l)},\ \ \boldsymbol{H}^*_{\{n\}}=\mathrm{e}^{k_s}\boldsymbol{H}_{\{n\}},\ \ \boldsymbol{I}^*_{\{n\}}=\mathrm{e}^{k_s}\boldsymbol{I}_{\{n\}},\ \ \cdots. \tag{4.21}$$

$$\bar{T}_{x_2}:\ t^*=t,\ \ \boldsymbol{x}^*=\boldsymbol{x}+k_{x_2},\ \ \boldsymbol{r}^*_{(l)}=\boldsymbol{r}_{(l)},\ \ \boldsymbol{H}^*_{\{n\}}=\boldsymbol{H}_{\{n\}},\ \ \boldsymbol{I}^*_{\{n\}}=\boldsymbol{I}_{\{n\}},\ \ \cdots. \tag{4.22}$$

$$\begin{aligned}
&\bar{T}_{\bar{U}_i}:\ t^*=t,\ \ \boldsymbol{x}^*=\boldsymbol{x},\ \ \boldsymbol{r}^*_{(l)}=\boldsymbol{r}_{(l)},\ \ \bar{U}^*_{i_{(0)}}=\bar{U}_{i_{(0)}}+k_{\bar{U}_{i_{(0)}}},\ \ \boldsymbol{H}^*_{\{n\}}=\boldsymbol{H}_{\{n\}}+\mathbf{C}_{\{n\}},\\
&\quad \boldsymbol{I}^*_{\{n\}}=\boldsymbol{I}_{\{n\}}+\boldsymbol{D}_{\{n\}},\ \ \cdots
\end{aligned} \tag{4.23}$$

and in fluctuating representation, correspondingly

$$\bar{T}'_s:\ t^*=t,\ \ \boldsymbol{x}^*=\boldsymbol{x},\ \ \boldsymbol{r}^*_{(l)}=\boldsymbol{r}_{(l)},\ \ \bar{U}^*_{i_{(0)}}=\mathrm{e}^{k_s}\bar{U}_{i_{(0)}},$$
$$R^*_{i_{(0)}i_{(1)}}=\mathrm{e}^{k_s}\left[R_{i_{(0)}i_{(1)}}+\left(1-\mathrm{e}^{k_s}\right)\bar{U}_{i_{(0)}}\bar{U}_{i_{(1)}}\right],\ \ \cdots. \tag{4.24}$$

$$\bar{T}_{x_2}:\ t^*=t,\ \ \boldsymbol{x}^*=\boldsymbol{x}+k_{x_2},\ \ \boldsymbol{r}^*_{(l)}=\boldsymbol{r}_{(l)},\ \ \bar{U}^*_{i_{(0)}}=\bar{U}_{i_{(0)}},\ \ R^*_{ij}=R_{ij},\cdots. \tag{4.25}$$

$$\bar{T}_{\bar{U}_i}:\ t^*=t,\ \ \boldsymbol{x}^*=\boldsymbol{x},\ \ \boldsymbol{r}^*_{(l)}=\boldsymbol{r}_{(l)},\ \ \bar{U}^*_{i_{(0)}}=\bar{U}_{i_{(0)}}+k_{\bar{U}_{i_{(0)}}},$$
$$R^*_{i_{(0)}i_{(1)}}=R_{i_{(0)}i_{(1)}}+\bar{U}_{i_{(0)}}\bar{U}_{i_{(1)}}-\left(\bar{U}_{i_{(0)}}+C_{i_{(0)}}\right)\left(\bar{U}_{i_{(1)}}+C_{i_{(1)}}\right),\ \ \cdots. \tag{4.26}$$

It turned out that the main ingredients for the log-law are Lie symmetry groups of the MPC equations (Oberlack 2001). Recently it was discovered that the log-law not only relies on symmetries which have their origin in classical fluid mechanics (see eq. (4.18-4.19)), in particular, Navier-Stokes equations, but one of the crucial symmetries for the log-law is of purely statistical nature (see eq. (4.21), (4.24)) and cannot be found in Navier-Stokes equations (Oberlack & Rosteck 2010). Application of the admitted set of the symmetries together with boundary conditions and observation that friction velocity u_τ is a symmetry breaking in the near-wall region led to the following classical functional non-dimensional form of the mean velocity

$$\bar{U}_1^+=\frac{1}{\kappa}\log(x_2^+ + A^+)+C^+. \tag{4.27}$$

Recently Moser, Bhattacharya & Malaya (2011) developed MPC model in LES of wall-bounded turbulence. In order to reconstruct velocity correlations they posited a model for small-separation MPCs. After successful modeling of the isotropic homogeneous turbulence they modeled anisotropy in a turbulent near-wall region.

4.4 Lie symmetry based turbulent scaling laws

One of the key objectives of the present analysis is to further develop and validate the Lie group theory for the multi-point statistics of turbulence employing the turbulent Poiseuille flow with wall transpiration. The first step to accomplish this objective is to find symmetry transformations which do not change the form of the TPC equation (2.64). The application of these symmetry groups will later facilitate us to find a group invariant solution of the TPC equation in fluid mechanics often of self-similar type. Finally, this leads to the reduction of the TPC equation and, at the same time, determines the functional form of the turbulent scaling law for the mean velocity. The final step of the analysis will be the validation of the new turbulent scaling law employing the present DNS data.

The starting point of this analysis was the observation, that the boundary condition (2.18), in particular for the transpiration velocity, may be symmetry breaking primarily in the core region of the flow. In the present section only an abbreviated approach will be presented, while more mathematical details are available in Oberlack & Rosteck (2010) and in the Appendix B of Oberlack (2001).

In order to derive a new turbulent scaling law for the present flow from the TPC equation, we need to consider the appropriate symmetry transformations. For the present problem it is sufficient to focus on the three scaling groups $(\bar{T}_1, \bar{T}_2, \bar{T}'_s)$, the translation group in space $(\bar{T}_{x_2})$ and the translation group of the averaged velocity $(\bar{T}_{\bar{U}_i})$ all to be defined below. In global form these transformation groups are defined as:

$$\begin{aligned}
\bar{T}_1 :\ & t^* = t,\ \ \boldsymbol{x}^* = e^{k_1}\boldsymbol{x},\ \ \boldsymbol{r}^*_{(l)} = e^{k_1}\boldsymbol{r}_{(l)},\ \ \bar{\boldsymbol{U}}^* = e^{k_1}\bar{\boldsymbol{U}},\ \ \bar{P}^* = e^{2k_1}\bar{P}, \\
& R^*_{ij} = e^{2k_1}R_{ij},\ \ \overline{pu_j}^* = e^{3k_1}\overline{pu_j},\ \ \overline{u_ip}^* = e^{3k_1}\overline{u_ip},\ \ \ldots\ , \qquad (4.28) \\
\bar{T}_2 :\ & t^* = e^{k_2}t,\ \ \boldsymbol{x}^* = \boldsymbol{x},\ \ \boldsymbol{r}^*_{(l)} = \boldsymbol{r}_{(l)},\ \ \bar{\boldsymbol{U}}^* = e^{-k_2}\bar{\boldsymbol{U}},\ \ \bar{P}^* = e^{-2k_2}\bar{P}, \\
& R^*_{ij} = e^{-2k_2}R_{ij},\ \ \overline{pu_j}^* = e^{-3k_2}\overline{pu_j},\ \ \overline{u_ip}^* = e^{-3k_2}\overline{u_ip},\ \ \ldots\ , \qquad (4.29) \\
\bar{T}'_s :\ & t^* = t,\ \ \boldsymbol{x}^* = \boldsymbol{x},\ \ \boldsymbol{r}^*_{(l)} = \boldsymbol{r}_{(l)},\ \ \bar{U}^*_i = \mathrm{e}^{k_s}\bar{U}_i,\ \ \bar{P}^* = e^{k_s}\bar{P}, \\
& R^*_{ij} = \mathrm{e}^{k_s}\left[R_{ij} + \left(1 - \mathrm{e}^{k_s}\right)\bar{U}_i\bar{U}_j\right],\ \ \overline{pu_j}^* = e^{k_s}\overline{pu_j} + (e^{k_s} - e^{2k_s})\bar{P}\bar{U}_j, \\
& \overline{u_ip}^* = e^{k_s}\overline{u_ip} + (e^{k_s} - e^{2k_s})\bar{P}\bar{U}_i,\ \ \ldots\ , \qquad (4.30) \\
\bar{T}_{x_2} :\ & t^* = t,\ \ \boldsymbol{x}^* = \boldsymbol{x} + k_{x_2},\ \ \boldsymbol{r}^*_{(l)} = \boldsymbol{r}_{(l)},\ \ \bar{\boldsymbol{U}}^* = \bar{\boldsymbol{U}}, \\
& \bar{P}^* = \bar{P},\ \ R^*_{ij} = R_{ij},\ \ \overline{pu_j}^* = \overline{pu_j},\ \ \overline{u_ip}^* = \overline{u_ip},\ \ \ldots\ , \qquad (4.31) \\
\bar{T}_{\bar{U}_i} :\ & t^* = t,\ \ \boldsymbol{x}^* = \boldsymbol{x},\ \ \boldsymbol{r}^*_{(l)} = \boldsymbol{r}_{(l)},\ \ \bar{U}^*_i = \bar{U}_i + k_{\bar{U}_i}, \\
& \bar{P}^* = \bar{P},\ \ R^*_{ij} = R_{ij},\ \ \overline{pu_j}^* = \overline{pu_j},\ \ \overline{u_ip}^* = \overline{u_ip},\ \ \ldots\ . \qquad (4.32)
\end{aligned}$$

Above and also further down, the dots denote the fact that in principle higher order correlations are part of the symmetry transformation since the full MPC equation is infinite dimensional. This, however, will not be considered presently and we only focus on the mean velocity and the TPC.

The first two scaling symmetries are well-known from the Euler and the Navier-Stokes equations describing scaling of space and time (see equations (4.20)). The third one is a rather new group and independent of (4.28) and (4.29). It represents the scaling of all TPC or MPC tensors (see equation (4.21) and (4.24)), and it is a purely statistical property of these equations (Oberlack & Rosteck 2010). In fact it is a property of all linear equations. One of the most crucial symmetries for the results to follow and also a key ingredient of the classical log-law (Oberlack 2001) is symmetry (4.32) (see also (4.23) and (4.26)). It is also of purely statistical nature and was discovered in the context of an infinite set of statistical symmetries in Oberlack & Rosteck (2010). It may be noted that the credit for the first hint toward (4.32) deserves Kraichnan (1965).

In local (infinitesimal) form the symmetries (4.28 - 4.32) are given by

$$\bar{\mathrm{X}}_1 = x_2\frac{\partial}{\partial x_2} + \bar{U}_i\frac{\partial}{\partial \bar{U}_i} + r_i\frac{\partial}{\partial r_i} + 2R_{ij}\frac{\partial}{\partial R_{ij}} + 3\overline{pu_j}\frac{\partial}{\partial \overline{pu_j}} + 3\overline{u_ip}\frac{\partial}{\partial \overline{u_ip}} + \ldots, \qquad (4.33)$$

$$\bar{\mathrm{X}}_2 = t\frac{\partial}{\partial t} - \bar{U}_i\frac{\partial}{\partial \bar{U}_i} - 2R_{ij}\frac{\partial}{\partial R_{ij}} - 3\overline{pu_j}\frac{\partial}{\partial \overline{pu_j}} - 3\overline{u_ip}\frac{\partial}{\partial \overline{u_ip}} + \ldots\ , \qquad (4.34)$$

$$\begin{aligned}
\bar{\mathrm{X}}_s = {} & \bar{U}_i\frac{\partial}{\partial \bar{U}_i} + \left(R_{ij} - \bar{U}_i\bar{U}_j\right)\frac{\partial}{\partial R_{ij}} + \left(\overline{pu_j} - \bar{P}\bar{U}_j\right)\frac{\partial}{\partial \overline{pu_j}} + \\
& \left(\overline{u_ip} - \bar{U}_i\bar{P}\right)\frac{\partial}{\partial \overline{u_ip}} + \ldots\ , \qquad (4.35)
\end{aligned}$$

$$\bar{\mathrm{X}}_{x_2} = \frac{\partial}{\partial x_2} \ , \tag{4.36}$$

$$\bar{\mathrm{X}}_{\bar{U}_i} = \frac{\partial}{\partial \bar{U}_i} + \dots \ . \tag{4.37}$$

As the latter groups are linearly independent, any linear combination of the symmetries (4.33 - 4.37), yield a new multi-parameter group which is also a symmetry of the TPC equation. From the latter we may finally construct the invariant surface condition (see e.g. Bluman et al. (2010)) encompassing all groups given above

$$\frac{\mathrm{d}x_2}{k_1 x_2 + k_{x_2}} = \frac{\mathrm{d}r_{(k)}}{k_1 r_{(k)}} = \frac{\mathrm{d}\bar{U}_i}{(k_1 - k_2 + k_s)\bar{U}_i + k_{\bar{U}_i}} = \cdots \ , \tag{4.38}$$

where any further invariance conditions for higher correlations are omitted.

4.5 New logarithmic scaling law

At this point non of the group parameters k_i in (4.38) are determined. In order to determine at least some of them we may invoke the BC (2.19), i.e. $\bar{U}_2 = v_0$, as this is the key influencing factor for altering the turbulent flow. Although the BC (2.19) corresponds to the Navie-Stokes equations and its averaged form, it is assumed that for TPC equations it will have similar form. As the BC acts primarily on the velocity we consider the concatenated global transformations for the mean velocity

$$\bar{U}_i^* = e^{k_1 - k_2 + k_s} \bar{U}_i, \tag{4.39}$$

taken from (4.28)-(4.30) and, for the moment, omitting any other part of the transformations. In order to comprehend the following, we may first recall that invariance, and in turn invariant reduction, requires at the first place the symmetries admitted by the underlying equation, here the TPC equation (2.64). In a second step, however, for the construction of a concrete solution, symmetries, or a combination of them, have to be consistent to the imposed boundary conditions. Presently this means (4.39) has to be conformal to (2.19) which, after implementing of the former into the latter, leads to

$$e^{-(k_1 - k_2 + k_s)} \bar{U}_2^* = v_0. \tag{4.40}$$

As the definition of symmetry implies form invariance, also for the boundary conditions, this provides the constraint

$$k_1 - k_2 + k_s = 0. \tag{4.41}$$

We may conclude that the transpiration velocity (v_0) is symmetry breaking, most likely in the core region of the flow but also in the near-wall region.

Imposing the latter constraint onto (4.38) and integrating the first with the third term leads to a new logarithmic scaling law for the streamwise mean velocity

$$\bar{U}_1 = A_1 \log\left(\frac{x_2}{h} + B_1\right) + C_1, \tag{4.42}$$

where A_1, B_1 and C_1 are simple functions of the group parameters k_i. If it may be presumed that v_0 is sufficiently large ($0.05 \leq v_0^+$) we will subsequently show that the latter new log-law is valid in the core region of a turbulent channel flow with wall transpiration.

For the wall-normal component of the mean velocity $\bar{U}_2$ a result similar to (4.42) is obtained from (4.38). Taking into account the additional constraint

$$k_{\bar{U}_2} = 0,$$

we obtain

$$\bar{U}_2(x_2) = C_2,$$

which nicely confirms the assumption (2.19) that the wall-normal component of mean velocity is a constant and is equal to the transpiration velocity v_0.

4.6 Conclusions

Lie group symmetry analysis performed in the present chapter was used to find a new logarithmic type mean velocity scaling law.

It was shown that transpiration velocity v_0 is an important scaling parameter that may be used in the core region and presumably in a near-wall region. As a result v_0 together with friction velocity u_τ is a scaling parameter that allows to collapse the mean velocity data in the core region of the channel flow with wall transpiration. Similarity of the functional form of the classical law of the wall (Oberlack 2001, Oberlack & Rosteck 2010) and a new mean velocity scaling law makes it possible to surmise that there is a correlation between these two velocity scales. However this question may be solved only with analysis of the DNS data.

Finally, it is important to mention that there was no high Reynolds number assumptions for the new log-law. Thus unlike classical log-law it is not high Reynolds number effect. As it will be shown in the next chapter the new log-law is present in the core region of the flow even at small Reynolds numbers such as $Re_\tau = 250$.

5 Mean velocity scaling laws of turbulent Poiseuille flow with wall transpiration

5.1 Introduction

It is well known that randomness and irregularity are characteristic properties of turbulence. The irregularity appears both in space and time and displays unpredictability of the turbulent flow patters, although turbulence is a solution of the (deterministic) Navier-Stokes equations. Irregularity results in extreme sensitivity of the solution of the Navier-Stokes equations to the small errors and to the initial and boundary conditions. Recently it was found that even in the deterministic systems this small differences may grow exponentially with time resulting in completely uncorrelated solutions (Lorenz 1993).

In order to overcome this sensitivity Reynolds proposed decomposition of the physical quantities into mean and fluctuating parts assuming that mean quantities are averaged both in space and time. This decomposition technique gave rise to the statistical methods for studying turbulent flows. Despite a number of other decomposition techniques developed in a last fifty years, like Galilean transformation or filtering fields (a Gaussian filter and proper orthogonal decomposition) decompositions, Reynolds decomposition still remains the most common method of describing turbulent velocity fields.

Another important property of turbulence that plays significant role in study of the turbulence phenomenon and, in particular, the wall-bounded turbulence is a certain statistical order that emerges from the irregularity of the turbulent flow. It was found that mean (averaged) quantities are regular, thus, it is possible to predict their values using certain similarity arguments. The most important result obtained in the wall-bounded turbulence is a finding of the logarithmic-like dependency of the mean streamwise velocity $\bar{U}_1$ on the non-dimensional wall normal coordinate x_2^+ in the near-wall region, i.e. the law of the wall (see eq. (1.18)). Due to the lack of a general theory that is both mathematically indisputable and mechanically correct the mean velocity distribution law still remains empiric. Moreover, it is at the center of controversy which asserts that power law (see eq. (1.19), (1.20), (1.21)) rather than log-law should be used for description of the region (all this different types of the scaling law were already described in the Introduction chapter of the present thesis).

Another important property of the turbulence that made the problem of derivation of the turbulent scaling laws from the first principles even more complicated is a multiscaling of the turbulence phenomenon (Richardson 1922, Kolmogorov 1941a, Kolmogorov 1941b). Due to a wide range of the scales of motion different regions of the wall-bounded flow have different length and velocity scales (Prandtl 1904), thus

scaling laws proposed for these regions should be functions of the admitted characteristic scales. Presently three different mean velocity scaling laws for the wall-bounded turbulent flows are found, these are: linear viscous sublayer law, near-wall log-law and core region velocity defect law.

A purely analytical study of the turbulent channel flow with wall transpiration was performed by Vigdorovich & Oberlack (2008). Employing the method of matched asymptotic expansions led them to the construction of the solutions for the near wall regions (both blowing/suction) as well as for the core region of the flow. The results therein did not give any scaling for the mean velocity or the correlation functions, but it allowed to describe the relation between the wall shear stress, the Reynolds number, and the transpiration velocity by a function of one variable.

It was an original idea of Townsend (1976) that turbulence intensities should also have logarithmic profiles in the near-wall (overlap) region

$$\overline{u_i^2}^+ = -A_i \log\left(x_2/h\right) + B_i. \tag{5.1}$$

This idea stem from his formulation of *the attached-eddy model*, and was further developed by Perry, Henbest & Chong (1986), Perry & Li (1990) and Kunkel & Marusic (2006) who performed a large amount of experiments in order to establish a logarithmic profile for $\overline{u_1^2}^+$. DeGraaff & Eaton (2000) raised the question of the scaling for the squared turbulence intensities in the overlap region and proposed *mixing velocity scale*. The first preliminary logarithmic-type profile for the streamwise and spanwise turbulence intensity scaled with friction velocity was obtained by Jiménez & Hoyas (2008) and Hutchins, Nickels, Marusic & Chong (2009).

In the present chapter the mean velocity scaling laws, i.e. viscous sublayer linear law and near-wall log-law will be analyzed by comparing the mean velocity profiles extracted from the DNSes of turbulent channel with wall transpiration presented in Chapter 3. A new mean velocity scaling law that was analytically derived in the Chapter 4 will be validated in section 5.4.

5.2 Viscous sublayer linear velocity scaling law

As it was mentioned in Introduction, the mean flow momentum equation (2.20) for the channel flow with wall transpiration has the following form

$$v_0 \frac{d\bar{U}_1}{dx_2} = -\frac{d\bar{P}}{dx_1} - \frac{d\overline{u_1 u_2}}{dx_2} + \nu \frac{d^2\bar{U}_1}{dx_2^2}. \tag{5.2}$$

It is integrable once leading to

$$v_0 \bar{U}_1 = -x_2 \frac{d\bar{P}}{dx_1} - \overline{u_1 u_2} + \nu \frac{d\bar{U}_1}{dx_2} + c_1. \tag{5.3}$$

since integration constant c_1 is proportional to the local friction velocities calculated at the walls, it has different values at the blowing and suction walls (see Basic Equations, page 17). For a local analysis we may in principle rewrite the momentum equation

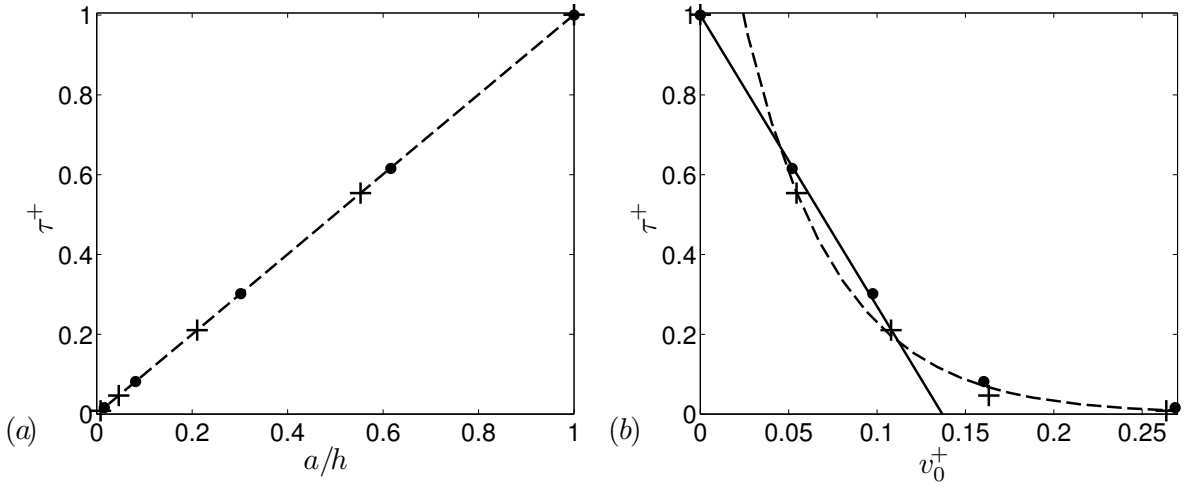

Figure 5.1: (a) Relation between zero-shear-stress point a/h and wall shear stress τ^+. (b) Relation between transpiration velocity in wall units and wall shear stress. •, $Re_\tau = 250$; +, $Re_\tau = 480$; -- , (a) linear relation between a/h and τ^+; (b) exponential relation between v_0^+ and τ^+ (valid only for channel flows with wall-transpiration); —, linear relation between v_0^+ and τ^+ (valid for small and moderate transpiration rates).

(5.3) for each wall using local friction velocities for definition of the c_1 constant and later normalize it on the respective local friction velocity.

Presently, however, we will follow a slightly different route and may first reformulate the local friction velocities according to (2.21) and (3.27) by the averaged friction velocity u_τ which is related to the streamwise pressure gradient

$$u_{\tau b}^2 = \frac{a}{h} u_\tau^2, \tag{5.4}$$

$$u_{\tau s}^2 = \frac{2h-a}{h} u_\tau^2. \tag{5.5}$$

The coefficients a/h and $(2h-a)/h$ represent the relations τ_{wb}/τ_w and τ_{ws}/τ_w respectively defined by (3.27), where a is a parameter that depends on the transpiration velocity. Validation of the equation (3.27) may be taken from figure 5.1(a), while dependency of the shear stress at the wall on the transpiration velocity is given in the figure 5.1(b). It is shown that at small and moderate transpiration rates ($v_0^+ \leq 0.1$) shear stress linearly decrease (increase) at the blowing wall (at the suction wall), while at high transpirations ($v_0^+ > 0.1$) the behaviour is exponential. It was naturally expected that relations τ_{wb}/τ_w and τ_{ws}/τ_w are impervious to the Reynolds number, it may be taken from the figure 5.1(b).

5.2.1 New viscous sublayer velocity scaling law for the blowing wall

Representations (5.4) and (5.5) facilitate a normalization of the terms of the momentum equation with the global u_τ rather than with local ones. The mean momentum

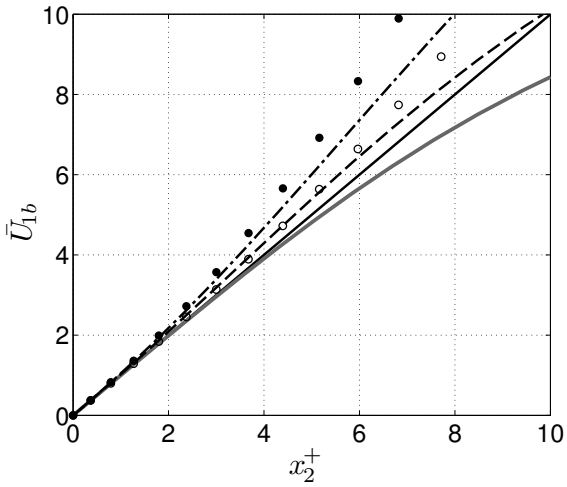

Figure 5.2: Mean velocity profiles and linear law at the blowing wall. —, linear laws (5.8); ——, $v_0^+ = 0$; - - , $v_0^+ = 0.05$; -.-, $v_0^+ = 0.1$; ●, $v_0^+ = 0.16$; ○, $v_0^+ = 0.26$.

equation (5.3) in integrated form and rewritten in non-dimensional form based on u_τ and ν for the blowing side yields

$$\frac{d\bar{U}_1^+}{dx_2^+} - v_0^+ \bar{U}_1^+ - \overline{u_1 u_2}^+ = \frac{a}{h} - \frac{x_2^+}{Re_\tau}. \tag{5.6}$$

Extending the usual universal near-wall region located in the vicinity of the wall where x_2^+ is the wall-normal coordinate and taking the limit $Re_\tau \to \infty$, with $x_2^+ = \mathcal{O}(1)$, the equation (5.6) reduces to

$$\frac{d\bar{U}_1^+}{dx_2^+} - v_0^+ \bar{U}_1^+ - \overline{u_1 u_2}^+ = \frac{a}{h}. \tag{5.7}$$

Finally, for the viscous sublayer at the blowing wall, we take the limit $x_2^+ \to 0$ to obtain $\overline{u_1 u_2}^+ \to 0$ and $v_0^+ \bar{U}_1^+ \to 0$ and hence linear velocity scaling law for the blowing side results

$$\bar{U}_1^+ = \frac{a}{h} x_2^+, \tag{5.8}$$

or in rescaled form

$$\bar{U}_{1b} = x_2^+, \quad \text{where} \quad \bar{U}_{1b} = \frac{\bar{U}_1}{u_{\tau b}} \frac{u_\tau}{u_{\tau b}} = \bar{U}_{1b}^+ u_{\tau b}^+. \tag{5.9}$$

We note that the true local shear stress derives from the pre-factor on the right hand side of the equation (5.8) and may be re-formulated to give a local shear stress based scaling law employing equation (5.4). Since in the classical Poiseuille flow without transpiration the point of zero shear stress coincides with the centreline of the flow, i.e. $a = h$, we observe that the modified scaling law (5.8) recovers the classical one for $v_0 = 0$.

In the presence of the convective momentum transport term $v_0\bar{U}_1$, the blowing shifts the viscous shear stress away from the wall towards the channel center as can be taken from figures 3.5(d-f) and 3.6(d-f). Since the viscous stress at the blowing wall is smaller than in a channel with impermeable boundaries, the viscous sublayer at the blowing side is thinner than for the classical flow. At very high transpiration rates ($v_0/u_\tau = 0.26$), when the local friction velocity becomes smaller than transpiration velocity ($v_0/u_{\tau b} = 2.9$), blowing creates a strong wall-normal flow in the vicinity of the blowing wall, and we see an increased validity of the linear scaling for $\bar{U}_1^+$ as it is obtained in figure 5.2. However, at such a high transpiration rate the viscous stress at the blowing wall is very small even at high Reynolds numbers, i.e. the streamwise velocity gradient in wall-normal direction is small, as can be taken from figures 3.5(f) and 3.6(f).

5.2.2 New viscous sublayer velocity scaling law for the suction wall

A similar analysis of the viscous sublayer on the suction side is not valid as the flow in that region may not be fully turbulent for large transpiration rates. However, in the limit $\overline{u_1 u_2} \to 0$ it is possible to find the velocity profile by integration of the mean momentum equation (1.4). In its final non-dimensional form the solution may be written as follows

$$\bar{U}_{1s} = \frac{2Re_{v_0}\, e^{2Re_{v_0}}}{1 - e^{2Re_{v_0}}(1 - 2Re_{v_0})} \left(1 - e^{-x_{2s}} + \frac{1 - e^{2Re_{v_0}}}{2Re_{v_0}\, e^{2Re_{v_0}}} x_{2s}\right), \tag{5.10}$$

where dimensionless variables in the near-suction-wall scaling have the following forms:

$$x_{2s} = \frac{x_2 v_0}{\nu}, \;\; \bar{U}_{1s} = \frac{\bar{U}_1}{u_{\tau s}} \frac{v_0}{u_{\tau s}} = \bar{U}_{1s}^+ v_{0s}^+, \;\; Re_{v_0} = Re_{\tau s} v_{0s}^+ = \frac{h v_0}{\nu}. \tag{5.11}$$

Note, that x_{2s} is the wall-normal coordinate, i.e. pointing in a different direction as in the rest of this paper, thus x_{2s} has been replaced by $2Re_{\tau s} - x_{2s}$. Taking the limit $Re_{v_0} \to \infty$, with $x_{2s} = \mathcal{O}(1)$, (5.10) reduces to the asymptotic suction profile (Griffith & Meredith 1936, Drazin & Riley 2006)

$$\bar{U}_{1s} = 1 - e^{-x_{2s}}. \tag{5.12}$$

In application to the turbulent wall-bounded flows with suction the near-wall solution (5.12) may have been obtained first by Tennekes (1965). However, due to too wide intervals between velocity traverses in his experiments velocity profiles did not coincide with the analytical solution (5.12). Presently, we verified (5.12) with the DNS, and the results are presented on figure 5.3(a, b). As it can be taken from figure 5.3(a, b), the mean velocity profiles at very high transpiration rates scales with equation (5.12) much better than at low or moderate transpiration rates. It is also important to note that with increasing Re_τ the domain of agreement between the data and (5.12) increases.

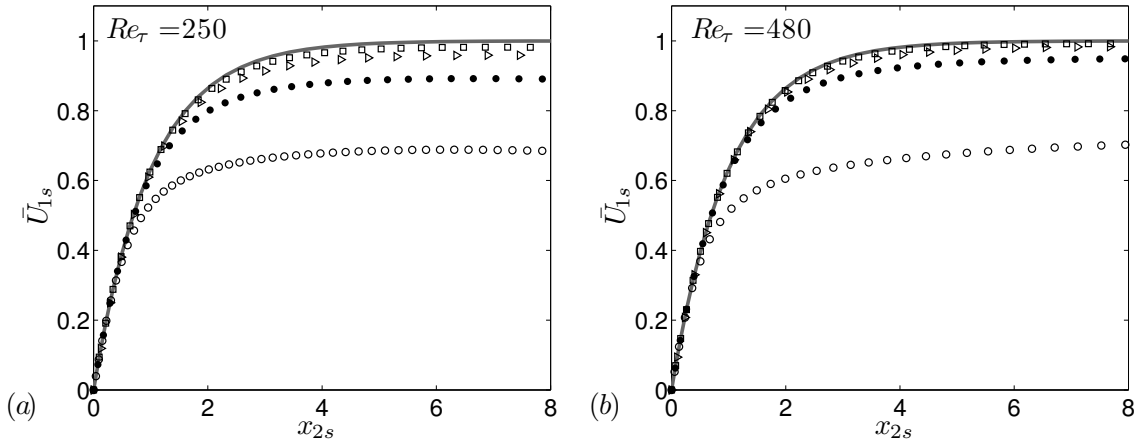

Figure 5.3: Mean velocity profiles and the asymptotic suction profile (5.12) at the suction wall at (a) $Re_\tau = 250$ and (b) $Re_\tau = 480$. ——, profile (5.12); ∘, $v_0^+ = 0.05$; •, $v_0^+ = 0.10$; △, $v_0^+ = 0.16$; □, $v_0^+ = 0.26$.

5.3 Near-wall logarithmic mean velocity scaling law

Historically, the derivation of the near-wall log-law traces back to the seminal work of von Kármán (1930), who introduced a new mixing length and later derived a log-law for the centerline velocity of the turbulent channel flow. He also found a slope constant to be $\kappa = 0.36$ and surmised that it might be a universal (Davidson, Kaneda, Moffatt & Sreenivasan 2011). Later (Millikan 1939), employed matched asymptotics to derive the logarithmic law of the wall as an overlap region. Presently we reconsider a derivation technique based on Lie group analysis, as it was used in Chapter 4 to derive the log in the core region of the channel flow with wall transpiration.

It was first shown in (Oberlack 2001) that the near-wall log has its roots in Lie symmetries based on a combination of statistical and fluctuating equations. Its first derivation based on the two- (TPC) and multi-point correlation (MPC) equations and in particular recognizing the importance of the statistical groups (4.30), (4.32) was obtained in (Oberlack & Rosteck 2010). The authors used the infinite set of MPC equations to derive the near-wall log-law

$$\bar{U}_1^+ = \frac{1}{\kappa} \log\left(x_2^+ + A^+\right) + C, \tag{5.13}$$

and showed that the friction velocity u_τ is the key symmetry breaking parameter in the near-wall region. The latter is a slightly generalized functional form of the usual near-wall scaling law, as it implies the offset A^+ as a displacement height, which gives an extended fit of (5.13) to the experimental data (see e.g. Lindgren et al. (2004)) and further appears, for example, in the log-law for rough-wall-bounded flows (Jackson 1981).

An apparent question arises how equation (5.13) may change under the influence of the wall-transpiration. In the present flow configuration the friction velocity u_τ and the transpiration velocity v_0 are of the same dimension and, to be shown below, are closely correlated. Further, as both are symmetry breaking for the velocity scaling a

functional form of the near-wall log-law obtained from Lie group analysis should be similar to the case without transpiration (5.13).

It was shown above that for the viscous sublayers on each wall the local friction velocity is the key normalization parameter in the equations (5.8) and (5.10), as would be naturally expected. This, however, does not appear to be true for the near-wall log-law. The collapse of the near-wall data appears to be due to the mean friction velocity u_τ, which is a measure of the pressure gradient. This, however, is very different from what was shown in (Nikitin & Pavel'ev 1998). They employed a local u_τ on the blowing wall and observed that the usual von Kármán constant κ varies with the blowing velocity.

In order to find the modified constants for the classical near-wall log-law in equation (5.13) due to wall transpiration we may adopt the classical notation given in (Millikan 1939). Since blowing increases turbulence it is preferable to derive unaltered near-wall log-law for this region.

According to the results obtained by (Jiménez et al. 2001) for the channel flow with permeable boundaries, transpiration only affects the log-law additive constant C, while von Kármán constant κ is largely unaltered in the overlap region if a global u_τ is used. As it will be shown below, the present DNS facilitate the latter finding and equation (5.13) may be rewritten in the following form

$$\bar{U}_1^+ = \frac{1}{\kappa}\log\left(x_2^+ + A^+\right) + C + C_1\left(\frac{v_0}{u_\tau}\right), \tag{5.14}$$

keeping in mind how it was normalized and the function C_1 which vanishes when transpiration is zero. Here κ and C are independent of v_0 and hence are universal constants obtained for the case without transpiration and based on the local u_τ.

As no first principle idea is known to determine $C_1(v_0/u_\tau)$ we employ a simple curve fitting procedure to fit the new additive function C_1 which comes down to the following power-law

$$C_1(v_0^+) = \alpha\left(\frac{v_0}{u_\tau}\right)^\beta, \tag{5.15}$$

where the constants are $\alpha = -90.62$ and $\beta = 1.188$. The validity of equation (5.15) may be taken from figure 5.4(d).

The results from the DNS and the modified log-law close to the blowing wall calculated from equation (5.14) with $A^+ = 0$ are compared in figure 5.4(a, b). We used $\kappa = 0.38$ as a slope constant, as it may be seen on the figure 5.4(c). We observe that for moderate transpiration rates ($0.04 < v_0/u_\tau < 0.1$) the log region does not change its size and location. However, for higher transpiration rates the validity of the scaling region becomes thinner and is shifted towards the core region of the channel. At high transpiration rates ($0.16 < v_0/u_\tau < 0.26$) the near-wall log-region almost vanishes, and cannot be validated with the expression (5.14).

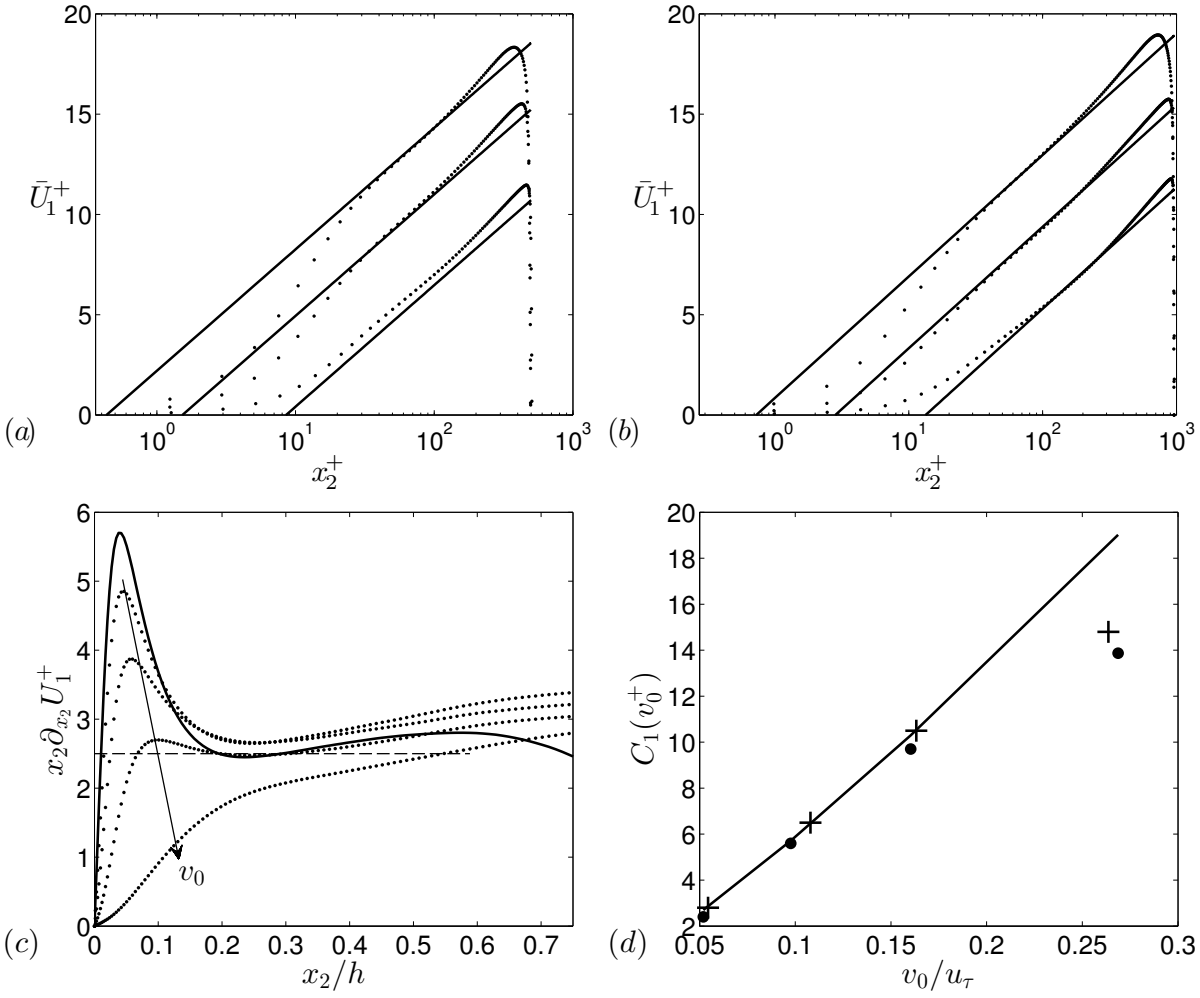

Figure 5.4: (a) Mean velocity profiles of a turbulent channel flow with wall transpiration at the blowing wall at $Re_\tau = 250$. Solid lines correspond to the log-law (5.14), where $A^+ = 0$. (b) Mean velocity profiles of a turbulent channel flow with wall transpiration at the blowing wall at $Re_\tau = 480$. From top to the bottom $v_0/u_\tau = 0.05, 0.1, 0.16$. (c) Mean velocity profile slope indicator function as computed from the DNS data. Solid line represents case without transpiration. Dotted lines represent cases with transpiration. The horizontal dashed line is at 2.5, corresponding to $\kappa = 0.4$. In direction of arrow: $v_0/u_\tau = 0.0, 0.05, 0.1, 0.16, 0.26,\ Re_\tau = 250$. (d) Scatter plot of the relationship between new log-law additive constant C_1 and transpiration rate v_0^+. ●, $Re_\tau = 250$; +, $Re_\tau = 480$; —, power-law (5.15).

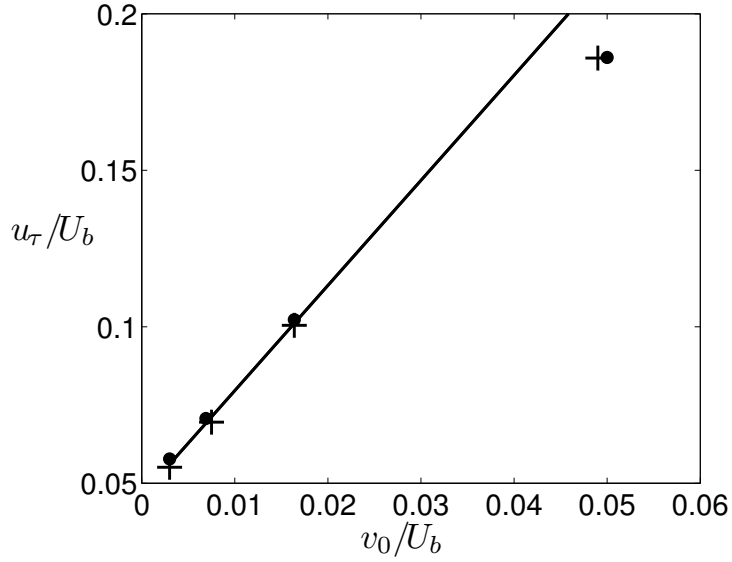

Figure 5.5: Relation between transpiration velocity and friction velocity. •, $Re_\tau = 250$; +, $Re_\tau = 480$; —, linear relation between v_0 and u_τ: $u_\tau = 3.36 v_0 + 0.046$.

5.4 New mean velocity scaling law

The scaling law (4.42) obtained using Lie symmetry method contains constants A_1, B_1 and C_1, that cannot be obtained using Lie group analysis alone. For this reason one of the main aims of the present study is to determine the constants employing the DNS results. An open question that arises immediately is a desired velocity scale, that will induce a collapse of the data in the considered region. Form invariance property of the symmetries have proven previously made assumption that transpiration velocity v_0 is a symmetry breaking constraint in the core region of the flow.

From this one may expect that v_0 is the appropriate velocity scale for the core region log-law (4.42). However, a changing of v_0/U_b also significantly changes u_τ/U_b and hence the proper velocity scale is not obvious in the first place. From dimensional reasons, the ratio of two velocities results in two non-dimensional groups with a unique functional relation

$$\frac{u_\tau}{U_b} = F\left(\frac{v_0}{U_b}\right). \tag{5.16}$$

The best fit to all data is obtained if instead of v_0 we invoke u_τ as the appropriate velocity scale. We recall that u_τ is a measure of the pressure gradient as the local $u_{\tau b}$ and $u_{\tau s}$ on each wall are very different. The analysis of the DNS results together with the employment of u_τ as a scaling velocity for A_1 leads to the fact that the overall scaling appears rather insensitive to the Reynolds numbers and the relative transpiration rates. The latter rescaling leads to $A_1 = u_\tau/\gamma$, where $\gamma = 0.3$ has been taken from the DNS data. Note that this is not the usual von Kármán constant κ.

The offset B_1 in the equation (4.42) was found to be a very small number. Further, a systematic and careful analysis of the best fitted values did not reveal a unique picture. Hence, B_1 has been set to zero for all cases, though a better fit of the DNS data to equation (4.42) may be obtained from a non-zero B_1.

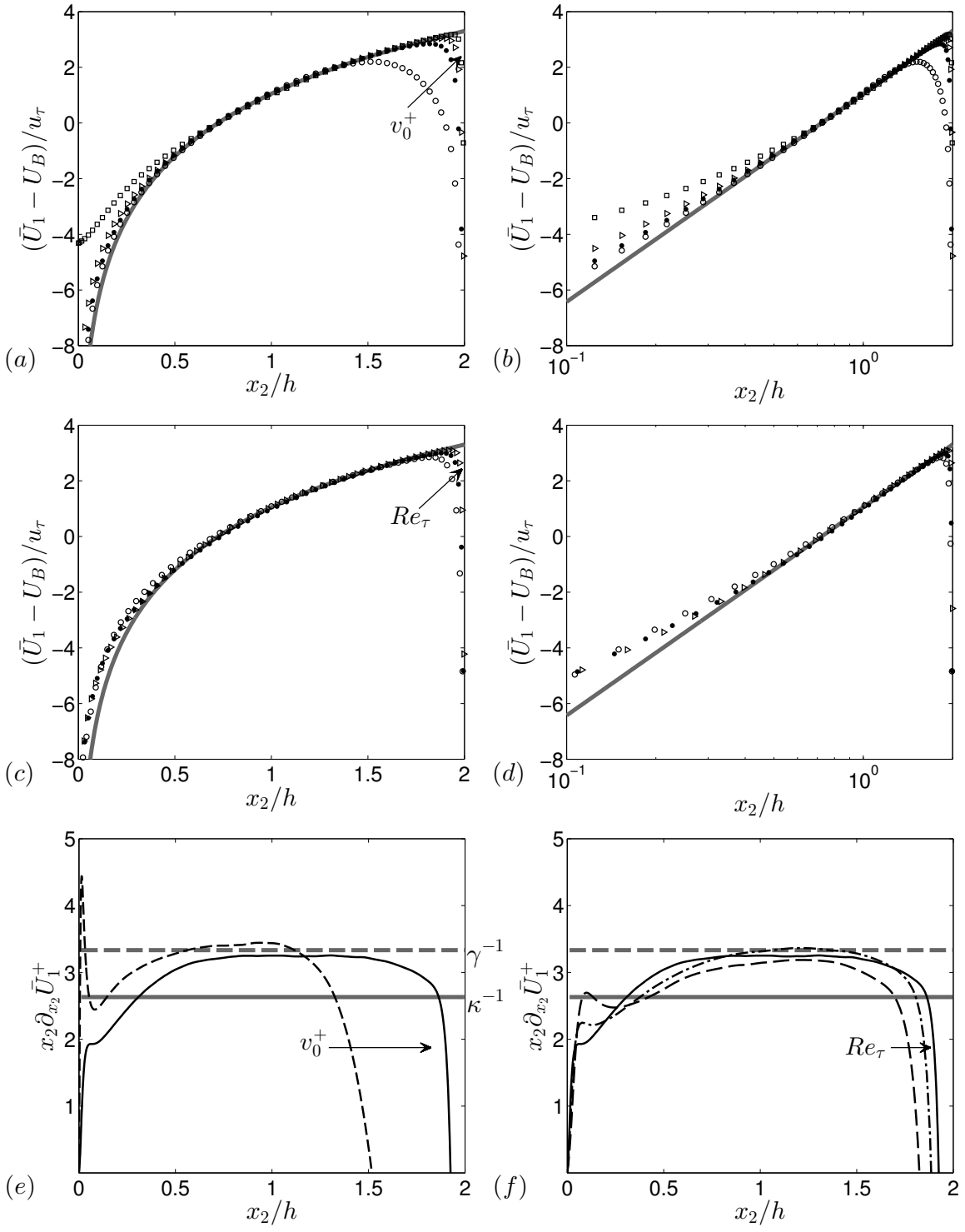

Figure 5.6: Mean velocity profiles at (a, b) constant Reynolds number $Re_\tau = 480$: ∘, $v_0^+ = 0.05$; •, $v_0^+ = 0.1$; ▷, $v_0^+ = 0.16$, □, $v_0^+ = 0.26$; and (c, d) constant transpiration rate $v_0^+ = 0.16$: ∘, $Re_\tau = 250$; •, $Re_\tau = 480$; ▷, $Re_\tau = 850$. (e, f) Indicator function $x_2\partial_{x_2}\bar{U}_1^+$. Grey lines represent slope constants used in the paper. For near-wall region: ——, $\kappa = 0.38$; for core region: - - , $\gamma = 0.3$. (e) Constant Reynolds number $Re_\tau = 850$: in direction of an arrow: - - , $v_0^+ = 0.05$; ——, $v_0^+ = 0.16$. (f) Constant transpiration rate $v_0^+ = 0.16$: in direction of an arrow: - - , $Re_\tau = 250$; - · , $Re_\tau = 480$; ——, $Re_\tau = 850$.

Since the new log-law is located in the center of the channel, our present knowledge of turbulent scaling laws suggests a defect type of scaling. Hence, a second global velocity scale is needed to determine C_1.

In turbulent boundary layer flows we use the free stream velocity U_∞ while in the classical Poiseuille flow U_{max} located in the center of the channel is the appropriate outer velocity scale. An analysis of the present DNS data disclosed C_1 to be the bulk velocity U_b (2.24) without an additional non-dimensional pre-factor.

In its final form the new logarithmic scaling law for the core region of the channel flow with wall transpiration is found to be

$$\bar{U}_1 = \frac{1}{\gamma} u_\tau \log\left(\frac{x_2}{h}\right) + U_b \tag{5.17}$$

or in deficit form

$$\frac{\bar{U}_1 - U_b}{u_\tau} = \frac{1}{\gamma} \log\left(\frac{x_2}{h}\right). \tag{5.18}$$

The new Lie symmetry induced scaling law (5.18) represents the velocity defect law that scales the data in the whole core region of the flow as may be taken from figure 5.6. This comparatively long log-region already appears at the low Reynolds numbers of $Re_\tau = 250$ and becomes even longer as the Reynolds number increased to $Re_\tau = 850$, as may be taken from figure 5.6(c,d). Most important, and as to be expected, the validity of (5.18) further increases with growing transpiration rate v_0 until the latter becomes only an order of magnitude smaller than the streamwise velocity.

An indicator function shown on figure 5.6(e, f) confirms once again that the new mean velocity scaling law (5.18) is valid in the whole core region of the flow. In particular, it is found that the indicator function has a plateau in the core region, and the slope constant for the new core region log-law was found to be $\gamma = 0.3$, as it is highlighted with a dashed line on figure 5.6(e, f). Further, the indicator function plot supports the fact that the scaling region of the new mean velocity scaling law increases with Reynolds numbers and moderate (up to $v_0^+ \leq 0.16$) transpiration numbers.

5.5 Turbulence intensity scaling laws

According to Townsend's *attached-eddy hypothesis* (Townsend 1976) the largest energy-containing eddies grow from the wall (they are attached to the wall) into the core region and have geometric lengths that scales with x_2. This leads to the following form of the streamwise (and also spanwise) turbulence intensity

$$\overline{u_1^2}^+ = B_2 - A_2 \log\left(\frac{x_2}{h}\right), \tag{5.19}$$

where $\overline{u_1^2}^+ = \overline{u_1^2}/u_\tau^2$ and h is the channel half-width. Perry & Chong (1982) proposed that logarithmic scaling of the streamwise turbulence intensity (5.19) and of the mean streamwise velocity (5.13) both are located in the overlap (logarithmic) region this assumption was confirmed only recently by Marusic, Monty, Hultmark & Smits (2013). They used data obtained from experiments at very high Reynolds numbers (up to

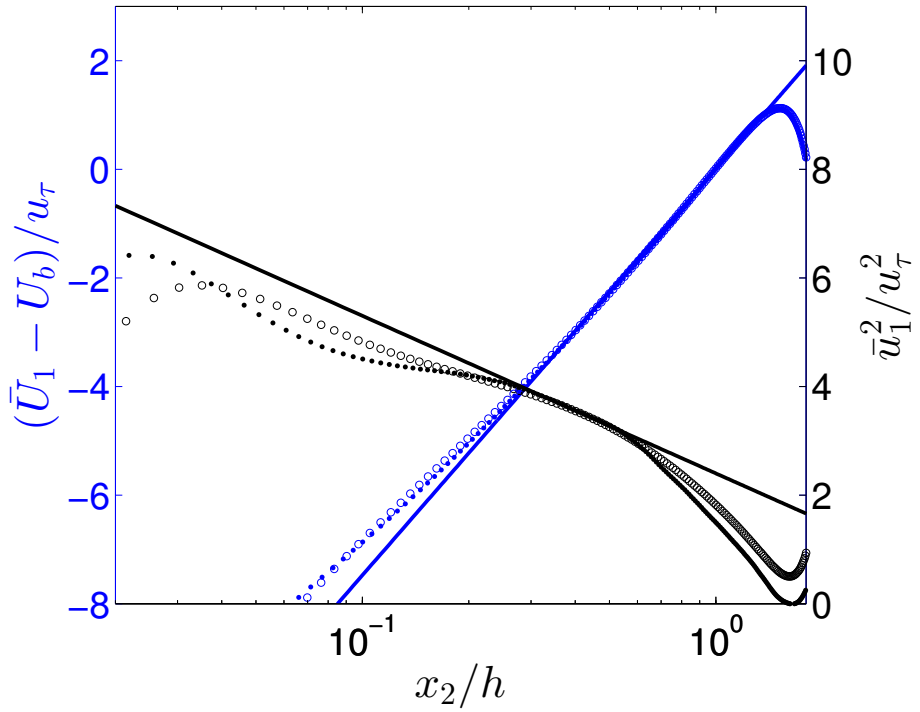

Figure 5.7: Mean streamwise velocity and streamwise turbulence intensity profiles. The solid lines correspond to equations (5.18) with $\gamma = 0.3$ and (5.19) with $A_2 = 1.26$. Open circles correspond to the DNS at $Re_\tau = 480; v_0/u_\tau = 0.05$. Filled circles to $Re_\tau = 850; v_0/u_\tau = 0.05$.

$Re_\tau \approx 628.000$) and tested universality of the mean velocity log-law and the streamwise turbulence intensity log-law. They have found that $A_2 = 1.26$ which is slightly different from the one proposed by Jiménez & Hoyas (2008) $A_2 = 1.15$.

Simple curve fitting of the DNS data obtained for the small transpiration rate ($v_0/u_\tau = 0.05$) at moderate turbulent Reynolds numbers ($Re_\tau = 480, 850$) helped us to verify their results. As it may be taken from figure 5.7 turbulence intensity log-law is found in the same region as a new mean velocity scaling law (see equation (5.18)). Scaling region grows in size as the Reynolds number increase, although it is still much smaller than the scaling region of the new mean velocity scaling law. This might be an indication that admitted Reynolds numbers are not high enough. It is important to note that the turbulence intensity scaling region does not appear in the channel flows without transpiration at similar Reynolds numbers. Thus, the new scaling law proposed here might be transpiration induced effect.

Another apparent feature shown in figure 5.7 is the growth of the near-wall peak of the streamwise velocity fluctuation as the Reynolds number increase. According to the Hoyas & Jiménez (2006) the growth of the peak is an evidence of the correctly selected velocity scale in the near-wall region, which in the present study is a friction velocity u_τ averaged on both blowing and suction walls.

Finally, according to Hutchins & Marusic (2007a) the logarithmic region of the streamwise turbulence intensity is an evidence for the presence of "superstructures", a very long meandering structures that scale on h. The magnitude of this events scales on u_τ^2

and it is widely accepted that these structures emerge at very high Reynolds numbers, when the near-wall logarithmic (overlap) region is long enough to clearly observe separation of the near-wall and core region scales. In more details the superstructures will be described in the following chapter.

5.6 Conclusions

In the present chapter we investigated the mean streamwise velocity and the turbulence intensity scaling laws that have been found in the channel flow with wall transpiration. In order to find the velocity scaling that will collapse all the data in the admitted region we have used the results obtained in the previous chapter and found that the viscous sublayer mean velocity scaling law is based on the local friction velocity $u_{\tau b}$, $u_{\tau s}$, while law of the wall is based on the global, averaged on both walls friction velocity u_τ.

It has been shown that wall transpiration alters the form of the classical mean velocity scaling laws. In particular, it was found that while von Kármán constant remains its classical value, an additive constant in the near-wall log-law depends on the wall conditions and has to be a function of transpiration velocity. Another interesting result is the counterbalance of the wall transpiration and high Reynolds number effects in the overlap region. This result agrees with the finding which was made in the previous chapter that at very high transpiration rates the region of the balance between turbulence production and dissipation rates disappears.

Apart from the classical mean velocity scaling laws we have found a new scaling law in the core region of the flow. As it was shown in this chapter it is also logarithmic type, however the slope constant is not von Kármán constant anymore and its value is $\gamma = 0.3$. Further it was found that scaling region of the new log-law depends not only on the transpiration number, which was naturally expected since transpiration shifts the point of the mean velocity gradient closer to the suction wall, but also that the scaling region depends on the Reynolds number. The size of the region increase at high Reynolds numbers. This indicates that in the core region these effects amplify each other. Which is oppositely to the effect that we see in the near-wall log-region.

Apart from the mean velocity scaling laws we have found a streamwise turbulence intensity scaling law. It was shown that the slope constant $A_2 = 1.26$ which was reported by Marusic et al. (2013) is supported by the present DNS results obtained at small transpiration and moderate (in comparison to their boundary layer experimental results) Reynolds numbers. The fact that the slope constant obtained by Jiménez & Hoyas (2008) for the channel flow without transpiration at $Re_\tau = 2000$ differs from the one used in the present study for $Re_\tau = 850$ indicates that the new streamwise turbulence intensity scaling law may be either a purely transpiration induced effect, or the result of an amplification of the transpiration and Reynolds number effects by each other which was found in the core region from analysis of the new mean velocity log-law.

6 Structural analysis of the near-blowing/suction regions

6.1 Introduction

Alongside the study of the scaling of the turbulent statistics presented in the previous chapter, an exploration of the nature of organized motions in instantaneous velocity and vorticity fields was performed. Although it is unclear what the organized motions are, their role in the understanding of the dynamics in the turbulent near-wall region cannot be overestimated. These organized motions are persistent in time and space and are called *coherent structures*. It is widely accepted that they play an important role in the scenarios of heat, mass and momentum transport.

According to the most recent studies of turbulence structures reviewed in detail in the following articles Marusic, McKeon, Monkewitz, Nagib, Smits & Sreenivasan (2010), Smits, McKeon & Marusic (2011), Jiménez (2012) there are four main types of structures identified in the near-wall region. The first two types of the coherent structures have been recognized for a long time. These are near-wall streaks of the streamwise velocity with a characteristic spacing in the spanwise direction of $100\nu/u_\tau$ (Kline et al. 1967) and streamwise individual vortices (Robinson 1991). The latter are also known as hairpin or horseshoe vortices with a minimum height of $100\nu/u_\tau$ (Theodorsen 1952). They are described in the introductory chapter of this thesis.

The most recent studies have revealed the presence of two other types of organized motions, particularly large-scale motions (LSMs) of scale $\mathcal{O}(h)$ and very large-scale motions (VLSMs) with streamwise length scales of $\mathcal{O}(10h)$. According to Adrian (2007) LSMs are packets of hairpin vortices aligned in streamwise direction, sometimes also called trains of hairpin vortices. These structures grow from the wall into the logarithmic region by a process of merging via a vortex reconnection mechanism (Wark & Nagib 1989, Tomkins & Adrian 2003) and generation of the new hairpin vortices upstream of the primary vortex (Zhou, Adrian, Balachandar & Kendall 1999). The heads of the hairpins in the packets are inclined at 20° to the wall. The packets lengths reaches $2-3h$ in the streamwise direction. A characteristic feature of the LSMs are the low-speed velocity streaks that are generated by the packets of the hairpins aligned in streamwise direction, which induce the regions of the low-streamise momentum between their legs.

VLSMs consist of narrow regions of low-speed streaks flanked by the regions of higher momentum fluid. As well as all other three types of the structures they have been found in all canonical flows. However, in pipes and channels they are usually called VLSMs (Adrian 2007) or global structures (del Álamo & Jiménez 2003, del Álamo et al. 2004), while in boundary layers they are referred to as "superstructures" (Hutchins & Marusic 2007a, Monty, Stewart, Williams & Chong 2007). VLSMs and superstructures

are very long in streamwise direction and they scale with outer variables. The important feature of the structures is the spanwise meandering that is believed to be a consequence of bursting events (Jiménez, Kawahara, Simens, Nagata & Shiba 2005). Due to the wavy nature of the VLSMs it is difficult to determine their typical streamwise scale. According to Hutchins & Marusic (2007b) the length of the superstructures exceeds 10-15 times the boundary layer thickness, while Monty et al. (2007) have found that in channel and pipe flows the length of VLSMs is 30 times the channel half-width or pipe radius. Finally, according to Jiménez (2012) VLSMs are quasi-independent in the streamwise direction, thus, it is possible to study these structures in much smaller, so-called minimal systems.

As we know, the near wall region is the most important part of the flow, where turbulent production dominates over dissipation. The fact that streaks and streamwise vortices are created in this region and that wall turbulence is a self-sustaining process, brings us to the conclusion that there should be a self-sustaining generation mechanism of these structures. Moreover, this generation process should be cyclic. A big amount of the generation scenarios have been proposed to characterize these time-independent interactions between streaks and vortices (Panton 2001). All the scenarios of the self-sustaining mechanisms may be conditionally subdivided into two broad classes. The first one is based on the linear perturbation analysis of the turbulent wall-bounded flows. It shows that instability of the streaks in the buffer region grows through the transient growth mechanism and produces much larger perturbations that form streamwise vortices (details on this formation mechanism may be found in Schoppa & Hussain (2000)). Within this class of scenarios it is assumed that the instability of the streaks is a crucial ingredient of the regeneration cycle. If the streaks were stable, they would not generate vortices and the latter ones will decay under the action of viscosity. Velocity streaks themselves would also decay and the whole flow will become laminar.

The generation of vortex-structures is the cornerstone for the second class of scenarios. It is assumed that hairpin-type vortices are fundamental elements for the description of the physical processes that occur in the near-wall region. According to this model quasi-streamwise vortices lift away from the boundary, form a hairpin-type structure that induces a low-speed streak between the legs of the hairpin vortex. If the hairpin is strong enough it will be able to generate secondary hairpins downstream and upstream, as well as the tertiary hairpin upstream and quasi-streamwise vorticies. The latter ones tend to curl back and weaken the primary hairpin vortex. All this generation process is described in detail in Zhou et al. (1999).

In the present chapter a visualization of near-wall structures will be performed. Effects of the blowing and suction on the near-wall coherent structures will be analyzed using visualizations of the instantaneous velocity and vorticity fields and the statistical data of vorticity fluctuations and the two-point correlations of velocity fluctuations.

6.2 Two-point correlations

It is well known that the two-point velocity correlations are able to provide important information about vortical structures present in turbulent flows. Analysis of the streamwise two-point cross correlation R_{12} have revealed that very close to the suction wall ($x_2 \to 2h$) R_{12} indicates a rather long correlation length as it decays slowly in r_1-direction, this may be taken from figure 6.1. The narrow region of long correlation length suggests that near-wall low-velocity streaks have very small wall-normal scale and are elongated in streamwise direction, prompting that suction creates a high velocity gradient region in the vicinity of the wall, see also figures 6.2($d-f$), 6.3($d-f$), 6.4($d-f$). In contrast, on the blowing side ($x_2 \to 0$) the correlations show a considerably shorter extent in streamwise direction. However, in wall-normal direction this region is three times wider then the former one. That indicates that velocity streaks at the blowing wall are lifted away from the boundary and have much smaller streamwise extent, see also figures 6.2($a-c$), 6.3($a-c$), 6.4($a-c$). That nicely agrees with the structural analysis of the near-wall region conducted by (Sumitani & Kasagi 1995). They have shown that the flow is highly populated with small scale coherent vortical structures near the blowing side, while vortical structures appear less frequently on the suction side coherent, however, at significantly larger scales.

The discovery of the near-wall coherent vortical structures makes clear that the dynamics of the near-wall region is much more complicated than it was assumed before. Since a large amount of research has been performed in order to identify these structures, and to study their statistical properties and importance to the dynamics of the flow in the near-wall region. Due to the complexity of the experimental study of the near-wall region, many aspects of the vortex dynamics have been discovered only after the development of numerical study techniques. One might name the relation between vorticity which is a point function and vortex-structure which is a multi-point phenomenon. To quote Robinson: "In the turbulent boundary layer, the association between regions of strong vorticity and actual vortices can be rather weak, especially in the near-wall region (Robinson, Kline & Spalart 1989)." (Robinson 1991), pp 614. However, it was recently found that the off-wall peak of the streamwise vorticity fluctuation ω_1^+ is an indicator for the quasi-streamwise vortices (Jiménez & Pinelli 1999). As it may be taken from figure 6.5(a), small blowing shifts the coherent vorticies away from the wall and at medium transpiration rates the peak is shifted further away from the wall and becomes smaller. At very high transpiration rates the peak does not appear at all, which suggests that vortical structures are destroyed in the near-wall region, and the regeneration cycle in which these structures are involved is broken. At the suction side the off-wall peak is also being shifted away from the wall by suction. Suction destroys quasi-streamwise vorticies much more effectively, see figure 6.5(b). Even at moderate suction rates the regeneration cycle is destroyed.

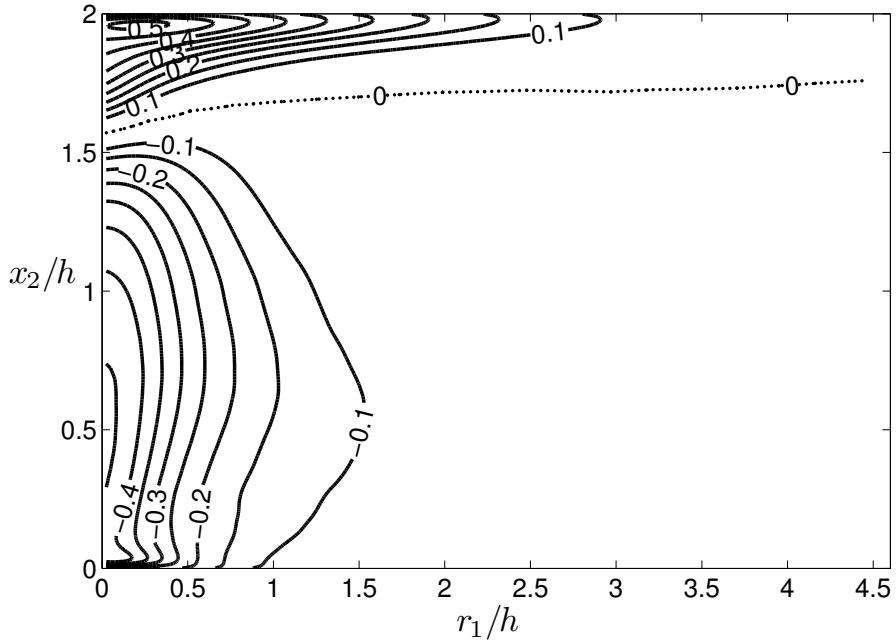

Figure 6.1: Iso-contours of the two-point cross-correlation function normalized on stresses, i.e. $R_{12}/\sqrt{(\overline{u_1 u_2})^2}$, as a function of the streamwise separation r_1/h and the wall-normal coordinate x_2/h. Further we have $r_2/h = r_3/h = 0$. The spacing of the contour lines 0.05; —, positive/negative; ····, zero.

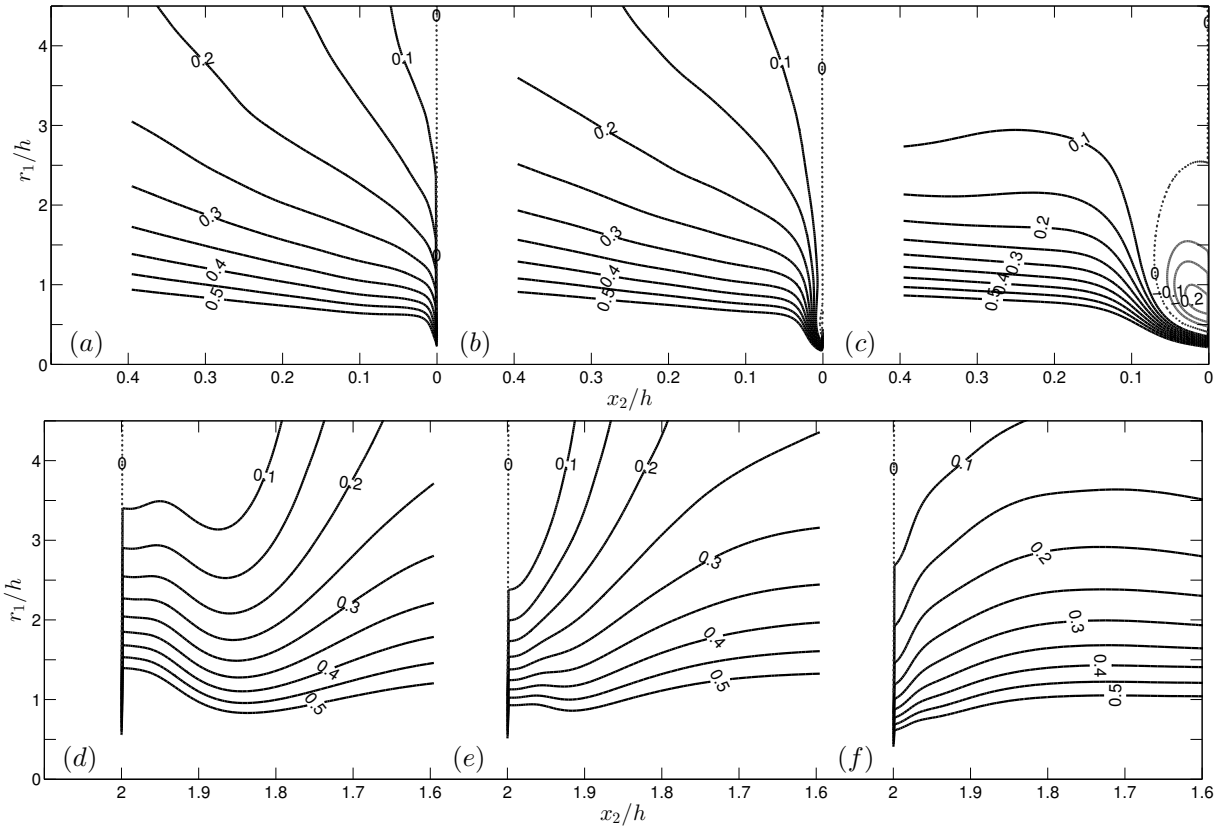

Figure 6.2: Iso-contours of the two-point streamwise-correlation function normalized on stresses, i.e. $R_{11}/\sqrt{(\overline{u_1 u_1})^2}$, as a function of the streamwise separation r_1/h and the wall-normal coordinate x_2/h. From left to right: $v_0^+ = 0.1, 0.16, 0.26$. (a)-(c) in the near-blowing wall region; (d)-(f) in the near-suction wall region. Further we have $r_2/h = r_3/h = 0$. The spacing of the contour lines 0.05; —, positive/negative; ····, zero.

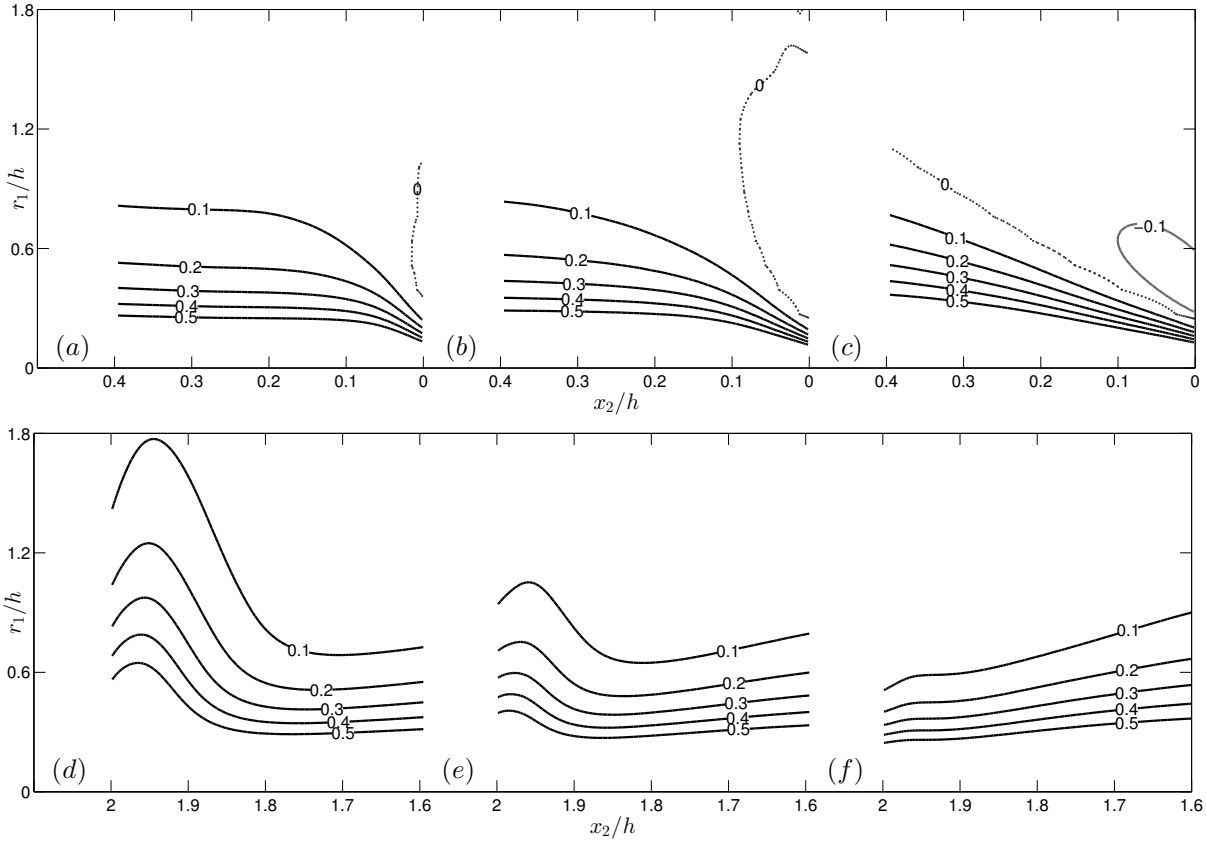

Figure 6.3: Iso-contours of the two-point streamwise-correlation function normalized on stresses, i.e. $R_{22}/\sqrt{(\overline{u_2u_2})^2}$, as a function of the streamwise separation r_1/h and the wall-normal coordinate x_2/h. From left to right: $v_0^+ = 0.1, 0.16, 0.26$. (a)-(c) in the near-blowing wall region; (d)-(f) in the near-suction wall region. Further we have $r_2/h = r_3/h = 0$. The spacing of the contour lines 0.1; —, positive/negative; ····, zero.

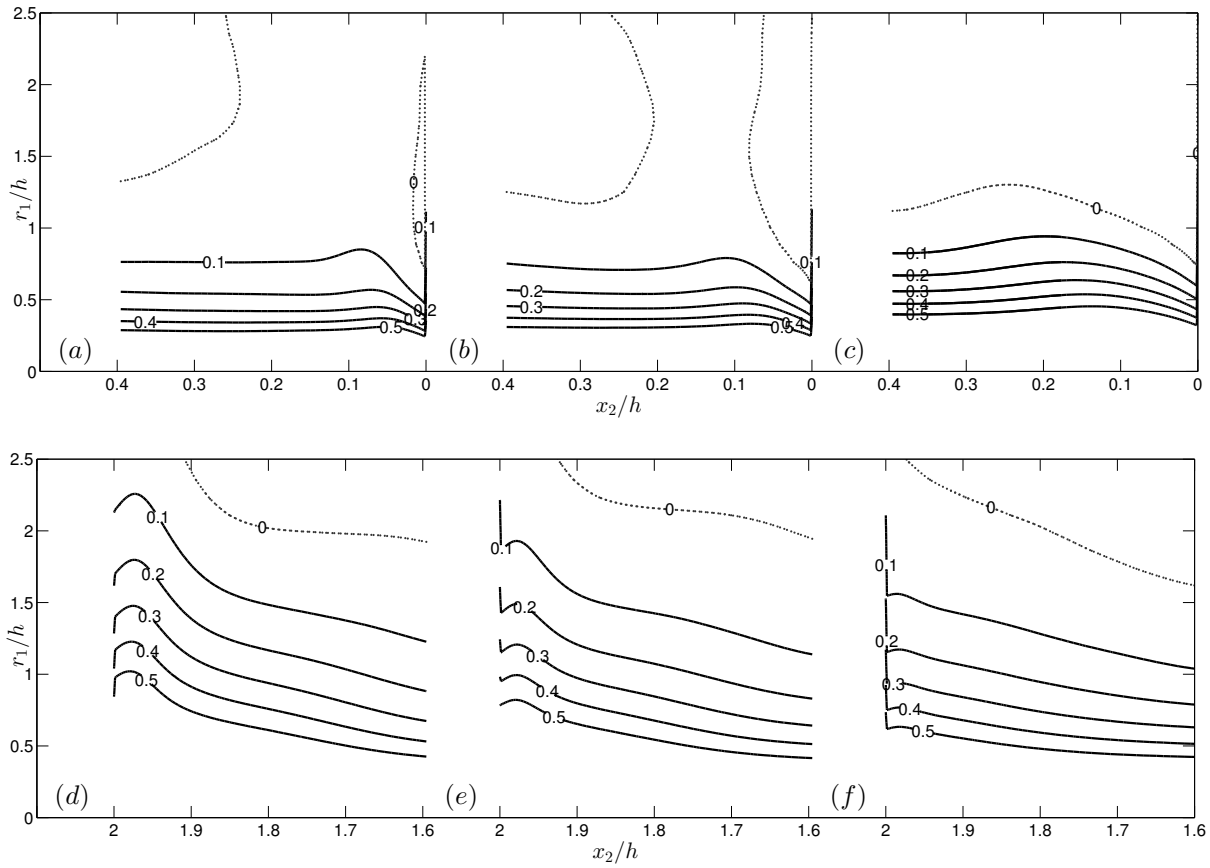

Figure 6.4: Iso-contours of the two-point streamwise-correlation function normalized on stresses, i.e. $R_{33}/\sqrt{(\overline{u_3u_3})^2}$, as a function of the streamwise separation r_1/h and the wall-normal coordinate x_2/h. From left to right: $v_0^+ = 0.1, 0.16, 0.26$. (a)-(c) in the near-blowing wall region; (d)-(f) in the near-suction wall region. Further we have $r_2/h = r_3/h = 0$. The spacing of the contour lines 0.1; —, positive/negative; ····, zero.

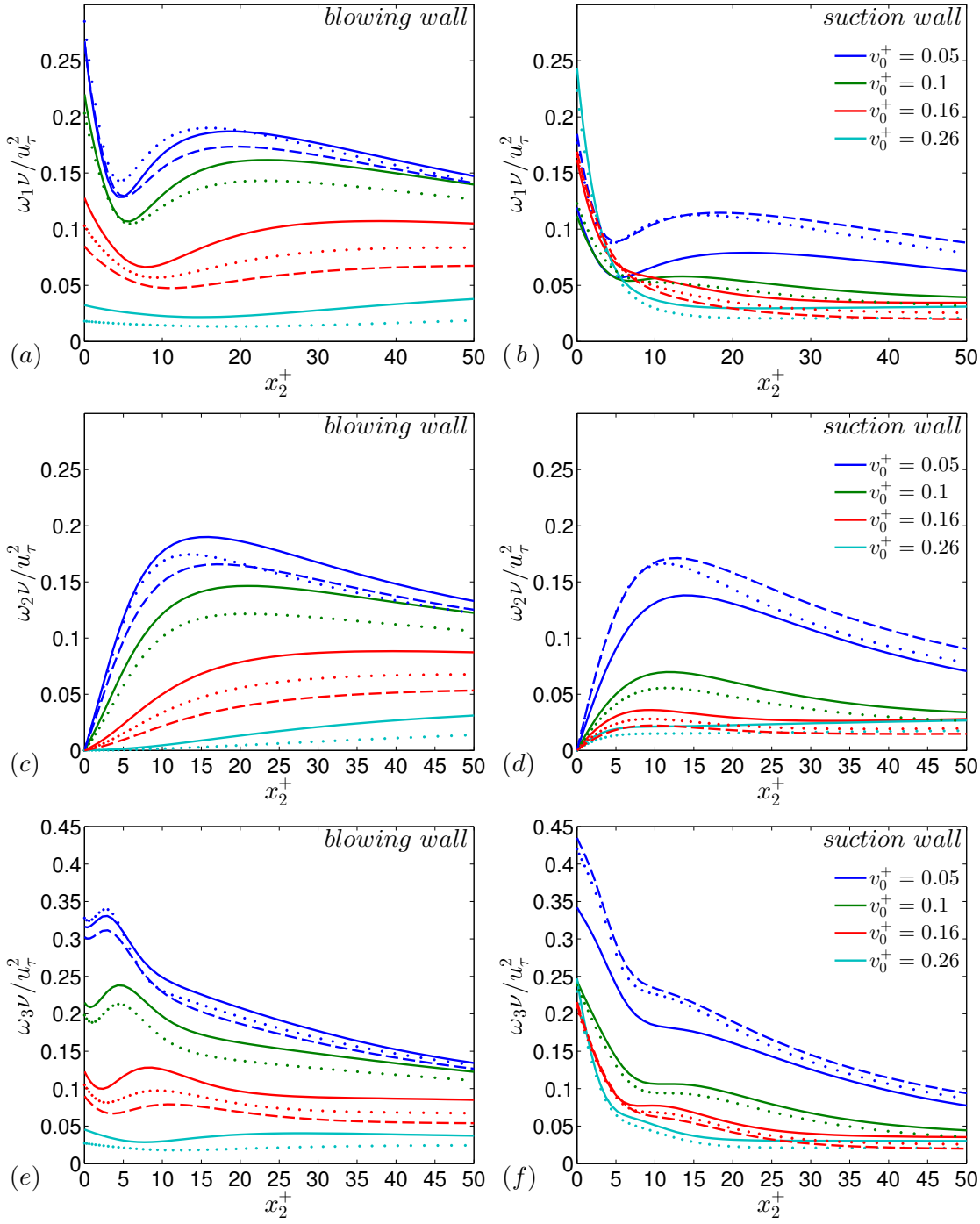

Figure 6.5: Vorticity fluctuations, (a)-(b) streamwise, (c)-(d) wall-normal, (e)-(f) spanwise, are plotted against the distance in wall units. On each plot profiles for four different transpiration rates and three Reynolds numbers are shown: $Re_\tau = 250$ —— ; $Re = 480$: ·····; $Re_\tau = 850$ - - .

It is well known that in the buffer layer ω_2 has a maximum peak that indicates the existence of velocity streaks. In fact this peak represents the maximum streak velocity, which is located at $x_2^+ \sim 15$ in canonical channel flow. The collapse of the wall-normal vorticity fluctuations at different turbulent Reynolds numbers that is found in this type of flows, suggests that there is an invariance of the low-speed streak spacing in wall units (Moser, Kim & Mansour 1999). In the case of channel flow with blowing and suction, wall-normal fluctuations do not collapse at the same transpiration rates in the buffer layer, where the streaks are usually located, as it may be taken from figures 6.5($c-d$). This effect is clearly visible on both, blowing and suction walls. Thus, both types of wall manipulation may affect the spacing of the near-wall velocity streaks. Away from the suction wall the profiles collapse, while at the blowing wall we do not see the same. That may be assumed to be another indication that blowing and suction introduce different types of anisotropy in the wall-bounded flow. While the latter is of local (near-wall) type, the former is of global type. Another important feature of the wall transpiration as it may be seen on figures 6.5($c-d$) is a decrease of the near-wall peak. At the suction wall the peak decrease much faster than at the blowing side with increase of the transpiration rate, which is in accordance with the previously made statement that suction is more effective in the destruction of the near-wall regeneration cycle.

As well as streamwise and wall-normal vorticity fluctuations, the spanwise component shows strong dependence on the transpiration rate on both sides (see figure 6.5($e-f$)). A distinguishable feature of the spanwise vorticity fluctuations at the blowing wall is an off-wall peak, which is located at $x_2^+ \sim 5$ and shifts to $x_2^+ \sim 10$ as transpiration increases, see figure 6.5(e). This peak does not appear in canonical flows. According to (Rajagopalan & Antonia 1993) in a canonical turbulent boundary layer the spanwise vorticity is strongly correlated with the sweep-like and ejection-like events at $x_2^+ = 10.7$. However, it is also well known that coherent vortical structures that are a direct consequences of sweeps and ejections in the near-blowing wall region, are smaller in size but larger in their amount (Sumitani & Kasagi 1995). Using these results we propose that the off-wall peak of spanwise vorticity fluctuations is an indicator of the increased amount of the sweep and ejection events, which take place in the near-blowing-wall region. At the suction wall the peak does not appear, yet, we may see a plateau which is located at $x_2^+ \sim 10$ and has length of $4-8$ wall units at low transpiration numbers, as it may be taken from figure 6.5(f). With increasing suction rate the plateau moves towards the wall. This plateau is also associated with the sweeps and ejections that are present in the near-wall region of the wall-bounded turbulent flow.

6.3 Instantaneous velocity and vorticity fields

In the previous section it has been shown that structures, which are present in the near-wall region are affected by uniform blowing and suction. These results where obtained from analysis of one- and two-point statistics of the fluctuating velocity and vorticity. In the present section we analyze instantaneous velocity and vorticity fields. And perform visualization of the low-speed streaks and coherent vortical structures

in the near-wall region using VisIt, a free interactive parallel visualization and graphical analysis tool.

In order to visualize LSM structures or clusters attached to the wall we plot the instantaneous point-wise Reynolds stresses normalized on the friction velocity $-\overline{u_1 u_2}/u_\tau^2$. It was reported by del Álamo & Jiménez (2006) that these structures contain most of the turbulent energy, while the detached ones dissipate with time and usually are much smaller then attached structures. As it may be taken from the figure 6.6, which represents the slice of the instantaneous $-\overline{u_1 u_2}/u_\tau^2$ field taken in the buffer layer (at $x_2^+ = 10; 490$), velocity streaks associated with these structures become shorter at the blowing wall and longer and thicker at the suction wall. This agrees with the structural analysis results obtained by Sumitani & Kasagi (1995), who reported that suction increases the size of the coherent structures.

According to the quadrant analysis method the region of the flow with positive streamwise and negative wall-normal component of the velocity fluctuations $u_1 > 0, u_2 < 0$ is different from the region with $u_1 < 0, u_2 > 0$. The difference results in the types of events taking place in these regions. In the latter case with ($u_1 < 0, u_2 > 0$) the fluid is being ejected from the wall, while in the former case with ($u_1 > 0, u_2 < 0$) the fluid is being swept to the wall. Both types of the events are usually associated with attached to the wall structures.

In order to plot sweep and ejection events that take place in the channel flow with blowing and suction we have applied contours of the positive and negative instantaneous wall-normal velocity on the slice plot shown in figure 6.6. The contours show us that at the blowing side all the regions with high negative instantaneous streamwise and wall-normal velocity product are formed by positive wall-normal velocity and negative streamwise velocity, as it may be seen in figure 6.6(a). As a result these structures represent ejection motions. It is important to note that amount of the sweep events at the blowing wall are much smaller than ejection ones, however it is not zero. Thus, it may be said that ejection events predominate in the near-blowing-wall region.

The distribution of the sweeps and ejections at the suction wall is completely different. Most of the high negative instantaneous velocity product structures on this side are of sweep type, as it may be taken from figure 6.6(b). In the central part of the flow we may see a very long $\mathcal{O}(h)$, conical structure that propagates in the streamwise direction. This structure may also be seen in figure 6.7 (yellowish region in the $x_2 - x_3$ plane). The nature of this structure is unclear so far, however, it may be related to the superstructures discussed above. As it can also be taken from the $x_2 - x_3$ plane in figure 6.7 the structures are quasi-periodic in the spanwise direction. The yellowish and reddish regions alternate with each other. At the upper wall we see the footprints of the long near-suction-wall low-speed velocity streaks with a characteristic length scale of $500-700$ wall units in streamwise direction. Due to the transpiration the point of the maximum velocity is shifted towards the suction wall, see figure 6.7.

Generally speaking, the instantaneous point-wise streamwise and wall-normal velocity product and velocity distributions presented in figures 6.6(a, b) and 6.7 clearly show how wall transpiration affects the flow at the walls and in the core region.

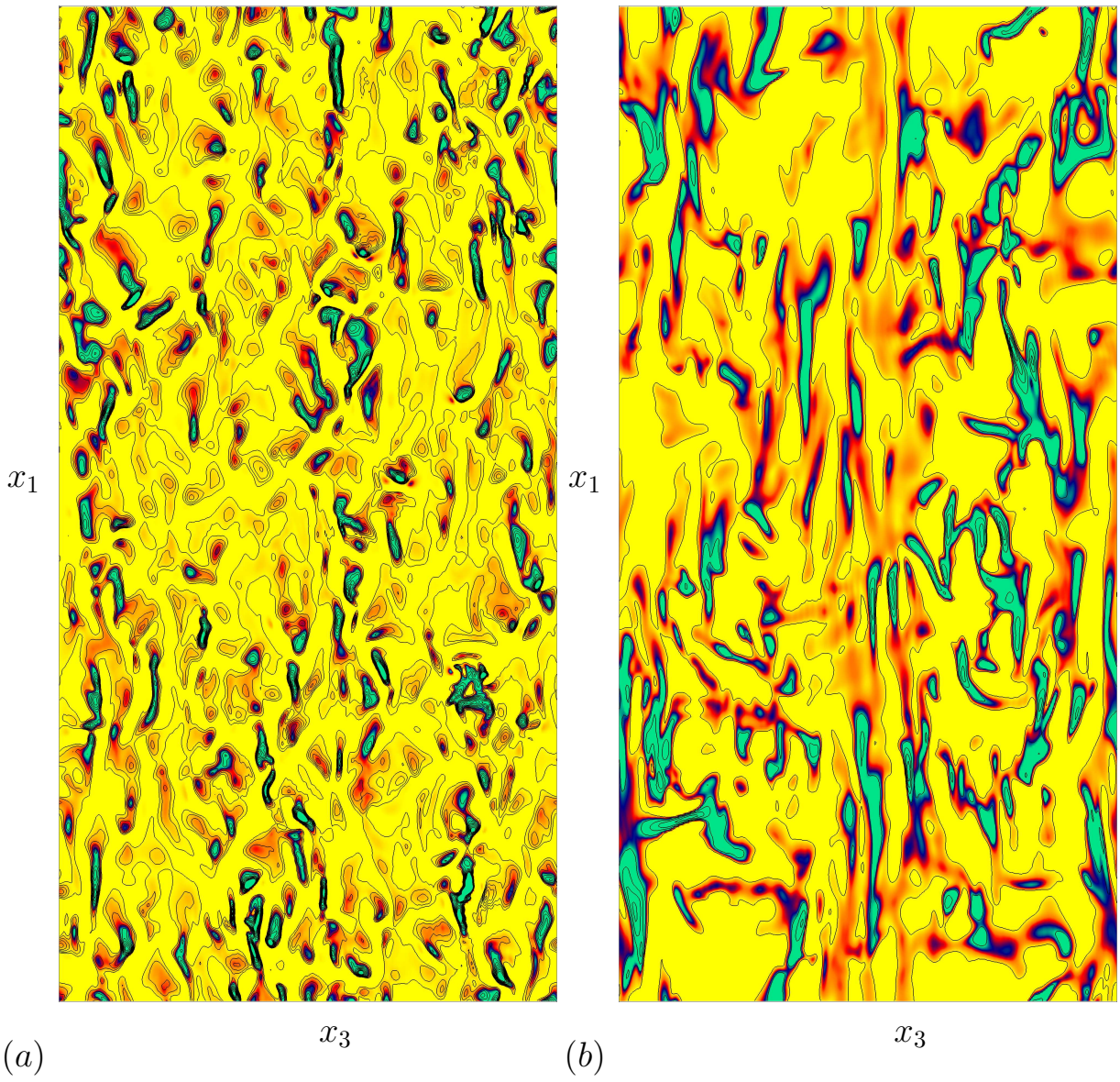

Figure 6.6: Instantaneous point-wise streamwise and wall-normal velocity product normalized on friction velocity $-U_1U_2/u_\tau^2$. Slices are taken at: (a) $x_2^+ = 10$ (at blowing wall); (b) $x_2^+ = 490$ (at suction wall). Yellowish areas represent the regions of zero Reynolds stress, while bluish areas show high Reynolds stress regions. Solid contour lines represent: (a) $u_2^+ < 0$; (b) $u_2^+ > 0$. The size of the plotted domain slice is: $4\pi \times 2\pi$. Parameters of the visualization are $v_0/u_\tau = 0.16, \;\; Re_\tau = 250$.

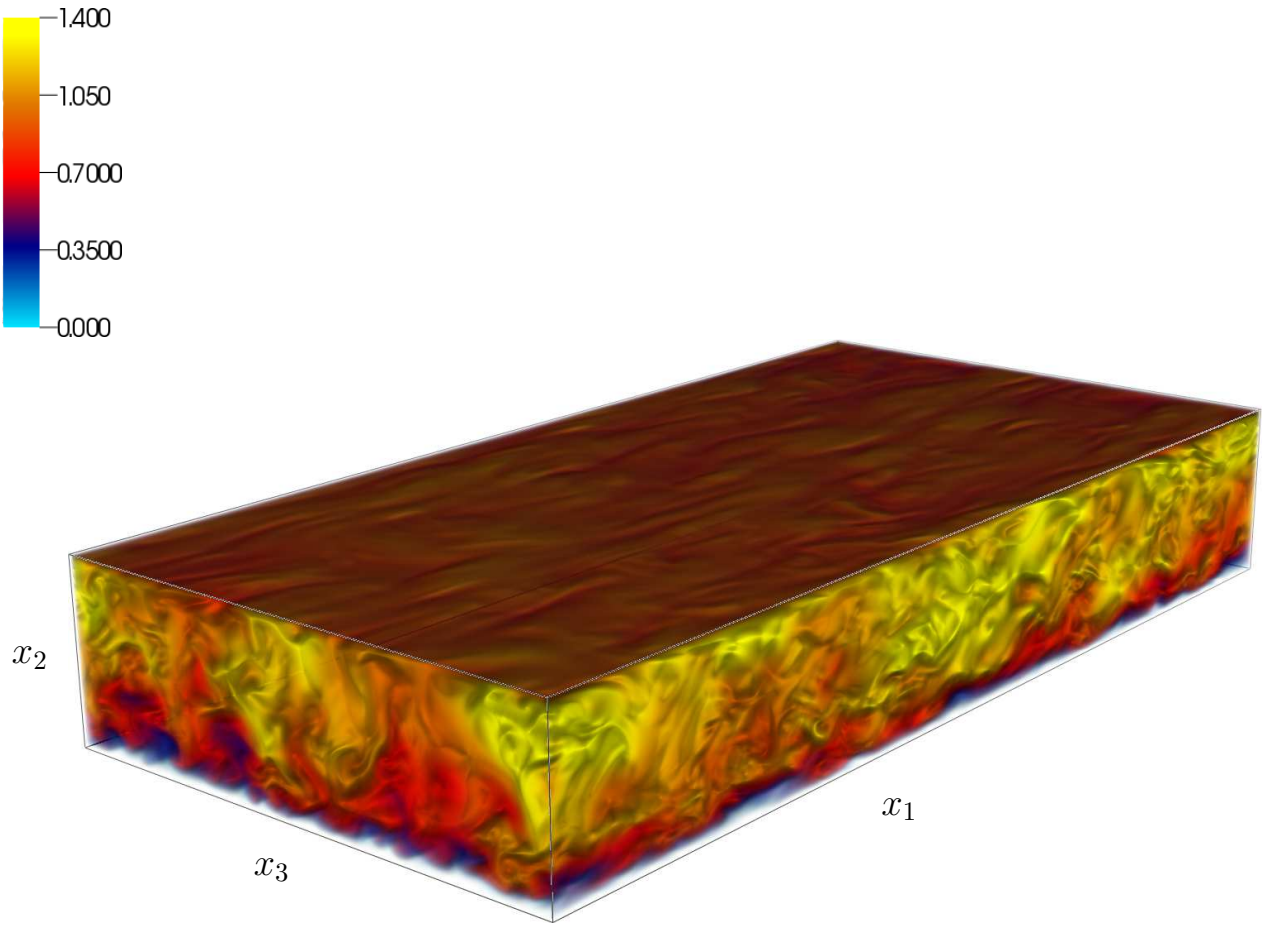

Figure 6.7: Three dimensional visualization of the positive part of the instantaneous streamwise velocity field. Blowing is applied at the bottom wall and suction at the upper wall. Parameters of the visualization are $v_0/u_\tau = 0.16$, $Re_\tau = 250$.

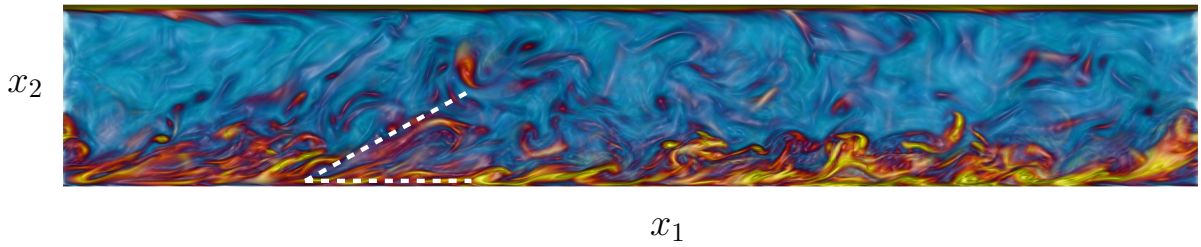

Figure 6.8: Instantaneous field of vorticity magnitude colored with streamwise component of vorticity. Blowing is applied at the bottom wall and suction at the upper wall. The flow propagates from left to right. The white dashed lines highlight the vertical growth angle. Yellow reddish structures are hairpin vortices and packets of hairpins. The colormap is the same as in figure 6.10. Parameters of the visualization are $v_0/u_\tau = 0.16, \;\; Re_\tau = 250$.

However, it is well known that low and high speed velocity streaks are not the only structures that are present in wall-bounded turbulence and are involved in the regeneration cycle.

In the buffer and logarithmic regions streamwise and spanwise coherent vortices are carrying most of the wall-normal momentum flux. They are aligned with the eigenvectors of the rate of strain tensor, which are at 45° in parallel shear layer flows (Theodorsen 1952, Robinson 1991). Alignment at this angle allows them to effectively extract the mean flow energy. The hairpin vortices created at the blowing wall are inclined at approximately 45° to the wall, thus wall-blowing does not change the orientation of these coherent structures. The heads of the hairpins are formed at $x_2^+ = 100$, as in the cases without transpiration (Robinson 1991, Adrian 2007). The length of the hairpin legs is also very similar to the classical case and varies from 200 to 300 wall units (Robinson 1991), as it may be seen on figure 6.9(a) (dashed line boxes are 400 wall units high). However, the packets of hairpins or LSM structures are much longer ($L_x \approx 5h$), whereas in canonical flows their length is $L_x \approx 3h$ (Jiménez 2012). The spanwise growth angle is also very different from the classical case and amounts to 24°, while according to Adrian (2007) it is about 12°. One of these structures is manually highlighted on figure 6.9(a) with dashed lines, which form 24° angle. The vertical growth angle, see figure 6.8, also amounts to 24°, which is in accordance with the *attached eddy* hypothesis (Townsend 1976).

Due to increased vertical and spanwise growth angles hairpin packets grow faster and penetrate deeper into the channel than similar structures in the classical case. Hence, they reach the core region, as it may be taken from figures 6.8 and 6.10. In the same figure we may also see that these structures do not form on the suction side. Thus, we may conclude that these structures are sensitive to the wall conditions and the growth angle increase is caused by wall-blowing. This result is in accordance with Flores et al. (2007), who reported that in the channel flow with roughness vertical and spanwise growth angle are 8°.

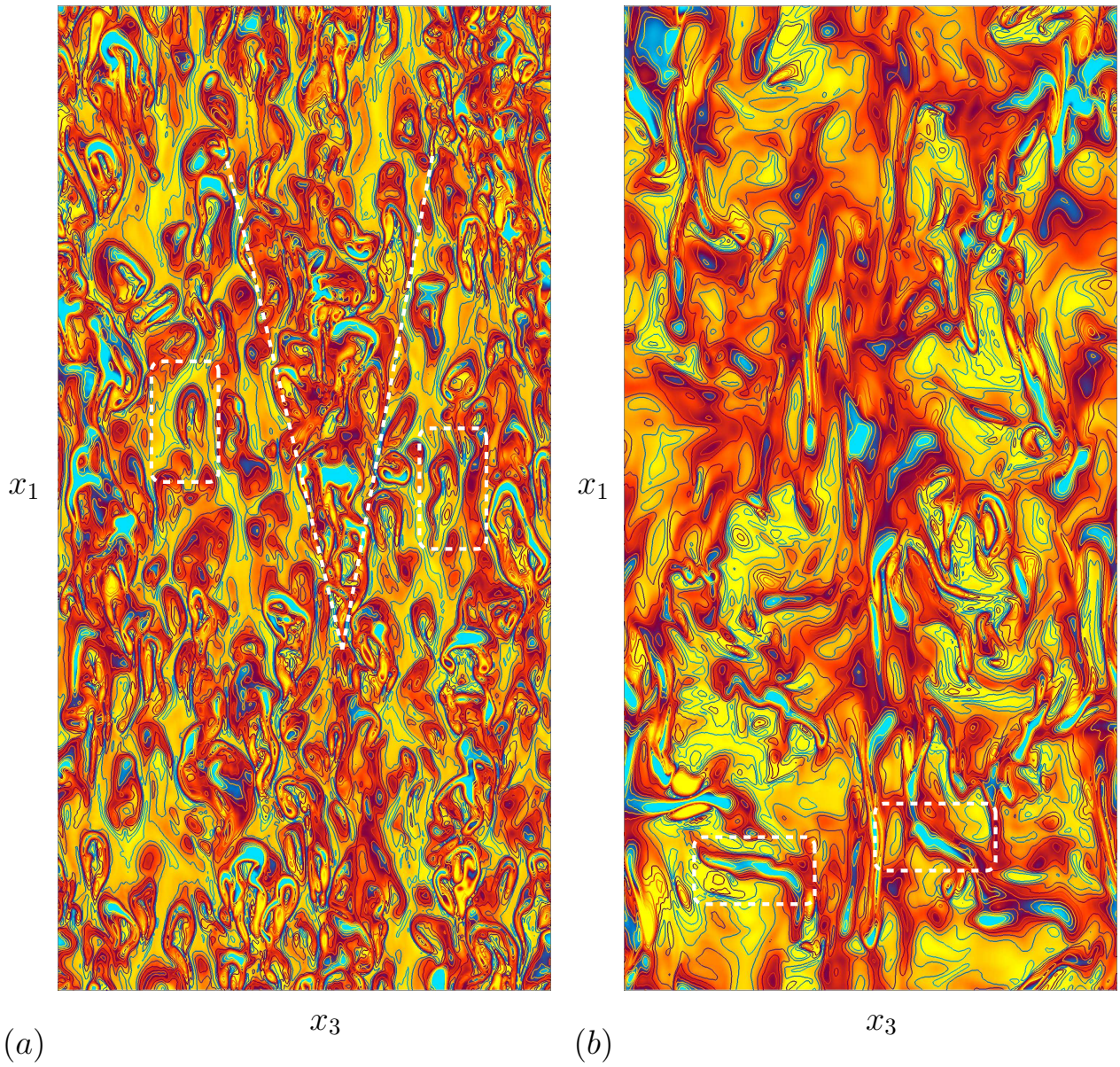

Figure 6.9: Instantaneous field of the spanwise vorticity ω_3. Slices are taken at: (a) $x_2^+ = 20$ (blowing wall); (b) $x_2^+ = 480$ (suction wall). White dashed line boxes show: (a) hairpin structures; (b) spanwise roller structures. White dashed lines highlight LSM structure at the blowing wall. These lines form a 24° angle. Yellowish areas represent the regions of zero vorticity, while bluish areas show the regions of high spanwise vorticity. Solid contour lines represent vorticity magnitude with inverted colormap: blueish contour lines show areas with zero vorticity magnitude, while yellowish lines areas of high vorticity magnitude. The size of the plotted domain slice is: $4\pi \times 2\pi$. Parameters of the visualization are $v_0/u_\tau = 0.16$, $Re_\tau = 250$.

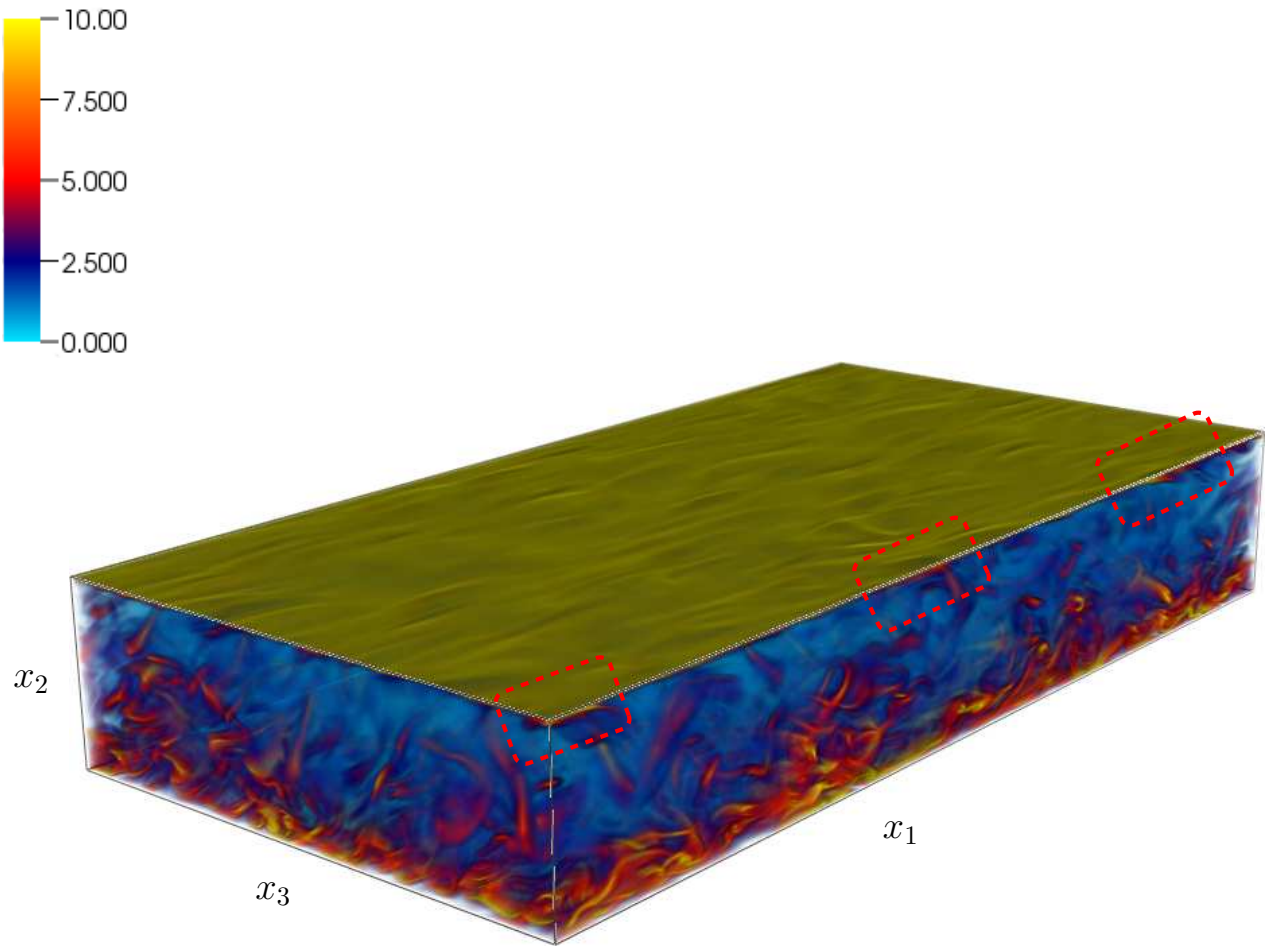

Figure 6.10: Three dimensional visualization of the instantaneous vorticity field, which magnitude colored with streamwise component of the vorticity. Blowing is applied at the bottom wall and suction at the upper wall. Red dashed boxes show random bursting events at the suction wall. Yellow reddish structures are hairpin vortices and packets of hairpins. Parameters of the visualization are $v_0/u_\tau = 0.16,\ \ Re_\tau = 250.$

On the suction side hairpin structures do not form. As it may be taken from figures 6.9(b) and 6.10, wall-suction does not allow arch structures to form a horseshoe and lift-up away from the wall. As a result arch structures transform into spanwise vortices or spanwise rollers, as they where named by Jiménez et al. (2001). These structures are manually highlighted with dashed boxes in figure 6.9(b). Apart from that we may find quasi-streamwise vortices at the suction wall, which correspond to the largest velocity streaks. Both types of coherent vortical structures have a very small wall-normal extent. Due to wall-suction they are localized in the near-wall region below 50 wall units. However, there are random bursting events that penetrate into the region above $x_2^+ = 100$ (red boxes in figure 6.10).

6.4 Conclusions

In the present chapter we have studied coherent structures that are present in wall-bounded turbulent flows and investigated how blowing and suction affect them. Using one- and two-point statistics we have found some important relations between single point and multi-point volume functions that represent coherent structures. In particular, it was found that the two-point cross correlation function $R_{12}/\sqrt{(\overline{u_1 u_2})^2}$, indicates the size of the velocity streaks in the flow, when normalized on the Reynolds stress.

Further, from the analysis of the single point vorticity fluctuations, it was found that strong blowing and suction may destroy the near-wall regeneration cycle. This result agrees with the one obtained from the production to dissipation rate analysis in the third chapter, namely that the flow becomes laminar at very high transpiration rates.

It was found that in the near-wall region blowing and suction affect the wall-normal component of vorticity fluctuations ω_2 through the term $\partial u_1/\partial x_3$ which serves as an indication of the presence of velocity streaks. Absence of the collapse of ω_2 profiles in the near-wall region indicates that wall-transpiration influences this purely high-Reynolds number effect.

A new indicator of sweep and ejection events was proposed from analysis of the spanwise vorticity fluctuations ω_3. In particular, it was proposed that the new off-wall peak of ω_3 at the blowing wall and plateau at the suction wall may indicate an increased amount of ejection and sweep events through the term $\partial u_1/\partial x_2$. Later, visualizations of the instantaneous velocity and vorticity fields have shown that ejections dominate at the blowing wall, where the big amount of hairpin-type vortical structures have been found, while at the suction wall we have only found sweep motions towards the suction wall. As a result no hairpin structures have been found in this region.

Finally, we have been found that hairpin packets (LSM structures), unlike single hairpins, may be affected by specific boundary conditions. In particular, vertical and spanwise growth angles increased at the blowing wall. As a result, these structures grow faster and penetrate into the core region of the flow.

7 Conclusions and future work

In the present thesis we have combined Lie symmetry analysis of the TPC equations and DNS to investigate the statistical characteristics of a turbulent channel flow with wall transpiration. The analysis of the numerical results performed in the third chapter revealed that the complexity of the system increased due to the flow asymmetry about the centerline. It has also been found that some of the high Reynolds number effects like the location of the peak of the streamwise velocity fluctuations (see figure 3.10) or collapse of the wall-normal component of vorticity fluctuations (see figure 6.5(c, d)) do not occur in the channel flow with wall transpiration.

Lie symmetry analysis has revealed a new mean velocity logarithmic type of scaling law that, afterwards, has been confirmed in the center of the channel and studied in detail by DNS. For the derivation of the new log-law we applied symmetry transformations, which have been previously derived in the two- and MPC equations (Oberlack 2001, Oberlack & Rosteck 2010). Although the completeness of the set of symmetry groups for turbulence statistics for the MPC equations has not been proven yet, it was sufficient to derive the new scaling law for the core region.

By using the new results from the DNS data it was found, that the slope constant (γ) of the new log-law is different from the von Kármán constant and that its value is $\gamma = 0.3$. The influence of the transpiration makes the log-region remarkably longer than that of the velocity defect law for the classical channel flow. The new scaling law covers 65% to 80% of the channel height depending on the transpiration rate. We have observed an increase of the new log-law scaling region with increasing transpiration rate, though no first principles theory may be given for this behaviour. The validity of the new scaling law may be obtained from the relation between friction and transpiration velocities, which is shown in figure 5.5. The law is only valid in the region $0 < v_0^+ \leq 0.16$, where the averaged friction velocity u_τ linearly depends on the transpiration velocity v_0.

The classical near-wall scaling laws, i.e. the linear law in the viscous sublayer and logarithmic law of the wall, have been validated in slightly modified form. Results of validation indicate that the permeability of the channel walls affects the near-wall region and in particular the wall shear stress. This conclusion, in a certain sense, is not new. However, the results obtained in the present thesis show that at very high transpiration rates the properties of the near-wall region are completely changed, which can be taken from figures 3.5(f), 3.6(f). We have shown that the convective momentum transport $v_0\bar{U}_1$ exceeds both viscous and Reynolds stresses at the blowing wall and at the same time leads to an almost zero Reynolds stress at the suction wall. From the same figures and also from the fact that the new scaling law (5.18) has been successfully validated with DNS data for moderate transpiration rates we may assume that the strong transpiration also has influence on the core region of the flow.

Further, it has been shown that the von Kármán constant is universal in the near-wall region, while the additive constant C had to be modified by the transpiration rate. A near-wall log region persisted only on the blowing side and only for moderate transpiration rates $0.05 \leq v_0/u_\tau \leq 0.1$. The most interesting conclusion we can draw from the figure 5.4 is that high Reynolds number and high transpiration rate effects counter balance each other in the log-region. The logarithmic region grows as the Reynolds number increases and decreases at high transpiration rates. The most plausible explanation for this effect is that transpiration shifts the buffer layer deeper into the channel, where the latter directly meets the core region of the flow at high transpiration rates and hence eliminates the logarithmic region.

Analysis of the near-wall coherent structures has revealed that high blowing and suction are able to destroy the near-wall regeneration cycle. It was found that near-suction wall region is saturated with sweep events, while ejections dominate at the blowing wall. Consequently, suction prevents hairpins from growing in wall-normal direction, while blowing does not affect these structures. Increased growth angles of the LSM structures at the blowing wall (see figures 6.8 and 6.9) and a shift of the production over the dissipation peak into the core region (see figure 3.8) indicates that these structures transfer a large amount of momentum deep into the core region of the channel. All the results obtained in the previous chapter support Townsend's *attached eddy hypothesis*.

The importance of the present contribution may be contemplated in a somewhat larger context as another brick in the turbulence theory based on Lie symmetries, applied to the multi-point correlation equation the reason being twofold. First, before the entire project started and before any DNS was conducted the new log-scaling laws has been forecasted from pure theoretical grounds. Second, the basis for the new log-law is partially based on two of the new statistical groups. These have no direct counterpart in the Euler and Navier-Stokes equations for the instantaneous velocities. Hence, have been proven one more time to be crucial for our general understanding of the statistics of turbulence.

The future research may concentrate on the analysis of the flow dynamics at very high transpiration rates and high Reynolds numbers. Results obtained in the present thesis suggest that at such transpiration numbers the near-wall logarithmic region will disappear and the buffer layer will be directly linked with the core region. The new mean velocity scaling law (5.18) will reduce in size and will cover up to 40% of the channel width. Taking into account that the streamwise turbulence intensity scaling law will also be present in the flow, we may suggest that large-scale coherent structures attached to the wall (hairpin packets) will dramatically grow in size. Due to the latter feature a much larger computational box should be used. As it may be taken from the results obtained in the previous chapter, the minimal computational box should be $8\pi h \times 2h \times 6\pi h$ for the high transpiration ($v_0^+ > 0.2$) and Reynolds number ($Re_\tau > 1000$) simulations. It has to be also taken into account that at very high transpiration rates flow tends to relaminarize, hence, high Reynolds number should be selected.

Another interesting future research topic may be a numerical study of the Couette flow with wall blowing and suction. Due to an additional moving wall velocity scale it is unknown how the new logarithmic mean velocity scaling law will be modified.

The finding of a similar type of log-law in the core region of the Couette flow with wall transpiration would proof that the new log-law is a purely transpiration induced phenomenon.

Appendix A

Laminar Poiseuille flow with uniform wall blowing and suction

As it is naturally expected it is possible to derive an exact analytical solution of the Navier-Stokes equations for the laminar flow with uniform wall blowing and suction.

The governing equations for a laminar channel flow, i.e. continuity and momentum equations, are

$$\frac{\partial U_k}{\partial x_k} = 0, \tag{A.1}$$

$$\frac{\partial U_i}{\partial t} + U_k \frac{\partial U_i}{\partial x_k} = -\frac{1}{\rho}\frac{\partial P}{\partial x_i} + \nu \frac{\partial^2 U_i}{\partial x_k \partial x_k}\,,\ i = 1, 2, 3, \tag{A.2}$$

where $U_i(x_i, t)$ and $P(x_i, t)$ are the velocity and pressure. For the incompressible and steady flow investigated, pressure can be normalized with the constant density as follows

$$P^* = \frac{P}{\rho}. \tag{A.3}$$

Assuming that

$$U_i = (U_1(x_2), v_0, 0) \ \text{ and } \ \frac{\partial P^*}{\partial x_i} = const, \tag{A.4}$$

the equation to be solved reduces to

$$v_0 \frac{\partial U_1}{\partial x_2} - \nu \frac{\partial^2 U_1}{\partial x_2 \partial x_2} = -\frac{\partial P^*}{\partial x_1}. \tag{A.5}$$

Therefore the solution of the linear second order non-homogeneous differential equation is a sum of the general solution of the homogeneous equation

$$v_0 \frac{\partial U_1}{\partial x_2} - \nu \frac{\partial^2 U_1}{\partial x_2 \partial x_2} = 0 \tag{A.6}$$

and the one particular solution of the non-homogeneous equation (A.5).

In order to find the solution of the homogeneous equation (A.6) I will make a following substitution

$$U_1 = e^{a x_2}, \tag{A.7}$$

where a is a constant to be found. Using (A.7) equation (A.6) reduces to

$$v_0 a e^{a x_2} - \nu a^2 e^{a x_2} = 0. \tag{A.8}$$

Solution of this equation yields $a = v_0/\nu$ and $a = 0$.
Thus general solution of (A.6) is given

$$U_{10}(x_2) = c_1 e^{v_0 x_2/\nu} + c_2. \tag{A.9}$$

Using no-slip boundary condition $U_1(x_2) = 0$ at $x_2 = 0$ leads to result that $c_1 = -c_2$.
A particular solution of the non-homogeneous equation (A.5) will have the form

$$U_1(x_2) = Ax_2, \tag{A.10}$$

where A is a constant to be found. Application of the (A.10) into the terms on the l.h.s. of the equation (A.5) facilitates to find a particular solution of this equation

$$U_{1p}(x_2) = -\frac{1}{v_0}\frac{\partial P^*}{\partial x_1}x_2. \tag{A.11}$$

General solution of equation (A.5) is

$$U_1(x_2) = U_{10}(x_2) + U_{1p}(x_2) = c_1\left(e^{v_0 x_2/\nu} - 1\right) - \frac{1}{v_0}\frac{\partial P^*}{\partial x_1}x_2. \tag{A.12}$$

In order to find the value of the constant c_1 we may use boundary condition $U_1(2h) = 0$, to yield

$$c_1 = -\frac{2h}{v_0(1 - e^{2hv_0/\nu})}\frac{\partial P^*}{\partial x_1}. \tag{A.13}$$

Finally, general solution of the equation (A.5) yields the following form

$$U_1(x_2) = \frac{1}{v_0}\left[2h\frac{1 - e^{v_0 x_2/\nu}}{1 - e^{2hv_0/\nu}} - x_2\right]\frac{\partial P^*}{\partial x_1}, \tag{A.14}$$

or in normalized on bulk velocity U_b (see eq. (2.24)) and channel half-height h form

$$\tilde{U}_1(\eta) = \frac{1}{\tilde{v}_0}\left[2\frac{1 - e^{\tilde{v}_0\eta Re}}{1 - e^{2\tilde{v}_0 Re}} - \eta\right]\frac{\partial \tilde{P}^*}{\partial(x_1/h)}, \tag{A.15}$$

where tilde denotes variables normalized on bulk velocity, $\eta = x_2/h$ and $Re = U_b h/\nu$. In order to determine the pressure gradient $\frac{\partial \tilde{P}^*}{\partial(x_1/h)}$ we may assume that it is constant and it exactly balances the mean shear stress at the walls

$$-\frac{\partial \tilde{P}^*}{\partial(x_1/h)} = \tau_w = \frac{1}{Re}\frac{\partial \tilde{U}_1}{\partial \eta}, \tag{A.16}$$

which in the present case reduces to the following form

$$-\frac{\partial \tilde{P}^*}{\partial(x_1/h)} = \frac{2}{Re}. \tag{A.17}$$

So, the general solution for the laminar channel flow with the wall transpiration has

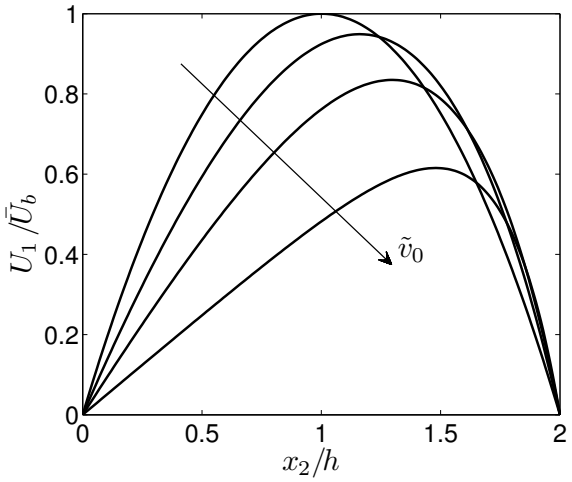

Figure A.1: Laminar velocity profiles of the channel flow with uniform wall blowing and suction. In the direction of the arrow: $v_0/U_b = 0.0005, 0.05, 0.1, 0.2;\ Re = 20$.

the form

$$\tilde{U}_1(\eta) = -\frac{2}{Re\tilde{v}_0}\left[2\frac{1-e^{\tilde{v}_0\eta Re}}{1-e^{2\tilde{v}_0 Re}} - \eta\right]. \tag{A.18}$$

Velocity profiles obtained with the present laminar solution may be taken from figure A.1.

B Bibliography

ADRIAN, R. J. (2007): Hairpin vortex organization in wall turbulence. *Phys. Fluids 19*, 4, 041301–1–16.

DEL ÁLAMO, J. C., JIMÉNEZ, J. (2003): Spectra of the very large anisotropic scales in turbulent channels. *Phys of Fluids 15*, 6, 41–44.

DEL ÁLAMO, J. C., JIMÉNEZ, J. (2006): Linear energy amplification in turbulent channels. *J. Fluid Mech. 559*, 205–213.

DEL ÁLAMO, J. C., JIMÉNEZ, J., ZANDONADE, P., MOSER, R. D. (2004): Scaling of the energy spectra of turbulent channels. *J. Fluid Mech. 500*, 135–144.

ANTONIA, R. S., KRISHNAMOORTHY, L. V., FULACHIER, L., ANSELMET, F., BENABID, T. (1986): Influence of wall suction on coherent structures in a turbulent boundary layer. 9th Australasian Fluid Mechanics Conference, Auckland, Australia, 346–349.

AVSARKISOV, V., OBERLACK, M., HOYAS, S. (2014): New scaling laws for turbulent Poiseuille flow with wall transpiration. *J. Fluid Mech. 746*, 99–122.

AVSARKISOV, V. S., OBERLACK, M., KHUJADZE, G. (2011): Turbulent Poiseuille Flow with Wall Transpiration: Analytical Study and Direct Numerical Simulation. *J. of Phys.: Conf. Ser. 318*, 022004, 1–6.

BARENBLATT, G. I. (1993): Scaling laws for fully developed turbulent shear flows. *J. Fluid Mech. 248*, 513–520.

BATCHELOR, G. K. (1967): *An introduction to fluid dynamics*. Cambridge university press.

BECHERT, K. (1941a): Differentialgleichungen der Wellenausbreitung in Gasen. *Annalen der Physik 39*, 357–372.

BECHERT, K. (1941b): Ebene Wellen in idealen Gasen mit Reibung und Warmeleitung. *Annalen der Physik 40*, 207–248.

BERNARD, P. S., WALLACE, J. M. (2002): *Turbulent Flow: Analysis, Measurement, and Prediction*. John Wiley and Sons.

BIRKHOFF, G. (1950): *Hydrodynamics*. Dover Publications, Inc. New York.

BLACK, T. J., SARNECKI, A. J. (1958): The turbulent boundary layer with suction or injection. Techn. Ber. 20, Cambrige University, Engineering Department.

BLUMAN, G., ANCO, S. (2002): *Symmetry and integration methods for differential equations., vol.154 of Applied mathematical sciences*. Springer-Verlag.

BLUMAN, G. W., CHEVIAKOV, A. F., ANCO, S. C. (2010): *Application of Symmetry Methods to Partial Differential Equations*. Springer.

BOISVERT, R. E., AMES, W. F., SRIVASTAVA, U. N. (1983): Group properties and new solutions of Navier-Stokes equations. *J. Eng. Math. 17*, 203–221.

BOUSSINESQ, J. (1887): Essai sur la théorie des eaux courantes. *Mem. Acad. Sci. Inst. Fra. 23*, 1, 1–64.

BUCHNEV, A. A. (1971): The Lie group admitted by the motion of an ideal incompressible fluid. *Dinamika Sploch. Sredi 7*, 212–214.

BYTEV, V. O. (1972): Group properties of the equations of Navier-Stokes in the plane, in collection: *Numerical methods of the mechanics of fluids*. *Comp. center Siberian Dep. Acad. Sci. USSR 3*, 13–17.

CARTAN, E. (1894): Sur la structure des groupes de transformations finis et continus. *Thesis* .

CARTAN, E. (1905): Sur la structure des groupes infinis de transformations. *Annales de lEcole Normale 22*, 219–308.

CARTAN, E. (1922): Sur une généralisation de la notion de courbure de Riemann et les espaces á torsion. *C. R. Acad. Sci. (Paris) 174*, 593–595.

CARTAN, E. (1923-1924): Sur les variétés á connexion affine et la théorie de la relativité généralisée. *Annales Scientifiques de l'Ecole Normale Superieure 41-42*, 1–25–17–88.

CARTAN, E. (1946): Les systèmes différentiels extérieurs et leurs applications géométriques. *Bull. Sc. math. 70*, 117–122.

CHAMPAGNE, B., HEREMAN, W., WINTERNITZ, P. (1991): The computer calculation of Lie point symmetries of large systems of differential equations. *Comp. Phys. Comm. 66*, 319–340.

CHUNG, Y. M., SUNG, H. J. (2001): Initial relaxation of spatially evolving turbulent channel flow with blowing and suction. *AIAA Journal 39*, 11, 2091–2099.

CHUNG, Y. M., SUNG, H. J., KROGSTAD, P.-A. (2002): Modulation of near-wall turbulence structure with wall blowing and suction. *AIAA Journal 40*, 8, 1529–1535.

CICOGNA, G., GAETA, G. (1993): Nonlinear Lie symmetries in bifurcation theory. *Phys. Letters A 172*, 361–364.

CLAUSER, F. H. (1956): The turbulent boundary layer. *Adv. Appl. Mech. 4*, 1–51.

CORINO, E. R., BRODKEY, R. S. (1969): A visual investigation of the wall region in turbulent ow. *J. Fluid Mech. 37*, 1, 1–30.

DARCY, H. (1857): *Recherches expérimentales relatives au mouvement de l'eau dans les tuyaux*. Mallet-Bachelier, Paris.

DAVIDSON, P. A. (2004): *Turbulence An introduction for scientists and engineers*. Oxford University Press.

DAVIDSON, P. A., KANEDA, Y., MOFFATT, K., SREENIVASAN, K. R. (2011): *A voyage through turbulence*. Cambridge University Press.

DEGRAAFF, D. B., EATON, J. K. (2000): Reynolds-number scaling of the flat-plate turbulent boundary layer. *J. Fluid Mech. 422*, 319–346.

DENNIS, S. C. R., INGHAM, D. B., COOK, R. N. (1979): Finite-difference methods for calculating steady incompressible flows in three dimensions. *J. of Comp. Phys.*

33, 3, 325–339.

DRAZIN, P. G., RILEY, N. (2006): *The Navier-Stokes equations: a classification of flows and exact solutions*. Cambridge University Press.

EHRENFEST-AFANASSJEWA, T. (1926): Dimensional analysis . . . theory of similitudes. *Phil. Mag. 1*, 257–272.

EULER, L. (1757): Principes généraux du mouvement des fluides. *Mém. Acad. Sci. Berl. 11*, 274–315.

FLORES, O., JIMÉNEZ, J. (2006): Effect of wall-boundary disturbances on turbulent channel flows. *J. Fluid Mech. 566*, 357–376.

FLORES, O., JIMÉNEZ, J., DEL ÁLAMO, J. C. (2007): Vorticity organization in the outer layer of turbulent channels with disturbed walls. *J. Fluid Mech. 591*, 145–154.

FOURIER, J. B. J. (1822): *Théorie analytique de la chaleur*. F. Didot, Paris.

FRISCH, U. (1995): *Turbulence*. Cambridge Univ. Press.

FROHNAPFEL, B., HASEGAWA, Y., KASAGI, N. (2010): Friction drag reduction through damping of the near-wall spanwise velocity fluctuation. *J Heat Fluid Flow 31*, 3, 434–441.

GALOIS, E. (1830): Analyse d'un Mémoire sur la résolution algébrique des équations. *Bulletin des Sciences mathématiques XIII*, 271–272.

GEORGE, W. K., CASTILLO, L. (1997): Zero-pressure-gradient turbulent boundary layer. *Appl. Mech. Rev. 50*, 689–729.

GÖRTLER, H. (1942): Berechnung von Aufgaben der freien Turbulenz auf Grund eines neuen Nherungsansatzes. *ZAMM 22*, 5, 244–254.

GRASS, A. J. (1971): Structural features of turbulent flow over smooth and rough boundaries. *J. Fluid Mech. 50*, 2, 233–255.

GRAUEL, A., STEEB, W.-H. (1985): Similarity solutions of the Euler equation and the Navier-Stokes equation in two space dimensions. *Inter. J. Theor. Phys. 24*, 3, 255–265.

GRIFFITH, A. A., MEREDITH, F. W. (1936): Possible improvement in aircraft performance due to use of boundary layer suction. Techn. Ber. 2315, Aero. Res. Counc., London.

GRÖTZBACH, G. (1987): Direct numerical and large eddy simulation of turbulent channel ows. *Encyclopedia of fluid mechanics* .

HAGEN, G. (1854): *Über den Einfluss der Temperatur auf die Bewegung des Wassers in Röhren*. Kgl. Akademie der Wiss. Berlin.

HANJALIĆ, K., LAUNDER, B. E. (1972a): Fully developed asymmetric flow in a plane channel. *J. Fluid Mech. 51(2)*, 301–335.

HANJALIĆ, K., LAUNDER, B. E. (1972b): Reynolds-stress model of turbulence and its application to thin shear flows. *J. Fluid Mech. 52(4)*, 609–638.

HINZE, J. O. (1959): *Turbulence, An Introduction to Its Mechanism and Theory*. McGraw-Hill.

HOYAS, S., JIMÉNEZ, J. (2006): Scaling of the velocity fluctuations in turbulent channels up to $Re_\tau = 2003$. *Phys. Fluids 18*, 011702–1–4.

HUTCHINS, N., MARUSIC, I. (2007a): Evidence of very long meandering streamwise structures in the logarithmic region of turbulent boundary layers. *J. Fluid Mech. 579*, 1–28.

HUTCHINS, N., MARUSIC, I. (2007b): Large-scale influences in near-wall turbulence. *Philos. Trans. R. Soc. Lond. A 365*, 647–664.

HUTCHINS, N., NICKELS, T. B., MARUSIC, I., CHONG, M. S. (2009): Hot-wire spatial resolution issues in wall-bounded turbulence. *J. Fluid Mech. 635*, 103–136.

IBRAGIMOV, N. (1995a): *CRC Handbook of Lie Group Analysis of Differential Equations, Volume 2: Applications in engineering and physical sciences*. CRC Press.

IBRAGIMOV, N. (1995b): *CRC Handbook of Lie Group Analysis of Differential Equations, Volume I: Symmetries, Exact Solutions, and Conservation Laws*. CRC Press.

IBRAGIMOV, N. (1996): *CRC Handbook of Lie Group Analysis of Differential Equations, Volume 3: New trends in theoretical developments and computational methods*. CRC Press.

JACKSON, P. (1981): On the displacement height in the logarithmic velocity profile. *J. Fluid Mech. 111*, 15–25.

JIMÉNEZ, J. (2004): Turbulent flows over rough walls. *Annu. Rev. Fluid Mech. 36*, 176–196.

JIMÉNEZ, J. (2012): Cascades in wall-bounded turbulence. *Annu. Rev. Fluid Mech. 44*, 27–45.

JIMÉNEZ, J., DEL ÁLAMO, J. C., FLORES, O. (2004): The large-scale dynamics of near-wall turbulence. *J. Fluid Mech. 505*, 179–199.

JIMÉNEZ, J., HOYAS, S. (2008): Turbulent fluctuations above the buffer layer of wall-bounded flows. *J. Fluid Mech. 611*, 215–236.

JIMÉNEZ, J., KAWAHARA, G., SIMENS, M. P., NAGATA, M., SHIBA, M. (2005): Characterization of near-wall turbulence in terms of equilibrium and 'bursting' solutions. *Phys. Fluids 17*, 015105–1–015105–16.

JIMÉNEZ, J., PINELLI, A. (1999): The autonomous cycle of near-wall turbulence. *J. Fluid Mech. 389*, 335–359.

JIMÉNEZ, J., UHLMANN, M., PINELLI, M., KAWAHARA, G. (2001): Turbulent shear flow over active and passive porous surfaces. *J. Fluid Mech. 442*, 89–117.

JOHNSON, R. W. (1998): *The handbook of fluid dynamics*. CRC Press LLC and Springer-Verlag GmbH.

VON KÁRMÁN, T. (1921): Über laminare und turbulente Reibung. *ZAMM 1*, 233–252.

VON KÁRMÁN, T. (1930): Mechanishe Ähnlichkeit und Turbulenz. *Nachr. Ges. Wiss. Göettingen, Math-Phys. Kl. 68*, 58–76.

VON KÁRMÁN, T. (1931): Mechanishe Ähnlichkeit und Turbulenz. *Proc. Third Internat. Congr. Appl. Mech. Stockholm 1*, 85–93.

KELLER, L., FRIEDMANN, A. (1924): Differentialgleichungen für die turbulente Bewegung einer kompressiblen Flüssigkeit. *Proc. First. Int. Congr. Appl. Mech.* , 395–405.

KENNEDY, C. A., CARPENTER, M. H., LEWIS, R. M. (2000): Low-storage, explicit Runge-Kutta schemes for the compressible Navier-Stokes equations. *J. of Appl. Num. Math. 35*, 177–219.

KILLING, W. (1889): Die Zusammensetzung der stetigen endlichen Transformationsgruppen. *Mathematische Annalen 34*, 57–122.

KIM, H. T., KLINE, S. J., REYNOLDS, W. (1971): The production of turbulence near a smooth wall in a turbulent boundary layer. *J. Fluid Mech. 50*, 1, 133–166.

KIM, J., MOIN, P., MOSER, R. (1987): Turbulence statistics in fully developed channel flow at low Reynolds number. *J. Fluid Mech. 177*, 133–166.

KLEIN, F. (1872): *Vergleichende Betrachtungen über neuere geometrische Forschungen*. Verlag von Andreas Deichert.

KLEIN, F. (1882): *Über Riemann's Theorie der Algebraischen Functionen und ihre Integrale*. Teubner, Leipzig.

KLINE, S. J., REYNOLDS, W., SCHRAUB, F. A., RUNSTADLER, P. W. (1967): The structure of turbulent boundary layers. *J. Fluid Mech. 30*, 4, 741–773.

KOLMOGOROV, A. N. (1941a): The local structure of turbulence in incompressible viscous fluids at very large Reynolds numbers. *Dokl. Akad. Nauk SSSR 30*, 299–303.

KOLMOGOROV, A. N. (1941b): Dissipation of energy in isotropic turbulence. *Dokl. Akad. Nauk SSSR 32*, 19–21.

KRAICHNAN, R. H. (1965): Lagrangian-history closure approximaiton for turbulence. *Phys. Fluids 8*, 4, 575–598.

KUNKEL, G. J., MARUSIC, I. (2006): Study of the near-wall turbulent region of the high-Reynolds-number boundary layer using an atmospheric flow. *J. Fluid Mech. 548*, 375–402.

LAUNDER, B. E., REECE, G. J., RODI, W. (1975): Progress in the development of a Reynolds-stress turbulence closure. *J. Fluid Mech. 68(3)*, 537–566.

LELE, S. K. (1992): Compact finite difference schemes with spectral-like resolution. *J. of Comp. Phys. 103*, 16–42.

LIE, S. (1874): Über Gruppen von Transformationen. *Göttinger Nachrichten 22*, 529–542.

LIE, S. (1888): *Theorie der Transformationsgruppen I*. B. G. Teubner.

LIE, S. (1891): *Theorie der Transformationsgruppen II*. B. G. Teubner.

LIE, S. (1896): *Theorie der Transformationsgruppen III*. B. G. Teubner.

LINDGREN, B., ÖSTERLUND, J. M., JOHANSSON, A. V. (2004): Evaluation of scaling laws derived from Lie group symmetry methods in zero-pressure-gradient turbulent boundary layers. *J. Fluid Mech. 502*, 127–152.

LORENZ, E. N. (1993): *The essence of chaos*. University of Washington Press.

MARUSIC, I., MCKEON, B. J., MONKEWITZ, P. A., NAGIB, H. M., SMITS, A. J., SREENIVASAN, K. R. (2010): Wall-bounded turbulent flows at high Reynolds numbers: Recent advances and key issues. *Phys. Fluids 22*, 065103–1–24.

MARUSIC, I., MONTY, J. P., HULTMARK, M., SMITS, A. J. (2013): On the logarithmic region in wall turbulence. *J. Fluid Mech. 716*, R3–1–11.

MCCOMB, W. D. (1990): *The Physics of Fluid Turbulence*. Oxford University Press.

MICKLEY, H. S., DAVIS, R. (1957): Momentum transfer for flow over a flat plate with blowing. Techn. Ber. 4017, MIT.

MILLIKAN, C. B. (1939): A critical discussion of turbulent flows in channels and circular tubes. *Proc. Vth Int. Congr. Appl. Mech.* , 386–392.

MIZUNO, Y., JIMÉNEZ, J. (2013): Wall turbulence without walls. *J. Fluid Mech. 723*, 429–455.

MONTY, J. P., STEWART, J. A., WILLIAMS, R. C., CHONG, M. S. (2007): Large-scale features in turbulent pipe and channel flows. *J. Fluid Mech. 589*, 147–156.

MOSER, R. D., BHATTACHARYA, A., MALAYA, N. (2011): Modeling multi-point correlations in wall-bounded turbulence. *Progress in Wall Turbulence: Understanding and Modeling ERCOFTAC Series 14*, 29–37.

MOSER, R. D., KIM, J., MANSOUR, N. N. (1999): Direct numerical simulation of turbulent channel flow up to $Re_\tau = 590$. *Phys. Fluids 11*, 4, 943–945.

NAVIER, C. (1822): Memoire sur les lois du mouvement des fluides. *Mém. Acad. Sci. Inst. Fra. 6*, 389–440.

NIKITIN, N., PAVEL'EV, A. (1998): Turbulent flow in a channel with permeable walls. DNS and results of three-parameter-model. *J. Fluid Mech. 33*, 6, 826–832.

NIKURADZE, J. (1932): Gesetzmässigkeit der turbulenten Strömung in glatten Rohren. *Forsch. Arb. Ing.-Wes. Heft 356*.

OBERLACK, M. (2000): Symmetrie, Invarianz und Selbstähnlichkeit in der Turbulenz. *Habilitation thesis* .

OBERLACK, M. (2001): A unified approach for symmetries in plane parallel turbulent shear flows. *J. Fluid Mech. 427*, 299–328.

OBERLACK, M., ROSTECK, A. (2010): New statistical symmetries of the multi-point equations and its importance for turbulent scaling laws. *Dis. and Cont. Dyn. Sys. S 3*, 3, 1–21.

OLVER, P. J. (1986): *Applications of Lie groups to differential equations*. Springer-Verlag.

PANTON, R. L. (2001): Overview of the self-sustaining mechanisms of wall turbulence. *Prog. Aerosp. Sci. 37*, 341–385.

PERRY, A. E., CHONG, M. S. (1982): On the mechanism of wall turbulence. *J. Fluid Mech. 119*, 173–217.

PERRY, A. E., HENBEST, S. M., CHONG, M. S. (1986): A theoretical and experimental study of wall turbulence. *J. Fluid Mech. 165*, 163–199.

PERRY, A. E., LI, J. D. (1990): Experimental support for the attached eddy hypothesis in zero pressure-gradient turbulent boundary layers. *J. Fluid Mech. 218*, 405–438.

PIOMELLI, U., FERZIGER, J., MOIN, P. (1989): New approximate boundary conditions for large eddy simulations of wall-bounded flows. *Phys. Fluids 1*, 6, 1061–1068.

POPE, S. (2000): *Turbulent flows*. Cambridge University Press.

PRANDTL, L. (1904): Über Flüssigkeitsbewegung bei sehr kleiner Reibung. *Ver. III Inter. Math.-Kong.* , 484–491.

PRANDTL, L. (1925): Bericht über Untersuchungen zur ausgebildeten Turbulenz. *ZAMM 5*, 136–139.

PUHNACHEV, V. V. (1960): Group properties of the equations of Navier-Stokes in the plane. *J. Appl. Mech. Tech. Phys. 1*, 83–90.

RAJAGOPALAN, S., ANTONIA, R. A. (1993): Structure of the velocity field associated with the spanwise vorticity in the wall region of a turbulent boundary layer. *Phys. Fluids 5*, 10, 2502–2510.

REICHARDT, H. (1951): Vollständige Darstellung der turbulenten Geschwindigkeitsverteilung in glatten Leitungen. *ZAMM 31*, 7, 208–219.

REYNOLDS, O. (1883): An experimental investigation of the circumstances which determine whether the motion of water shall be direct or sinuous, and of the law of resistance in parallel channels. *Phil. Trans. R. Soc. 174*, 935–982.

REYNOLDS, O. (1895): On the dynamical theory of incompressible viscous fluids and the determination of the criterion. *Phil. Trans. R. Soc. 186*, 123–164.

RICHARDSON, L. F. (1922): *Weather prediction by numerical process*. Cambridge University Press.

ROBINSON, S. K. (1991): Coherent motions in the turbulent boundary layer. *Annu. Rev. Fluid Mech. 23*, 601–639.

ROBINSON, S. K., KLINE, S. J., SPALART, P. R. (1989): A review of quasi-coherent structures in a numerically simulated turbulent boundary layer. Techn. Ber. TM-102191, NASA.

ROSTECK, A., OBERLACK, M. (2011): Lie algebra of the symmetries of the multi-point equations in statistical turbulence theory. *J. Nonlinear Math. Phys. 18*, 1, 251–264.

RUARK, A. E. (1935): Inspectional analysis: a method which supplements dimensional analysis. *Jour. Elisha Mitchell Sci. Soc. 51*, 127–133.

RUELLE, D., TAKENS, F. (1971): On the nature of turbulence. *Commun. math. Phys. 20*, 167–192.

SCHLATTER, P., ÖRLÜ, R. (2011): Turbulent asymptotic suction boundary layers studied by simulation. *J. Phys. Conference Series 318*, 1–10.

SCHOPPA, W., HUSSAIN, F. (2000): Coherent structure generation in near-wall turbulence. *J. Fluid Mech. 453*, 57–108.

SCHUMANN, U. (1975): Subgrid scale model for finite difference simulations of turbulent flows in plane channels and annuli. *J. Comut. Phys. 18*, 4, 376–404.

SEDOV, L. I. (1945): On unsteady motions of a compressible fluid. *Doklady U.R.S.S. 47*, 91–93.

SHERRING, J., HEAD, A. K., PRINCE, G. E. (1997): Dimsym and LIE: Symmetry determination packages. *Mathl. Comput. Model. 25*, 8/9, 153–164.

SMITS, A. J., MCKEON, B. J., MARUSIC, I. (2011): High-reynolds number wall turbulence. *Annu. Rev. Fluid Mech. 43*, 353–375.

SPALART, P. R., MOSER, R. D., ROGERS, M. M. (1991): Spectral methods for the Navier-Stokes equations with one infinite and two periodic directions. *J. of Comp. Phys. 96*, 2, 297–324.

SPEZIALE, C. G. (1987): On the advantages of the vorticity-velocity formulation of the equations of fluid dynamics. *J. of Comp. Phys. 73*, 2, 476–480.

STEVENSON, T. N. (1963a): A law of the wall for turbulent boundary layers with suction or injection. Techn. Ber. 166, The College of Aeronautics Cranfield.

STEVENSON, T. N. (1963b): A modified velocity defect law for turbulent boundary layers with injection. Techn. Ber. 170, The College of Aeronautics Cranfield.

STOKES, G. (1845): On the theories of the internal friction of fluids in motion, and of the equilibrium and motion of elastic solids. *Cambridge Phil. Soc.* , 287–305.

SUMITANI, Y., KASAGI, N. (1995): Direct numerical simulation of turbulent transport with uniform wall injection and suction. *AIAA Journal 33*, 7, 1220–1228.

TENNEKES, H. (1965): Similarity laws for turbulent boundary layers with suction or injection. *J. Fluid Mech. 21(4)*, 689–703.

TENNEKES, H., LUMLEY, J. L. (1972): *A First Course in Turbulence*. The MIT Press.

THEODORSEN, T. (1952): Mechanism of turbulence. *Proc. Midwest. Conf. Fluid Mech., 2nd, Columbus, Ohio* , 1–18.

THOMSON, W. (1887): Stability of motion. Broad river flowing down an inclined plane bed. *Phil. Mag. Series 5 24*, 148, 272–278.

TOMKINS, C. D., ADRIAN, R. J. (2003): Spanwise structure and scale growth in turbulent boundary layers. *J. Fluid Mech. 490*, 37–74.

TOWNSEND, A. A. (1961): Equilibrium layers and wall turbulence. *J. Fluid Mech. 11*, 1, 97–120.

TOWNSEND, A. A. (1976): *The structure of turbulent shear flow*. Cambridge University Press.

VIGDOROVICH, I., OBERLACK, M. (2008): Analytical study of turbulent Poiseuille flow with wall transpiration. *Phys. Fluids 20*, 055102–1–9.

WALLACE, J. M., ECKELMANN, H., BRODKEY, R. S. (1972): The wall region in turbulent shear flow. *J. Fluid Mech. 54*, 1, 39–48.

WARK, C. E., NAGIB, H. M. (1989): Relation between outer structures and wall-layer events in boundary layers with and without manipulation. *Proc. 2nd IUTAM Symp. on Structure of Turbulence and Drag Reduction, Zurich, Switzerland* , 467–474.

WILLMARTH, W. W., LU, S. S. (1972): Structure of the Reynolds stress near the wall. *J. Fluid Mech. 55*, 1, 65–92.

WOSNIK, M., CASTILLO, L., GEORGE, W. (2000): A theory for turbulent pipe and channel flows. *J. Fluid Mech. 421*, 115–145.

ZHAPBASBAYEV, U., ISAKHANOVA, G. (1998): Developed turbulent flow in a plane channel with simultaneous injection through one porous wall and suction through the other. *J. Appl. Mech. Tech. Phys. 39*, 53–59.

ZHAPBASBAYEV, U., YERSHIN, S. (2003): Developed turbulent flow in a channel with mass exchange through porous walls. *Symposium on Turbulence, Heat and Mass Transfer* , 173–180.

ZHOU, J., ADRIAN, R. J., BALACHANDAR, S., KENDALL, T. M. (1999): Mechanisms for generating coherent packets of hairpin vortices in channel flow. *J. Fluid Mech. 387*, 353–396.

Curriculum Vitae

Victor Avsarkisov

Personal Data:

Date of Birth:	7^{th} of June, 1984
Place of Birth:	Tbilisi, Georgia

Education:

Jan. 2010 - Nov. 2013:	PhD student at Chair of Fluid Dynamics, Department of Mechanical Engineering, Technische Universität Darmstadt, Germany
Sep. 2005 - Oct. 2007:	Master student at Faculty of Exact and Natural Sciences, I. Javakhishvili Tbilisi State University, Georgia Master thesis: *"Transient growth and mode coupling of the perturbations with a constant vertical shear in geostrophic flows"*
Sep. 2001 - Jul. 2005:	Bachelor student at Faculty of Physics, I. Javakhishvili Tbilisi State University, Georgia
Sep. 1990 - May 2001:	Primary school, secondary school

Employment:

Jan. 2010 - Apr. 2014:	Research Scientist, Chair of Fluid Dynamics, Department of Mechanical Engineering, Technische Universität Darmstadt, Germany
Jan. 2008 - Dec. 2009:	Research Scientist, M.Nodia Institute of Geophysics, Tbilisi, Georgia